LL

JET–P(97)42

Many Authors

JET Posters Presented at the 16th Symposium on Fusion Energy (SOFE)

(San Diego, USA. 6-10th October 1997)

JOINT EUROPEAN TORUS

JET–P(97)42

JET Posters Presented at the 16th Symposium on Fusion Energy (SOFE)

(San Diego, USA. 6–10th October 1997)

Many Authors

JET Joint Undertaking, Abingdon, Oxfordshire, OX14 3EA, UK

October 1997

Title	Main Author	Page No.
The JET Active-Phase Gas Introduction Systems for Neutral Beam Injection and Beamline Commissioning and Operation with Tritium	L Svensson	1 – 8
The Relation Between Halo Currents and Plasma Displacement/Deformation in JET	P Andrew	9 – 16
Preparations for the Fully Remote Exchange of JET Divertor Modules	A Rolfe	17 – 24
Engineering a Remote Survey of JET's Divertor Structure under Conditions of Restricted Access using Digital Photogrammetry	B Macklin	25 – 32
Closure of the Bypass Leakage around the JET Divertor with Polymer Seals	H Altmann	33 – 40
Plasma Vertical Stabilisation at JET using Adaptive Gain Adjustment	M Lennholm	41 – 48
The Development and Testing of a 66kA By-Pass Switch with ARC Commutation Capability for the ITER Coil Power Supply System	T Bonicelli	49 – 56
Asymmetric Vertical Displacement Events at JET	V Riccardo	57 – 64
An Active Phase Compatible Protection System to prevent Excessive Neutral Beam Shinethrough during JET Plasmas	S Cox	65 –72
Operator Interfaces for JET Remote Handling Equipment	P Carter	73 – 74

The JET Active Phase Gas Introduction Systems for Neutral Beam Injection and Beamline Commissioning and Operation with Tritium

L Svensson, A Bickley, A Browne, C D Challis, S Cox, H de Esch, H D Falter, D Godden, T T C Jones, A Konarski, D Martin, D Young

JET Joint Undertaking, Abingdon, Oxon, OX14 3EA, UK

ABSTRACT

During the first part of the active phase of JET, the Deuterium and Tritium Experiment 1 (DTE1), the tritium was delivered to the plasma mainly by Neutral Beam Injection. T_2 and D_2 were delivered from uranium beds in the Active Gas Handling System (AGHS) and were introduced to the Positive Ion Neutral Injectors (PINIs) at ground potential via a new specially developed Tritium and Deuterium Gas Introduction System (TDGIS).

This poster describes the function of the TDGIS, the installation and the commissioning of the system. It also describes the operation of the Neutral Beam System up to 160 kV with tritium beams.

FUNCTION AND DESIGN OF THE TRITIUM AND DEUTERIUM GAS INTRODUCTION SYSTEM

The JET Neutral Beam Injection System consists of two Injector boxes with 8 Positive Ion Neutral Injectors (PINI) modules each. A new Gas Introduction System has been built to supply all PINIs with either tritium or deuterium. The two parts of the system are called TDGIS4 and TDGIS8.

The Active Gas Handling System:

- The tritium and the deuterium is stored on uranium beds in Product Storage (PS) in the Active Gas Handling System (AGHS). [1].

- Accurate gas accounting is performed in AGHS by using pressure and temperature sensors together with calibrated volumes.
- These gases are then expanded into the Gas Distribution Box (GD).
- The limited amount of tritium available for the experiment made it necessary to only use the pipes as the reservoir for the tritium gas.
- The dimensions were critically assessed to verify that the pressure drop over the 100 meters length of pipe was less than 10 %.

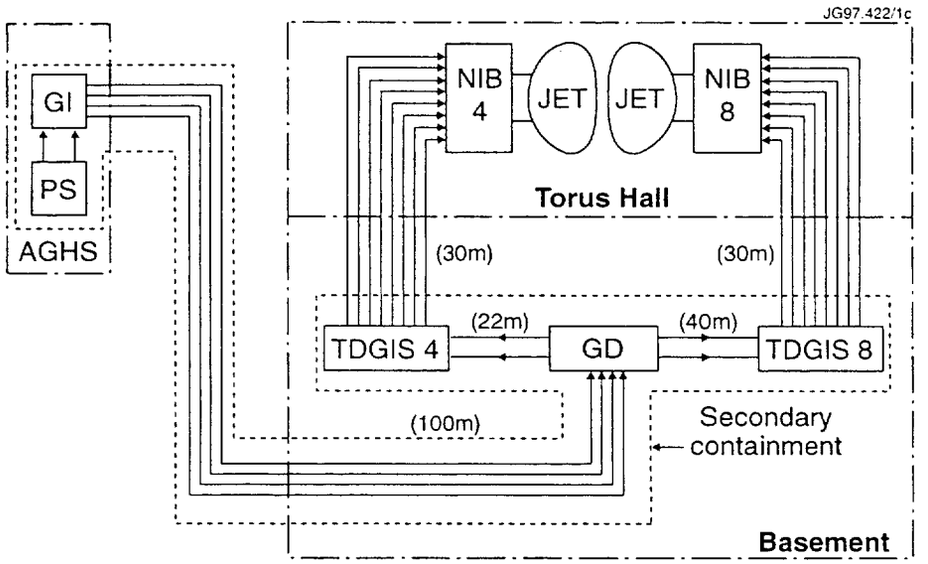

Fig.1: The complete gas system for the Neutral beam Injectors. (Distances in meters are in brackets.)

THE TDGIS

- The system can provide tritium or deuterium to any PINI pairs simultaneously.
- All components are installed inside a secondary containment consisting of a pressure vessel.
- The vessel was built in two parts and can be separated to provide access to the internal components without breaching the primary containment.
- All pipes carrying pressurized gas have a secondary containment.
- The secondary containment is continuously purged with nitrogen. If a tritium leak is detected by Ionisation chambers in the AGHS system, all valves in the GI are closed.
- A stable and reproducible gas flow for the PINIs is achieved using pressure regulators and needle valves.
- In order to prevent gas mixing, the selection valves can not be operated without the pressure in that section being < 1 kPa.

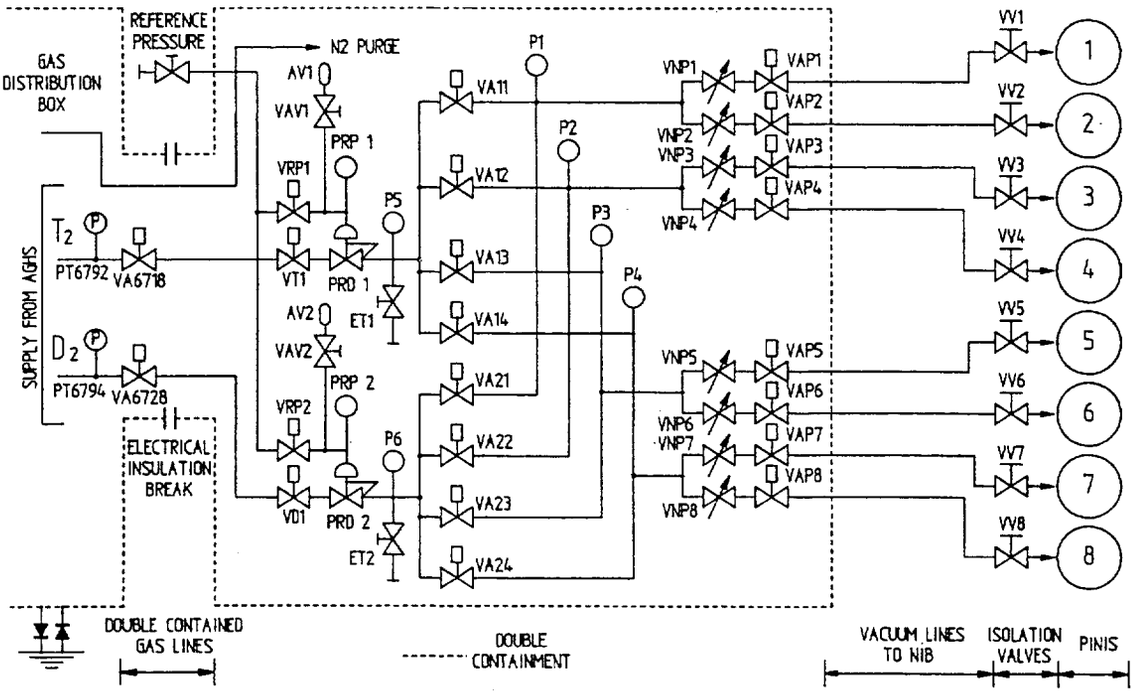

Fig. 2. The Tritium and deuterium gas introduction system.

CONTROL AND INTERLOCKS:

- The set-up program (SCHEDULER) is used to set the parameters and timing for the TDGIS.
- A pre-pulse checking program (NIBLECH) is used to confirm the correct set-up of the whole system.
- The BLIPS program checks the consistency of beam parameters for the selected gas during the pulse.
- There is one interlock key switch for enabling of the system.
- There are also four gas selection key switches to enable tritium, one for each PINI pair.
- The Central Interlock System (CISS) [2] is used to enable the operation of the TDGIS when the Neutral Beam System is in a Normal state. It also switches to Emergency Shutdown if one of the following criteria is met:
  - Either of the valves VRP1 or VRP2 are NOT closed.
  - Either of the reference pressures PRP1 or PRP2 are outside their allowed window.
  - The status signals from the gas selection valves are not correct for the selected gas. The selection of gas is made with the gas selection key switches.
- The Fast Beam Interlock System (FBIS) [3] is used in parallel to CISS and uses the same input signals as CISS for the interlocks. The difference between CISS and FBIS is mainly that FBIS acts within 1 ms, while CISS acts in 125 ms.

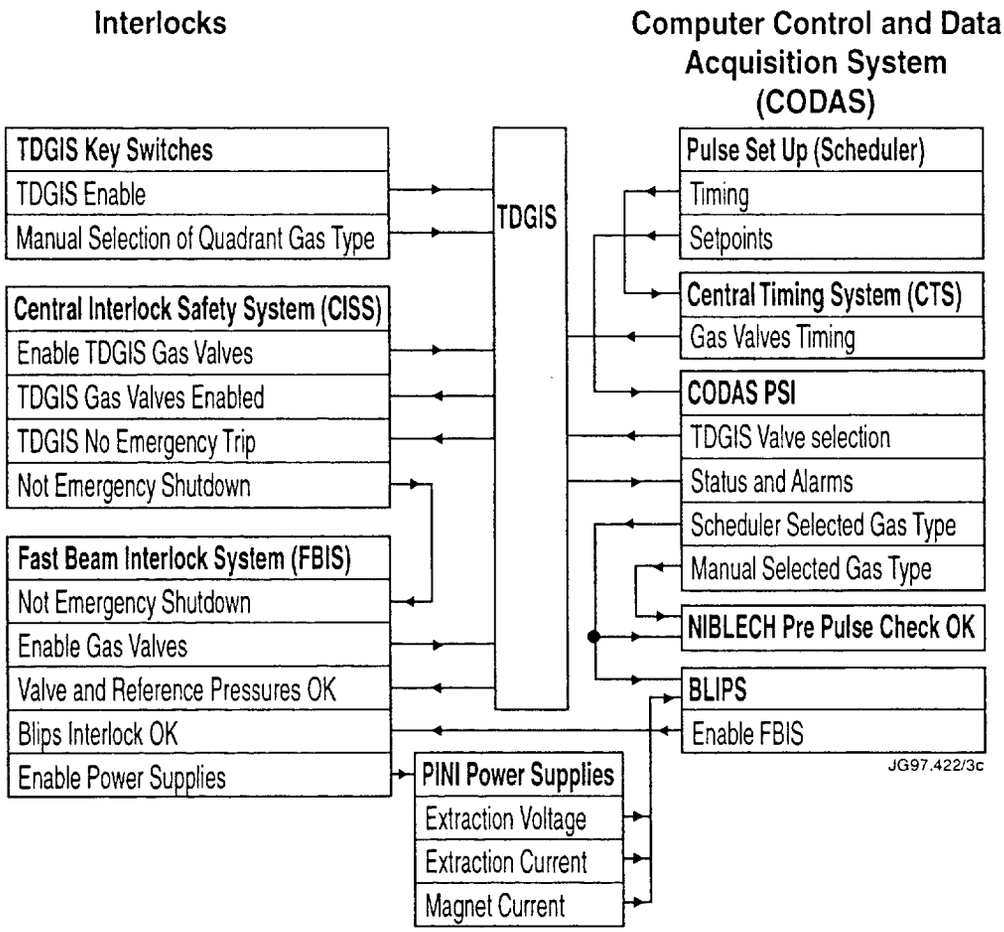

Fig. 3. The Control and Interlocks for the TDGIS

CONSTRUCTION

- The TDGIS was assembled in a clean room. Each component was cleaned to UHV standards and leak tested prior to assembly. Most components were welded together and the weld integrity was checked with radiography. Some components eg. the pressure gauges and the pressure regulators, were connected with UHV approved stainless steel couplings with nickel gaskets.

- The secondary containment for each of the two parts of the TDGIS was constructed as a pressure vessel It was leak tested to 1×10^{-9} mbls^{-1} and pressure tested to 1.1MPa.

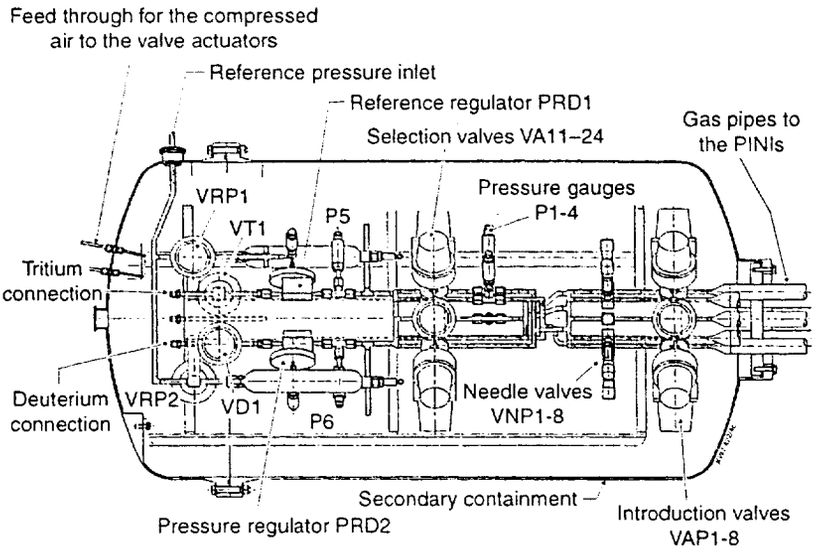

Fig. 4. A cross section of one of the two TDGIS units.

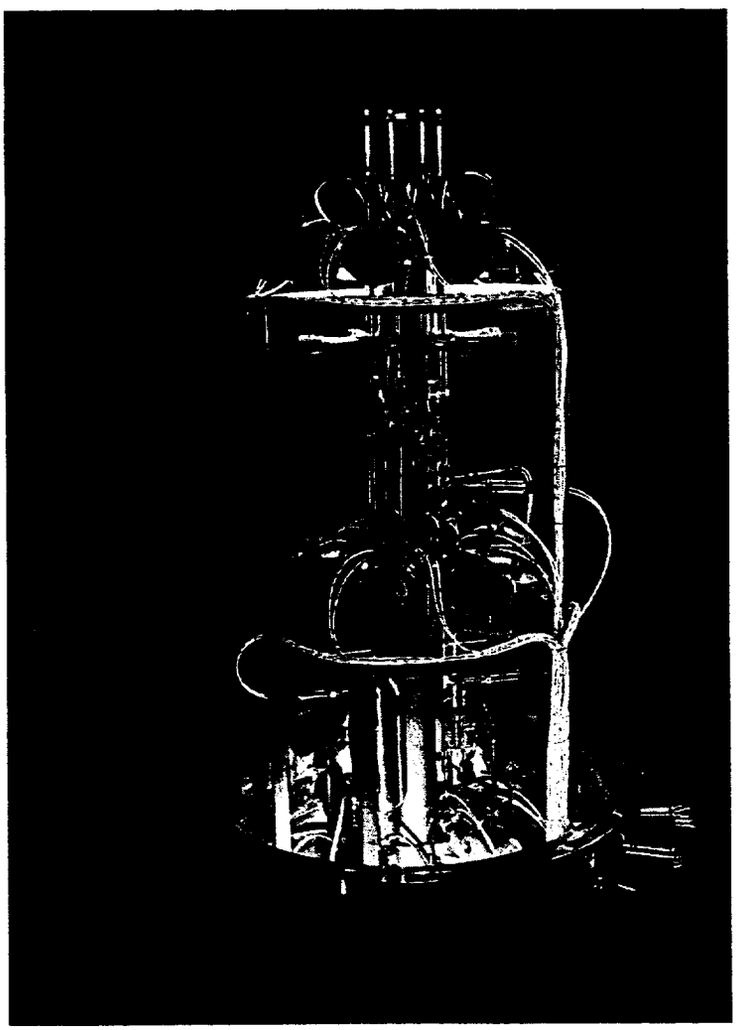

Fig. 5. One of the gas modules during assembly.

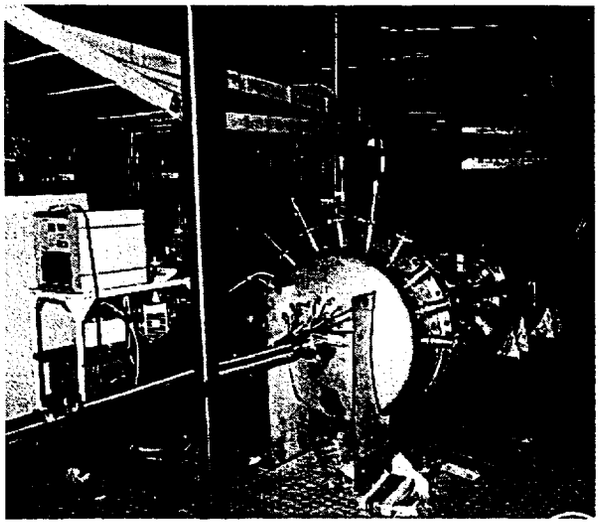

Fig. 6. TDGIS 8 installed. The secondary containment is open.

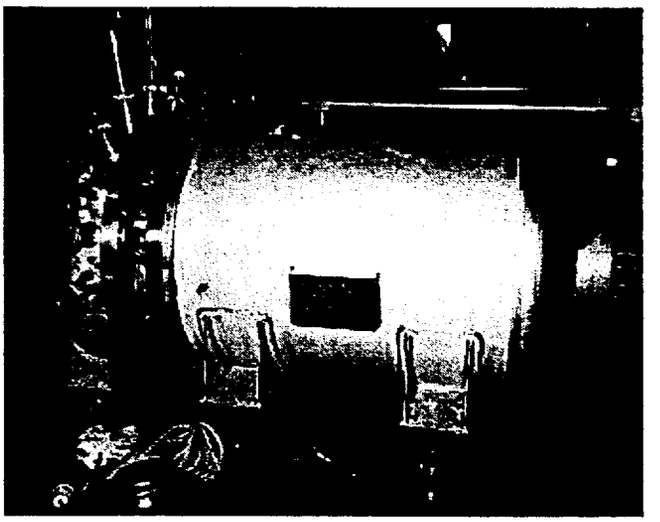

Fig. 7. TDGIS 4 with the secondary containment almost closed.

B Commissioning

The system was run for over two month in deuterium. In this phase we discovered two important things:

- The operation of the High Current 80 kV tetrode PINIs on the Octant 4 NIB had proven to be unexpectedly difficult. The operational window for the gas flow rate was found to be very small. At the low side of the window we noticed gas starvation of the Ion source and on the high side we were limited by high voltage breakdowns. In addition to the operation difficulties the extracted power was decreased with 20 %.
- The all metal seal valves with stellite inserts that were used had started to develop small leaks only after a few hundreds of cycles. All valves were replaced with new ones that had Vespel inserts instead of all metal. Since the replacement with Vespel seated valves, ~ 3000 cycles have been performed supplying gas and no leaks have been detected.

The four bending magnets (one for each PINI pair) [4] for the non neutralized beams interract with each other at high magnetic fields. When deuterium and tritium are used in paralell (but in different PINI pairs), correction factors are used for the magnet currents. These correction factors depend on the extracted voltage and gas for each PINI pair.

OPERATION OF THE TDGIS

The initial operation with the TDGIS was with deuterium. During this phase the PINIs on the octant 8 Injector were conditioned to run reliably between 155 - 160 kV. A period of injection of a mixture of 1% tritium in 99% deuterium then followed.

The conversion to tritium operation on all PINIs was done in three stages:

- The filaments in the ion sources were heated, until no deuterium release was observed. Each filament was heated 3 times for 10 seconds.
- Two 5 second PINI plasma source shots were then done to remove any residual deuterium from the PINIs.

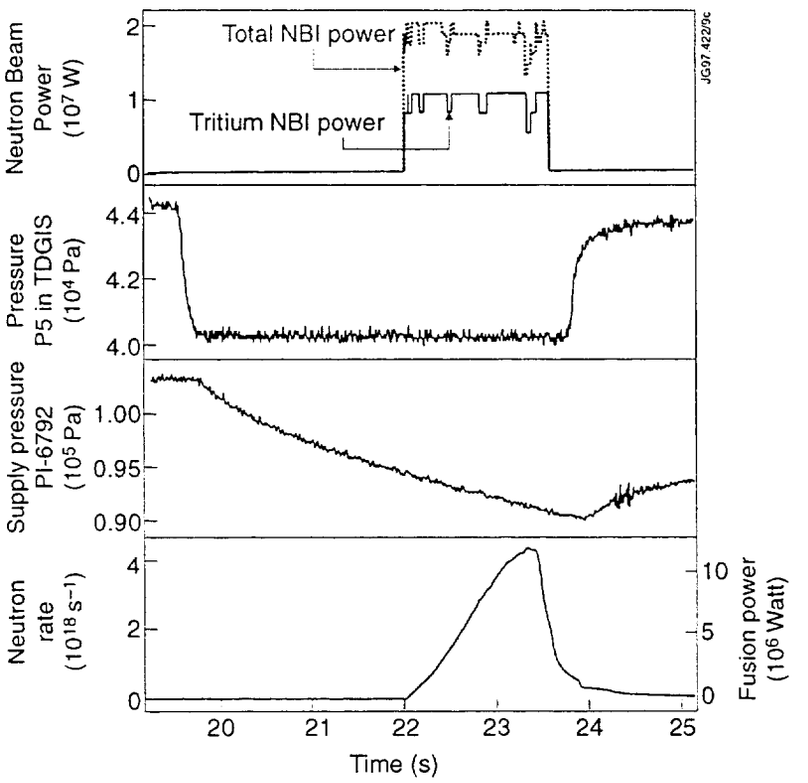

Fig.8: JET Pulse 42676 with 10.6MW of Tritium Beam Injection

- Beams were then produced. In the first pulse the ON-time was 300ms at 120 kV. The beam alignment and Ion dump profiles were checked in this shot. Beam current scans were performed at 120 kV and 150 kV to establish the minimum beam divergence. Approximately 50 tritium pulses were done in Asynchronous mode (beams fired into beam stopping element) before they were injected into JET.

- The safe operating limits were established to be 160 kV for ten seconds for all 8 PINIs but two PINIs were restricted to 150 kV due to problems with conditioning.

A pulse with 10.6MW of tritium beams for 1.6 seconds is shown in Fig 8. The total NBI power was more than 18MW. During the beam extraction the manifold pressure P5 was kept constant by the regulator. The supply pressure can be seen dropping throughout the pulse. The increase in the supply pressure after the pulse was due to the equalisation of the pressure in the 140 meter long pipe between the GI and the TDGIS.

12.9MW of Fusion Power was achieved in this pulse.

REFERENCES

[1] R. Lässer, et. al. "Commissioning tests and enhancements to the JET Active Gas handling Plant, " Proc. 19th Symposium on Fusion technology (SOFT), Lisbon, 1992

[2] H. van der Beken, et. al, J. Fusion Technology, 11 (1987) pp. 126-127.

[3] D.Cooper et.al, J Fusion technology, 11 (1987) vol.2, pp 1096-1100.

[4] G. Duesing, et. al. "Neutral Beam Injection System" J. Fusion Technology, 11 (1987) pp. 163 -180.

The Relation between Halo Currents and Plasma Displacement / Deformation in JET

P Andrew, P Noll, V Riccardo.

JET Joint Undertaking, Abingdon, Oxon, OX14 3EA, UK

I. INTRODUCTION

The disruption of an elongated plasma is generally accompanied by a vertical displacement of the plasma. The vertical displacement can be either the result or the cause of the disruption.

When the plasma collides with the vessel, large currents are observed to flow out of the plasma through the vacuum vessel, and back into the plasma. The halo current transfers the force experienced by the displaced plasma to the vessel. The halo current forces are observed indirectly in two ways:

1) The vacuum vessel is observed to react to forces which cannot be accounted by eddy current forces alone

2) In-vessel components are observed to have experienced large, destructive forces which, again, cannot be accounted by eddy current forces alone.

II. METHOD OF MEASUREMENT

1) Current shunts in mushroom tiles

2) Current shunts in conducting divertor support structure

3) Toroidal field pick-up coils

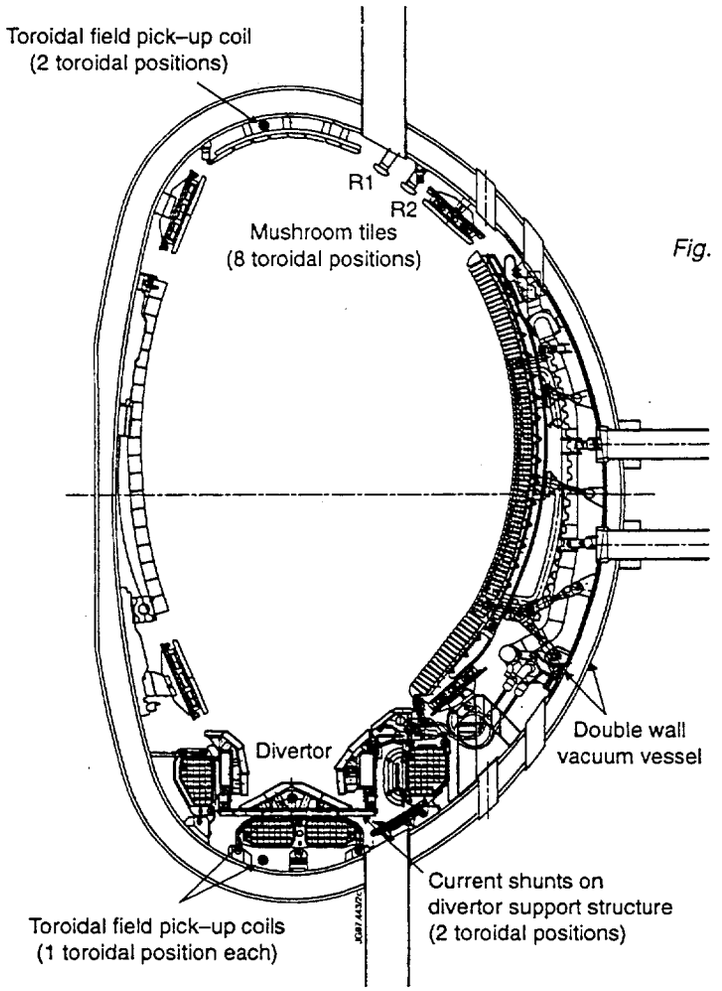

Fig. 1 Cross section of the JET vessel

- JET MKII divertor has 0.6 mΩ toroidal resistance and approximately 0.1 mΩ poloidal resistance (including electrical connection to the vessel via earth straps)
- Graphite tiles are mounted so as not to create an electrical path above the support structure.

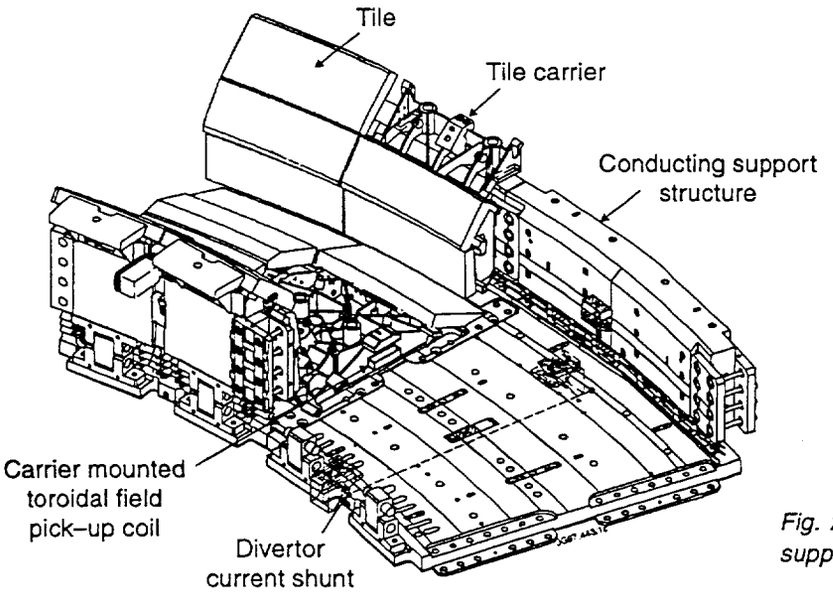

Fig. 2 Segment of the divertor support structure

III. TOTAL HALO CURRENT

- The total poloidal halo current is determined from the measured toroidal field change. Any n=1 component is factored out by using the average of 2 pick-up coil signals for upward disruptions or 2 divertor shunts for downward disruptions.

- The data fall within a limiting envelope, $(I_H)<0.8\ I_{po}/q_{95}$, where I_{po} is the initial plasma current. There are many observations where the halo current is a small fraction of the limiting value.

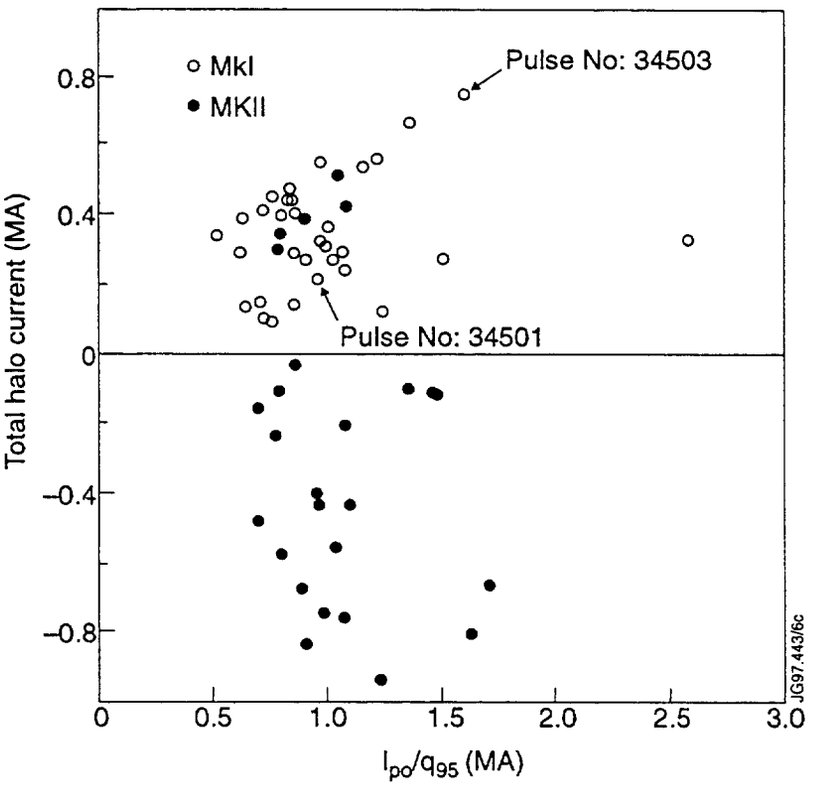

Fig. 3 Peak total halo current measured for the JET MKII divertors. In the MKI campaign, halo current could only be measured for upward displacements. $I_n<o$ signifies a downward disruption.

- Fig. 4a illustrates a disruption where a small plasma current vertical moment ($I_p\Delta z$) is achieved.

- The decay of the plasma current is followed by a loss of vertical position control.

- I_H is observed to be a small fraction 0.074, of the initial plasma current.

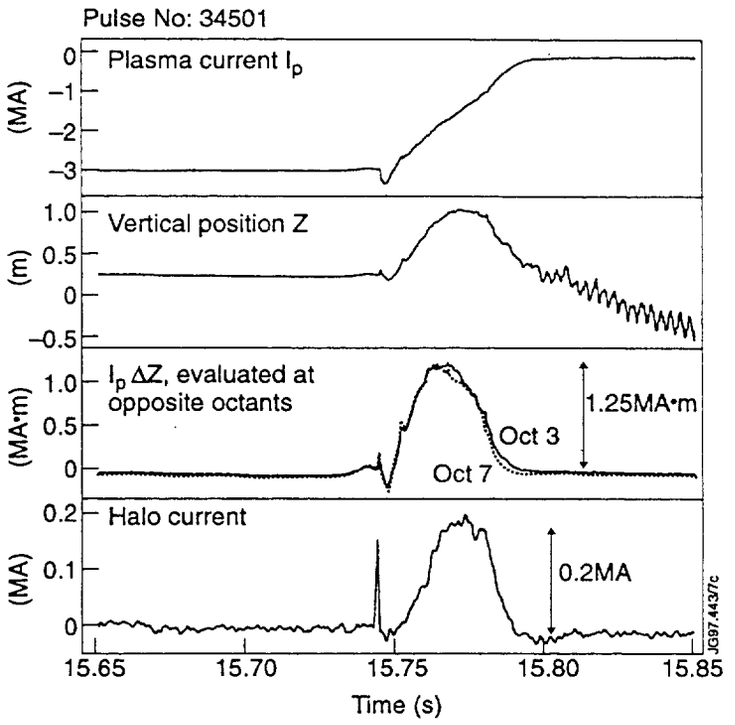

Fig. 4a Disruption with a small vertical current moment

- Fig. 4b illustrates a disruption where a large value of $I_p \Delta z$ is achieved.
- The current decays only after the vertical position has moved ~ 1m from the equilibrium position.
- I_H is observed to be a large fraction 0.19, of the initial plasma current.

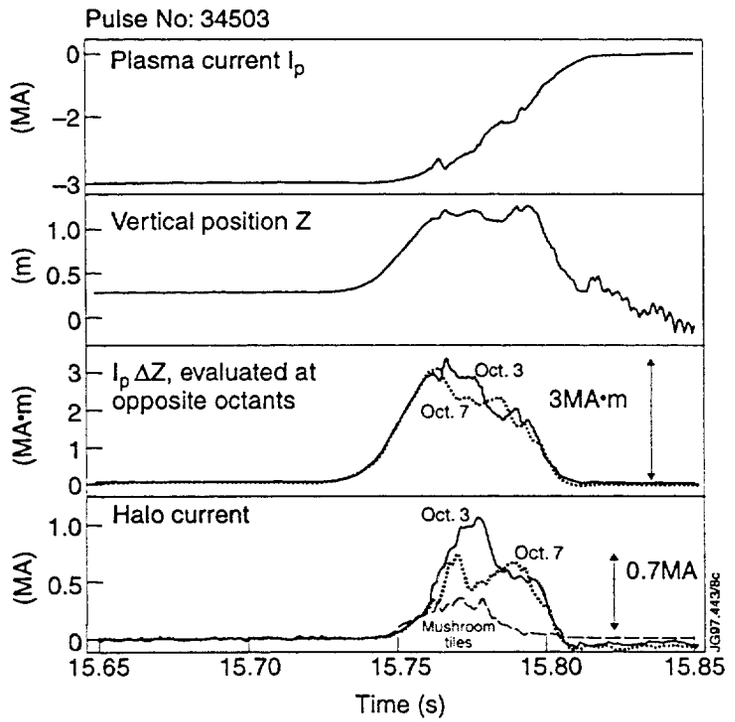

Fig. 4b Disruption with a large vertical current moment

- The role of the plasma current vertical moment is consistent with a force balance model:

halo current force ∝ vertical destabilizing force

$$I_H B_\phi W \propto (I_p \Delta z) I_{po}$$

or

$$I_H \propto (I_p \Delta z) \cdot \frac{I_{po}}{wB_\phi}$$

where w = radial width of halo current recirculation in the vessel

- I_H vs. $I_p \Delta z$ (Fig. 5) gives a tighter grouping of the data.
- The downward disruptions have a larger I_H for a given $I_p \Delta z$. This could be due to
  - i) a large destabilizing force due to the up down asymmetry of the poloidal field coil positions
  - ii) the up/down asymmetry of the first wall
    e.g. relatively narrow throat of divertor could lead to smaller w

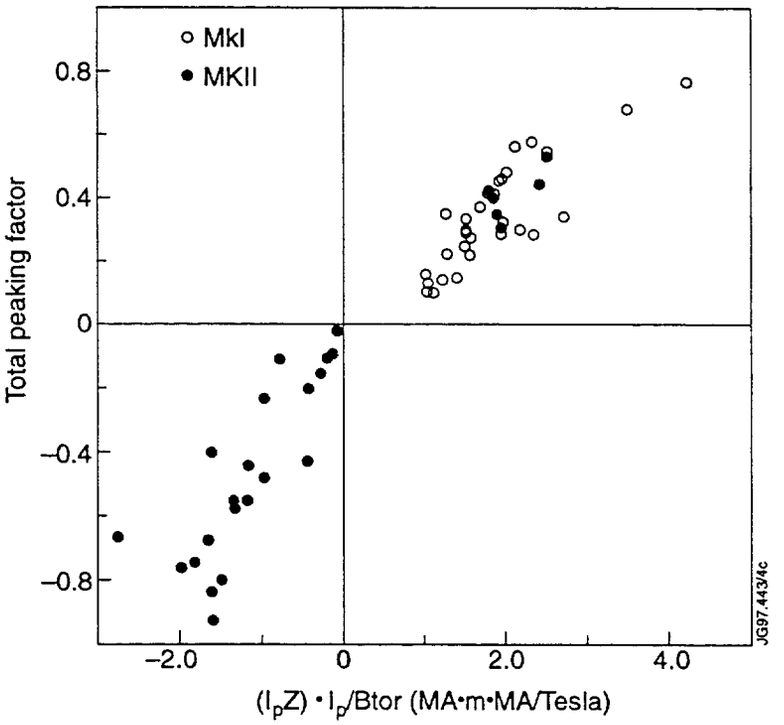

Fig. 5 Peak halo current vs. peak vertical moment

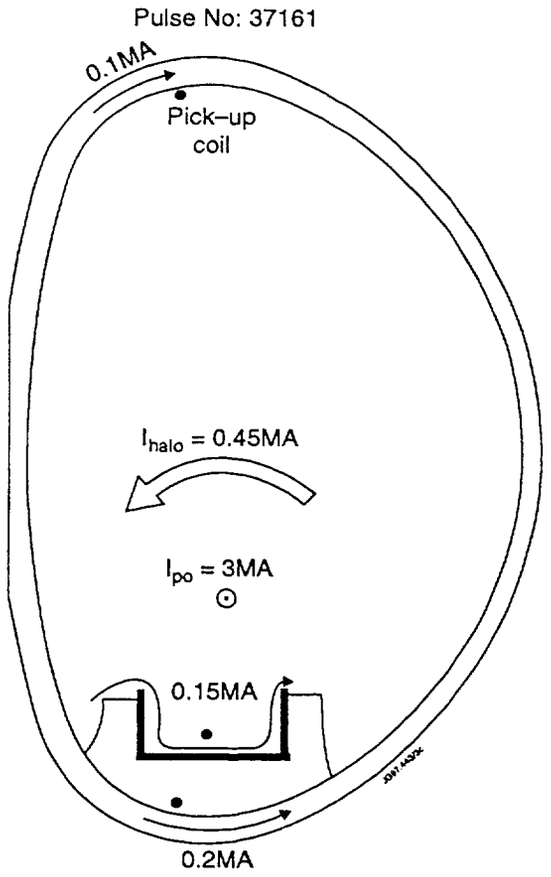

- Fig. 6 illustrates the branching of halo current for a downward disruption. The results are based on measurements from a single octant, scaled up to 360°.

- The sharing of current between the divertor support structure and vessel wall greatly reduces the forces on the divertor.

Fig. 6 Schematic showing the branching of halo current within the vessel components for a downward disruption

- Time traces for this pulse show that the plasma current vertical moment is very similar in opposite octants (typical of downward disruptions).

- The current shunts, however, indicate a departure from toroidal symmetry starting at 11.315 sec.

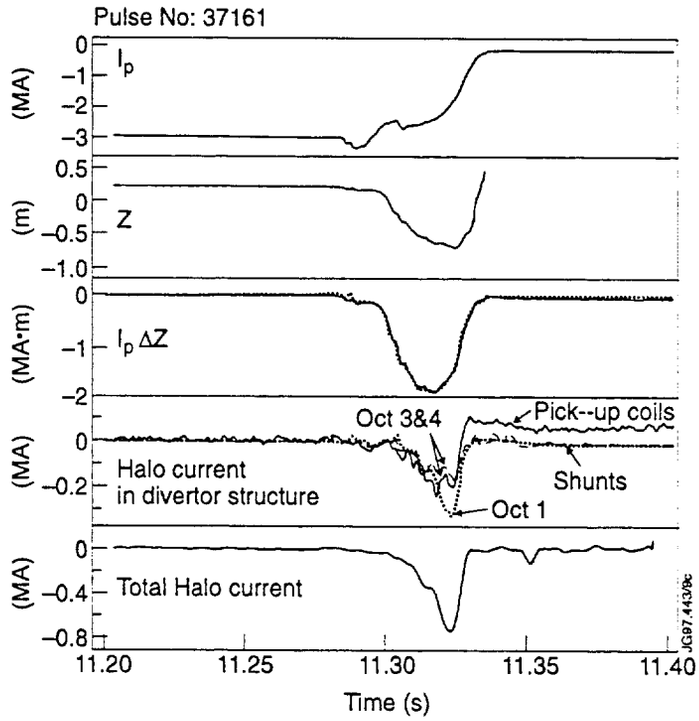

Fig. 7 Disruption following a downward excursion of the vertically unstable plasma

IV. ASYMMETRIES IN THE HALO CURRENT

$$\text{Toroidal Peaking Factor} \equiv \frac{\text{Peak halo current density}}{\text{Toroidally averaged halo current density}}$$

(note: TPF in Fig. 8 evaluated using measurements at only 2 toroidal positions).

- TPF is not observed to decrease with increasing I_H/I_p. This is consistent with the force balance model: if the plasma has poor contact in one toroidal location, the halo current force will have to increase elsewhere to maintain the required total force.

- TPF is smaller, on average, for downward disruptions. Downward disruptions exhibit almost no asymmetry in plasma current vertical moment.

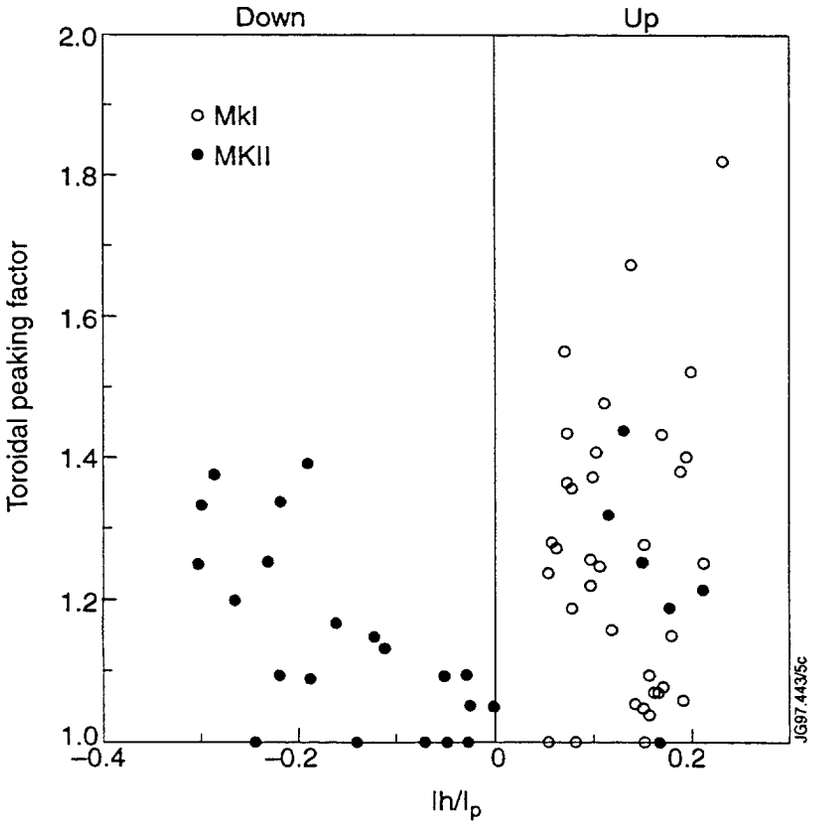

Fig. 8 Toroidal peaking factor, measurement at the peak total halo current.

V. CONCLUSIONS

- The magnitude of the total poloidal halo current is found to be closely related to the value of the plasma current vertical moment achieved during the disruption.

- The halo current density (current per unit toroidal length) is observed to be largest in the cases of toroidally asymmetric halo currents: this is consistent with a force balance model.

- In cases of upward disruptions, the halo current toroidal asymmetry is consistent with the sideways displacement experienced by the vessel. However in downward disruptions, toroidally asymmetric current is also observed to flow in the divertor, but is not accompanied by an asymmetry in the plasma current vertical moment.

Preparations for the Fully Remote Exchange of JET Divertor Modules

A C Rolfe, H Altmann, P Brown, P Carter, R Cusack, P Edwards, A Gaberscik, L Galbiati, B Haist, F Hurd, M Irving, D Locke, R Horn, A Loving, P Martin, S Mills, R Minchin, J Palmer, G Preece, S Sanders, S G Sanders, R Stokes

JET Joint Undertaking, Abingdon, Oxon, OX14 3EA. UK.

ABSTRACT

At the beginning of 1998 it is planned to replace all 144 JET MK II Divertor carrier modules with new modules. This exchange operation will be performed entirely remotely by means of the JET Mascot servo-manipulator transported inside the Torus on the Articulated Boom. The Mascot will deploy specially designed tooling to handle modules to and from their torus location and will transport them to and from a separate transfer system interfacing between the inside and outside of the torus.

This paper describes the preparations being made for this first fully remote handling shutdown for JET.

INTRODUCTION

The 1997 JET operations include a 3 month campaign of DT experiments (DTE1) which result in a significant increase in the in-vessel dose rate to a level which renders the in-vessel inaccessible to personnel for anything other than the most brief tasks for around one year.

The JET Divertor study programme requires that immediately after DTE1 the MkIIa divertor should be replaced with the MkIIGB divertor. Accordingly preparations are being made to undertake this work using fully remote handling techniques. This will be the first remote handling shutdown of the JET programme.

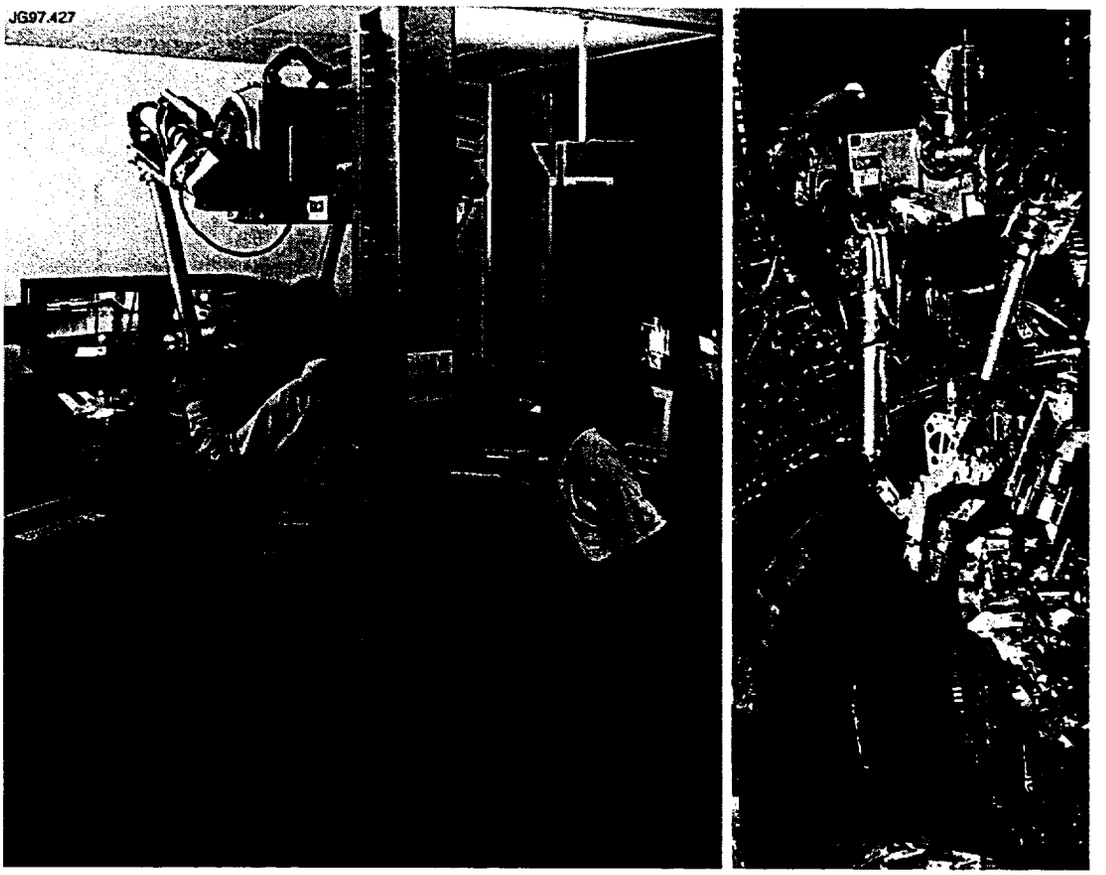

OVERVIEW OF THE OPERATIONAL SCENARIO

It is required to remove 144 MkIIa divertor modules and to replace them with 192 MkIIGB divertor modules. In addition it is required to clean four Beryllium evaporators, vacuum clean the divertor region, replace a number of small diagnostic components, inspect the First Wall tiles and undertake a 3-dimensional survey of the Divertor structure using Videogrammetry techniques.

All in-vessel work will be done fully remotely by means of the Mascot servo-manipulator transported into the torus on the JET Articulated Boom. All other equipment required inside the torus will be transferred through an opposite port using a special handling device. After removal the MkIIa divertor modules will be stored on trolleys within removable ISO cabins.

The dose rates expected to prevail in areas outside the torus vacuum vessel fall rapidly to levels which allow 95% of all ex-vessel work to be performed manually. The only exception to this is the handling and storage of activated MkIIa modules removed from the torus which require the use of fully remote handling transfer to shielded storage cabins.

During the entire shutdown period the torus and the attached operational areas will be purged with air and maintained at a depression relative to the surrounding Torus Hall for contamination control.

DIVERTOR DESIGN

The MkII Divertor was designed to facilitate an exchange in an activated environment by remote handling.

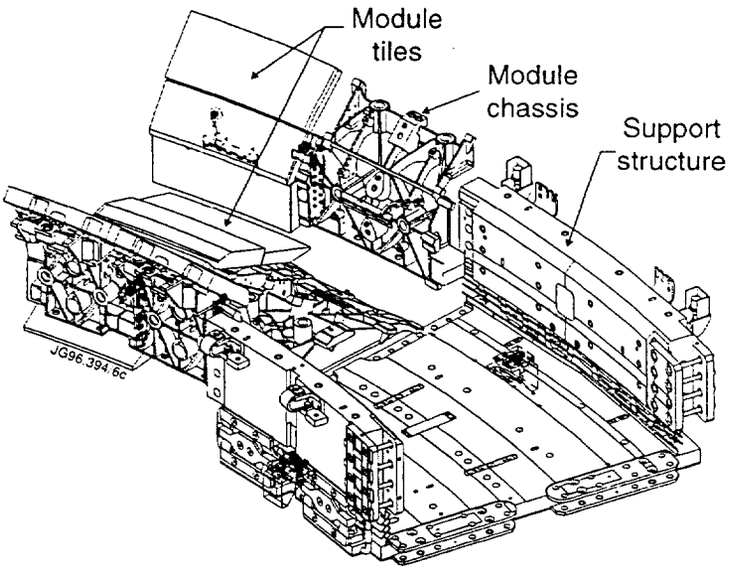

The design is based on a solid "U" shaped water cooled ring-structure which serves as a support to which Divertor modules are bolted. The ring-structure incorporates dowel slots to ensure the precise alignment of modules as well as serving to cool the target tiles by radiation. It also incorporates pre-wired electrical sockets into which diagnostics attached to the Divertor modules can be remotely plugged. The first set of modules installed in the Mark II structure, the Mark IIa Divertor, are designed with large carbon fibre reinforced carbon composite (CFC) tiles supported by accurately machined Inconel modules with the tile corner supports shared between adjacent modules. The precise tile alignment thus achievable is dependent only on the accuracy of the tile machining (±0.05mm).

The Divertor target tiles are fixed to the module structure by locating dowels and spring loaded bolts. The material strength across the fibre direction is enhanced with tie rods in tension to avoid crack initiation and also to ensure that in the very rare circumstance of a tile cracking no parts will fall off the modules.

Diagnostic sensors are attached either on to the modules themselves or directly to a remote handling compatible plug.

The Divertor modules have features incorporated which make them compatible with the remote handling tools. The captive bolt assemblies float within the modules to prevent side loads on the bolts and thereby minimise the risk of seizure during operation. In the unlikely event that they become damaged both the bolts and the aluminium bronze nuts to which they attach are remotely replaceable.

REMOTE HANDLING EQUIPMENT

The general philosophy for remote handling at JET has been to develop a flexible system based on a man-in-the-loop control strategy able to be deployed to undertake any one of a large number of potential remote repair type tasks. This approach has resulted in a system which has been able to be readily adapted for application to this new task.

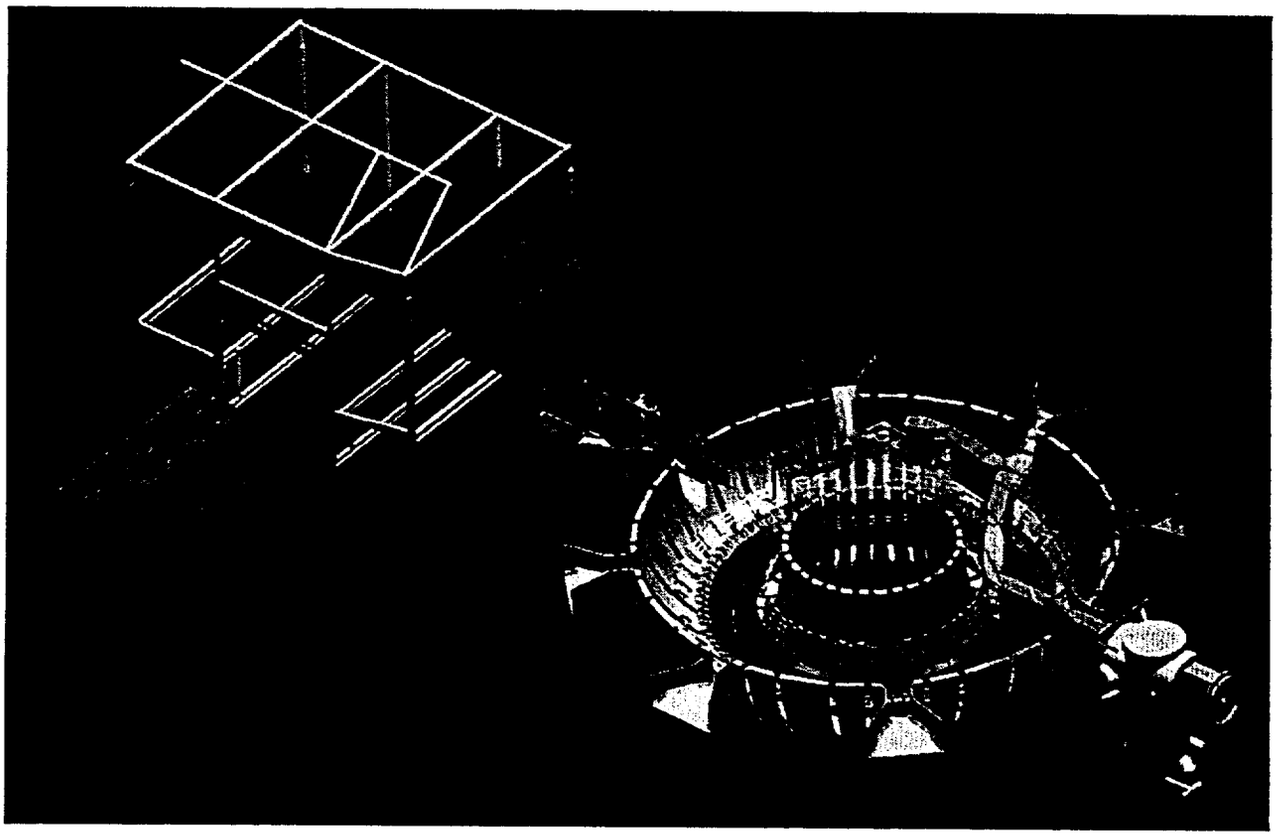

The Articulated Boom is housed within a contamination control enclosure which will be sealed to the torus. The Boom has one camera mounted on a 1m long robotic arm. The Mascot servomanipulator is configured with two wrist cameras and one pan/tilt camera. General purpose viewing in-vessel will be by means of four pan/tilt camera units and two miniature mobile cameras. Also available is a 50kg winch mounted between the Mascot shoulders.

The Tile Carrier Transfer Facility (TCTF) enclosure is sealed to the torus and the storage ISO cabins are sealed to the TCTF enclosure by means of a large double door system designed and developed for this shutdown.

DIVERTOR MODULE REMOTE HANDLING TOOLS

A concept for handling of the Divertor modules was derived to satisfy the objectives of minimising the complexity of the tasks whilst maximising the safety and speed of operation. This was achieved by designing handling tools which deskilled the repetitive tasks by transferring the high risk module alignment control to the tools themselves.

The gaps between the adjacent tiles can be as small as 1.4mm and it is crucial that installation or removal be achieved without damage to the sharp tile edges.

The handling tools form the interface between the Mascot and the Divertor modules and their primary function is to support the weight of the modules and transport them within the torus. They also provide a means of handling that prevents damage to the critical edges of the tiles and guidance for the hexagonal keys which must pass between the tiles to reach the module fixing bolts.

The interlocking design of the MkIIa Divertor requires the installation of modules between two other previously installed modules. This is safely achieved by leaving the module handling tools attached to the two already installed modules during the fitting of the third module which enables features on them to be used as accurate guides for the handling tool on the third module. Once these guide features are interlocked it is impossible for the modules to collide. The same handling concept is used during module removal.

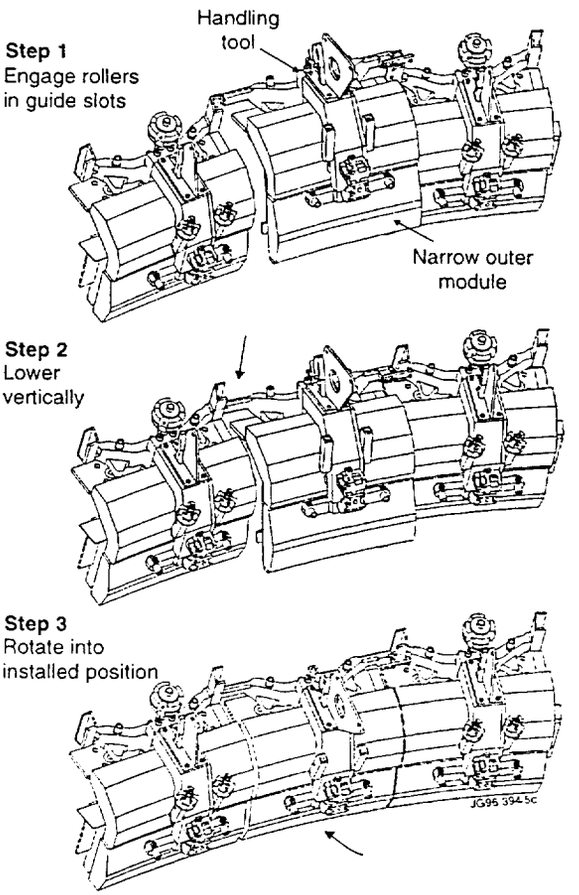

Divertor module fixing bolts are driven with hexagonal keys which locate in guides on the handling tools. Bolting operations are performed with tools directly operated using Mascot. A ratchet driver is used to run the bolts in "finger tight". Using alternate grasping features it can also be used for unbolting. It employs virtually friction free roller clutches so that it works even when the bolt is very loose.

OPERATIONAL PREPARATIONS

Reliability and Response to Faults

Fault reporting and fault isolation procedures are vital to the maximisation of overall Availability. A formal Fault Recording and Corrective Action System has been in operation at JET since 1994. The system provides operators with facilities to record details and actions taken for each fault. A systematic process of weekly fault report review and action has resulted in an environment of continuous development and reliability improvement.

Equipment Maintenance and Support

An essential element in the management of operations is the efficient isolation and repair of faults. A strategy for fault isolation has been adopted which creates a hierarchy of corrective actions that personnel of different skill levels are allowed to perform. Detailed instructions have been produced for the operators and if these do not correct a fault then a trained maintenance specialist and finally the engineer responsible for the design of the equipment are called in.

Equipment Recovery from Failure

A fail safe and fail recoverable policy has been applied to all aspects of JET remote handling equipment design. In the case of a failure of parts of the remote handling equipment that will operate within the torus, methods have been devised to withdraw the equipment from the torus for repair. In the worst case it may be necessary to deploy ex-vessel remote handling equipment into the torus through a second port to render the equipment into a recoverable state.

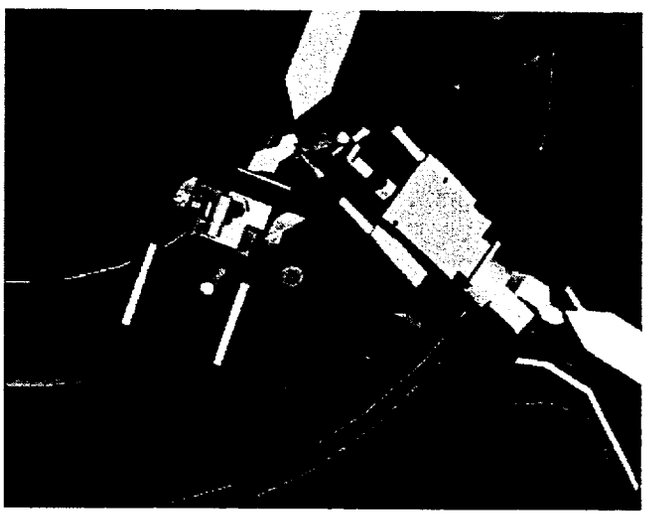

Contingencies for Unplanned Events

Considerable effort and resources have been invested in making contingency provisions for dealing with unplanned events. All of the divertor modules have been designed to enable their handling even if the tiles are cracked or broken, if the bolts fixing the module to the support structure are seized or if the primary attachment points for the handling tools to the modules is obstructed. In the event that it is required to undertake tasks as a result of failures for which no specific preparations have been made the problem will be tackled making use of the inherent adaptability of the remote handling equipment and operations facility to implement the task as if it were being done by hand.

OPERATIONAL TRIALS

Mock-up Programme

Many years of manual shutdown experience at JET has shown that to ensure efficient in-vessel work it is essential to comprehensively prepare procedures and train operators using full scale mock-ups. This is even more relevant for remote handling tasks where unexpected procedural problems can cause severe delays. This has been fulfilled by constructing a full size mock-up using dimensional information taken from the tokamak "as-built" metrological surveys and by deploying the real remote handling equipment for handling trials.

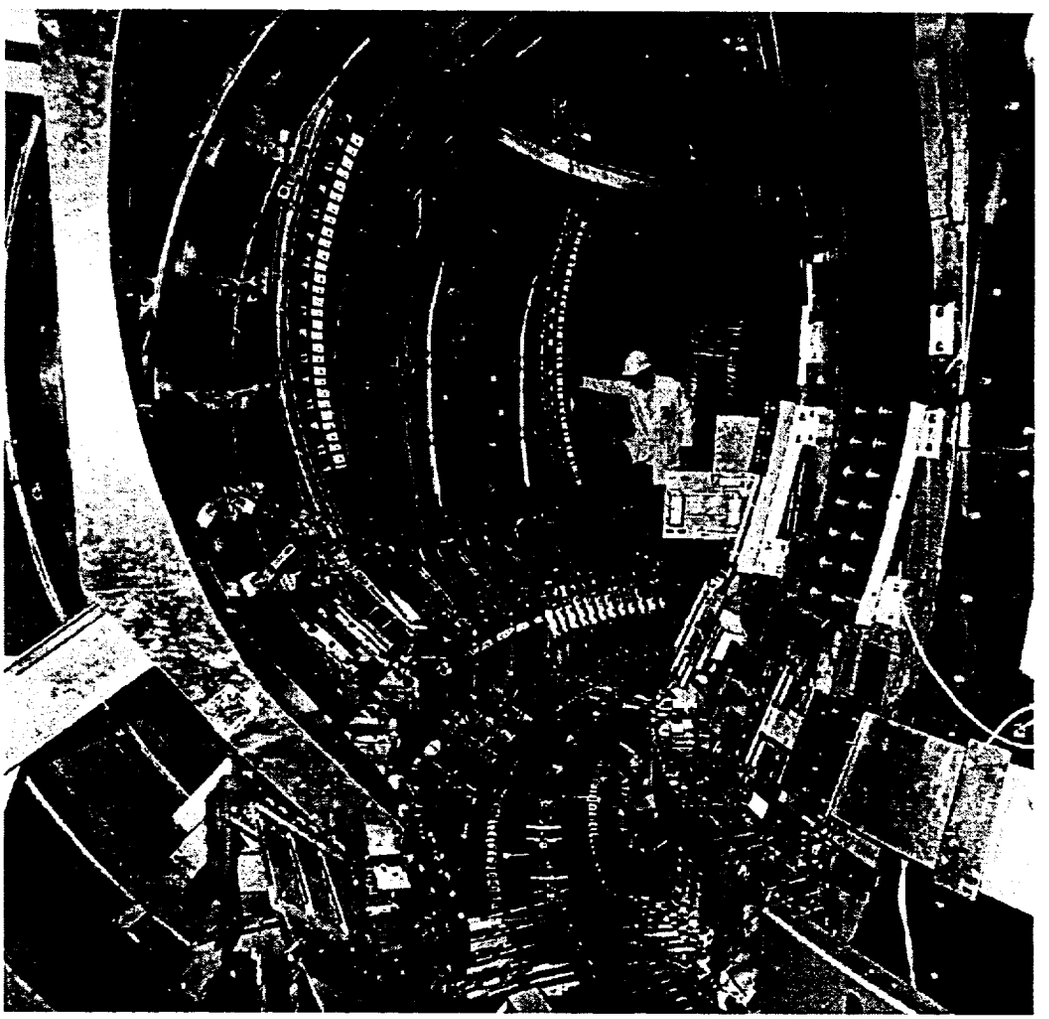

Extensive mock-up operations have already taken place and all required tasks have been proven to be feasible. The final shutdown preparations phase is now using the mock-up facility for procedural validation, operator training and rehearsal.

JET Torus Trials

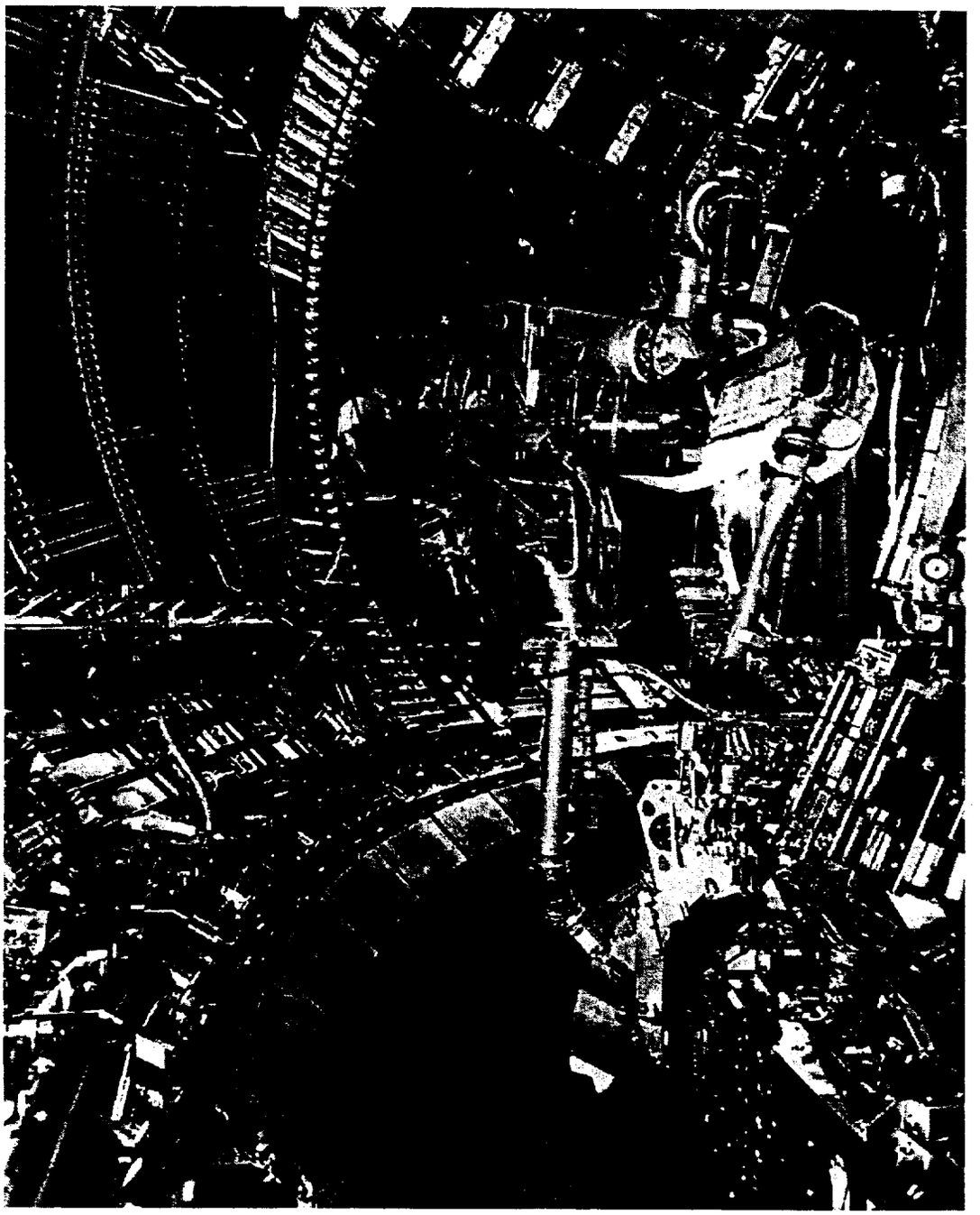

In order to prove that preparations made by use of the full scale mock-up facility are valid when transferred to the actual torus, the opportunity was taken during the MkIIa Divertor first installation shutdown to install 33 divertor modules by fully remote handling inside the real torus.

Engineering a Remote Survey of JET's Divertor Structure under Conditions of Restricted Access using Digital Photogrammetry

B Macklin, R Brade, F Hurd, S F Mills, S Sanders, R Stokes, J Tait.

JET Joint Undertaking, Abingdon, Oxon, OX14 3EA, UK.

INTRODUCTION

JET is currently planning to install its new Gasbox Divertor remotely. In line with JET's policy and philosophy it was decided to survey the divertor structure remotely to confirm its position, shape and integrity prior to installing the new tile configuration. A remote survey to metrology standards is required i.e. with sub-millimetric accuracy. While remote surveys have been carried out in the past, they have not been to this level of accuracy.

I. MKII DIVERTOR SUPPORT STRUCTURE

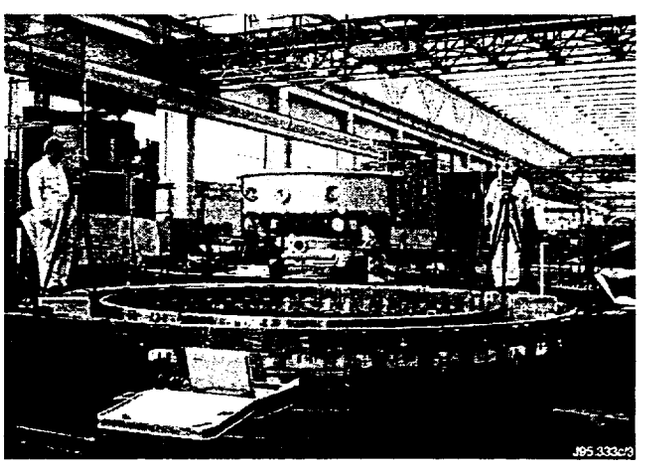

Fig.1 Divertor structure being surveyed during manufacture

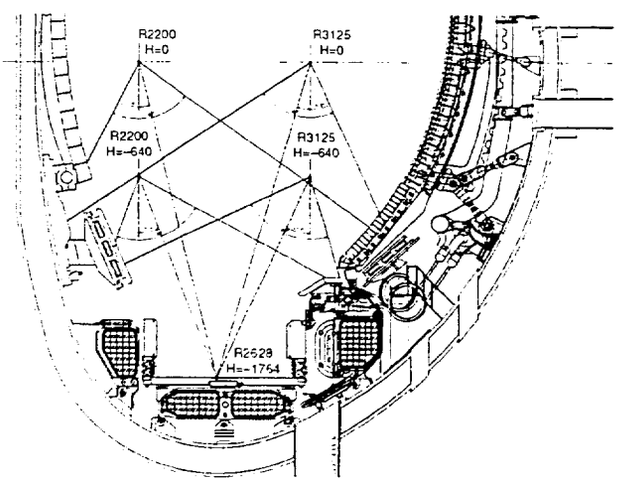

Fig. 2 Typical camera positions and orientation.

Design and Installation

The water cooled support structure, comprising twenty-four modules, is the main component of the JET MKII divertor system [1]. The inconel support structure was manufactured as twenty four sub assemblies which were assembled together once inside the vacuum vessel. JET's CAT (Computer Aided Theodolite) system was used to check the large fixture used for the final machining and assembly sequences of the structure at the manufacturers. The CAT system was also used in-vessel to ensure the accurate installation and positioning of the structure with respect to the magnetic centre of the machine [3]. The tile carriers, which are fully remote handleable, are designed as a lightweight and rigid structure, holding tiles and diagnostics.

MKIIGB Divertor

The existing MKII Divertor structure will be the support for the MKIIGB Divertor. As the structure had already been accurately manufactured and installed in-vessel it seemed that no surveying should be required during the installation of the MKIIGB. However, it was considered prudent to plan to confirm the integrity of the structure after the removal of the MKIIA tile system. There are a number of highly stressed components which position the structure. As many of these components are not directly visible, even with manned access, surveying the structure to confirm its shape and position is now considered to be essential.

II. SURVEY SYSTEM SELECTION

When the need for a remote survey inside the vacuum vessel was identified, a study of systems available on the market was undertaken. The criteria for system selection were that the system:

1. **Could be operated remotely and used with JET's remote handling articulated boom [7].**
2. **Should be suitable for use without targets, to provide sub-millimetric accuracy**
3. **Should be suitable for use in the multiple set-up format required by JET's difficult geometry.**
4. **Provide data, via existing internal wiring of articulated boom, in an easy to use format, compatible with JET's existing survey systems.**
5. **Be fully commercially available.**

Many potentially suitable systems were found, most of which are based on some form of laser scanning. However, these were still at the prototype stage and not yet capable of meeting the accuracy and other requirements.

Digital Photogrammetry

Finally it was decided that a digital photogrammetry system called V-stars [6] was the most suitable.

- Photogrammetry is a technique with which JET already has some experience, mainly in the form of film-based convergent photogrammetry.
- Digital photogrammetry is based on the same principles but uses a CCD camera instead of the film-based camera. JET's experience with optical systems and photogrammetry meant that a good assessment of the suitability of digital photogrammetry could be made.
- V-stars uses a six million pixel camera called INCA (Intelligent Camera), which has a built-in 486 chip for pre-processing of data. This means that the camera can communicate as a computer via an ethernet link.
- Although V-stars is not a targetless system, the contract survey company ESIC, which had previously carried out photogrammetry surveys at JET, have developed software called SCANTIF which allows features e.g. holes, corners, edges of components to be selected with the cursor on-screen.
- Provided the camera positions are known accurately and the same feature can be seen in two or more pictures the software will determine the co-ordinates of the feature by triangulation from the known camera positions.

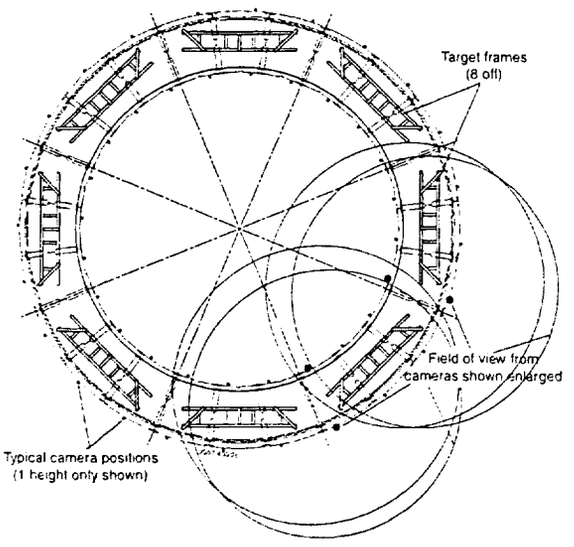

Fig. 3 Layout of Target Frames on Divertor Structure.

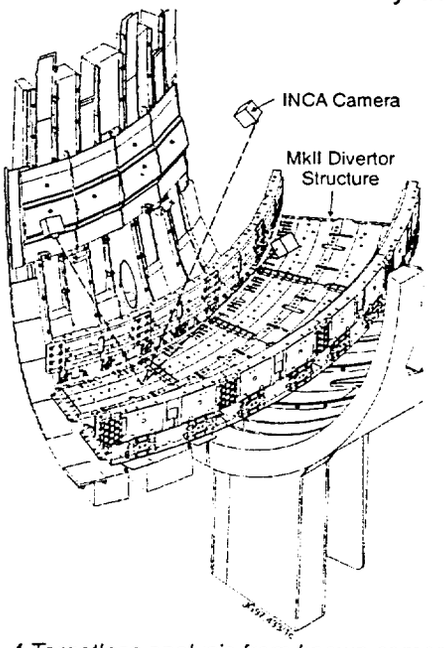

Fig. 4 Targetless analysis from known camera positions

V-stars output data is fully compatible with the Leica systems and software already used extensively at JET [2,3,4]. This compatibility capitalised on the experience and familiarity of the operators with existing manipulative software. It also allowed the protocols which had been developed for the two-way flow of information with JET's CAD system to continue. Digital photogrammetry was seen as the natural evolution of the systems and techniques already employed at JET and has the advantage of being suitable for use in conjunction with these systems on other increasingly important ex-vessel applications.

III. SURVEY CONCEPT

- To determine the co-ordinates of untargeted features it is essential that the camera positions are known as accurately as possible. This requires the use of retro-reflective targets. However, it was clear that it would not be practical to install several hundred individual targets remotely.
- Instead, it was decided to design a three dimensional frame which could be fitted with targets ex-vessel. The complete frame could then be installed in-vessel using the remote articulated boom.
- Eight frames were envisaged which would provide a network of targets to be used to determine the camera positions.
- A number of prototype frames were manufactured and used to optimise the frame geometry and to develop a preliminary survey technique, bearing in mind that the camera positions would have to be achieved with the camera mounted on the articulated boom.
- Survey results and techniques were validated by comparing with JET's CAT system
- It was decided to exploit the frame design further by designing it to locate on the baseplate and radially on the outer ring of the structure. When the target co-ordinates and, therefore, the frame positions have been determined, the shape and position of the outer ring and the height and level of the baseplate can be established relatively quickly.
- Targetless analysis, which is relatively tedious, will only be required to yield the shape and position of the inner ring and information which may be required about specific features e.g. to check the fishplates for deformation.

IV. VESSEL DATUM SYSTEM

- In order to compare the position of the divertor structure with its installed position, the photogrammetry survey must refer to the datum system used during the installation i.e. the vacuum vessel datum system.
- The vacuum vessel datum system consists of a series of bosses welded to the vacuum vessel wall. These bosses are fitted with targets during shutdowns to allow survey data to be referenced to the machine datum system, which is concentric with the magnetic centre of JET.
- The datum system was originally established by surveying with the CAT system and was first used for the installation of the MKI Divertor and associated components [2]. The datum system has been periodically resurveyed since.
- In preparation for the remote survey of the divertor, the vacuum vessel datum system target bosses were fitted with permanent targets.
- These targets will be selected during survey analysis using the Scantif software and will allow the divertor position to be determined with respect to the vacuum vessel datum system. This position can then be compared with the original installation position and allows an assessment to be made of the status of the structure.

V. TARGET FRAME DESIGN

- The target frame was designed to have three dimensional geometry appropriate to the survey.
- The frame had to fit through the main horizontal port of the vacuum vessel, which imposed the maximum cross sectional dimensions of the frame. The distance from the outer to the inner wall of the vacuum vessel determined the maximum length. The frame was designed to be as light as possible.
- The frame was equipped with the necessary features to allow it to be handled by the mascot on the remote articulated boom.
- It was fitted with machined feet to allow it to sit on the machined surface of the divertor structure, while tooling balls and a locking mechanism ensured radial location against the outer ring of the divertor structure.
- Finally each frame was equipped with an invar strip to provide a scale independent of temperature.

VI. REMOTE HANDLING TRIALS

JET's remote articulated boom is 10 meters long, with 19 degrees of freedom and is fitted with the Mascot servo-manipulator which provides the 'arms' for carrying out manipulative tasks. It is an extremely sophisticated tool and has the capability to operate on the basis of 'teach and repeat' files. Accordingly, JET's In-vessel Training Facility (IVTF), a mock-up of the interior of the vacuum vessel, was upgraded and used to practise and develop all of the handling techniques for all components. It was also used to train personnel and ultimately to generate the teach files. Preparation for the remote survey was included in this extensive programme of work.

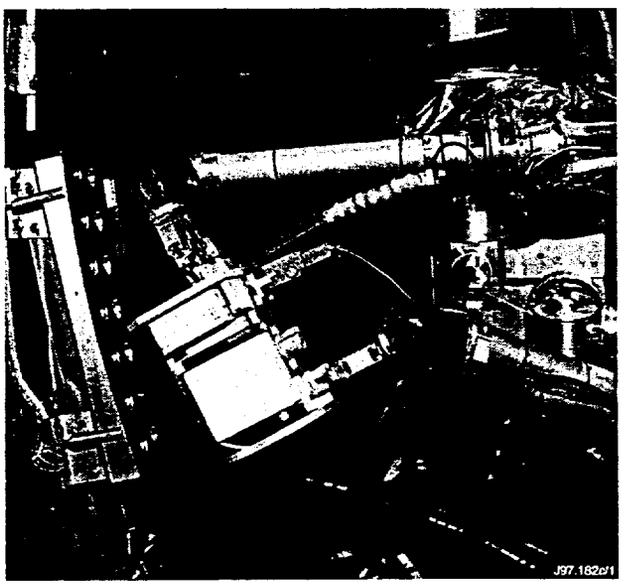

Fig. 5 Handling the INCA camera.

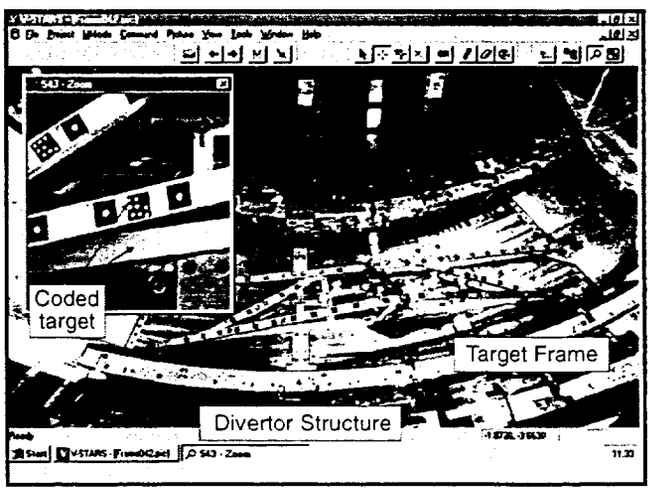

Fig. 6 Analysis of digital images.

Target Frame Handling

- A campaign of development and extensive handling trials was undertaken in the IVTF to establish and develop the techniques necessary to handle the target frames.
- Initial work was done using prototype target frames.
- The frame design was upgraded to reflect the requirements of the remote handling team after the initial trials. Changes included extra gripping features and an attachment point for a safety lanyard. It was also found that the frame length could be extended.

Camera Handling

Having established desirable camera positions from a survey geometry point of view, it was necessary to develop the handling of the camera with the boom and mascot to achieve these positions. A frame fitted with mascot grip features and into which the camera could be locked was designed. The camera frame provided a degree of additional protection for the camera and included a socket which allowed electrical connections to the boom to be made with remote-handling plugs on a flying lead.

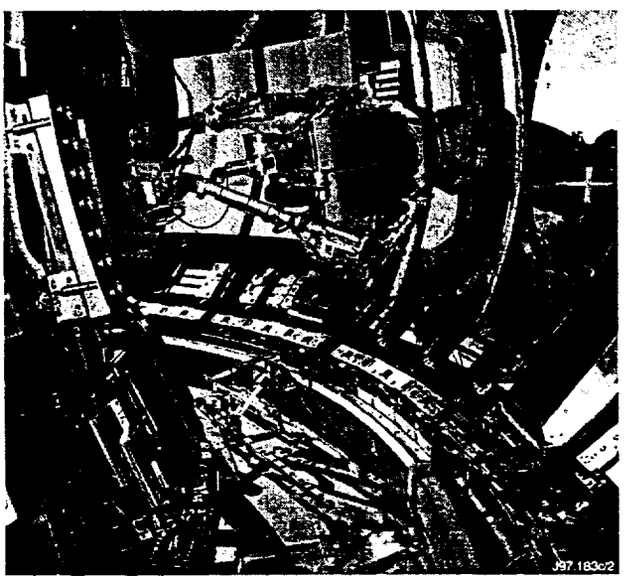

Fig. 7 Target frames in use during trials in IVTF

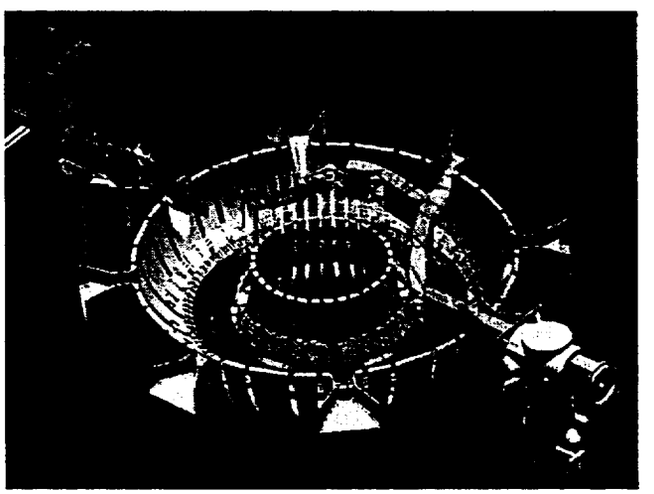

Fig.8 KISMET being used to develop boom manoeuvres.

- Initially the concept for camera handling was developed on KISMET (virtual reality software for planning boom manoeuvres). The challenge was to exploit the enormous flexibility of the boom/Mascot to achieve around on hundred camera positions reasonably accurately (±20mm) in the shortest possible time.
- The detailed preparation paid dividends as for most octants the desired camera positions were achieved relatively easily when the remote trials began. In fact, only the generic position had to be achieved and this was then copied for the other octants.
- Octant five, however posed difficulties as this is the octant where the boom enters the vacuum vessel. To achieve the desired camera positions entailed doubling the boom back on itself. A significant proportion of the development time available was spent on this task.
- Testing of electrical connections through the remote handling boom, data download to the control room and the remote survey concept for three octants took place during this period. Suitable camera parameters for shutter speed and flash were selected at this stage. This was the first opportunity to assess the stability of the boom, which proved to be excellent.

VII. DATA PROCESSING

Determination of Camera Position using Coded Targets

- When digital photogrammetry was selected for JET, and indeed during the one month evaluation phase, it was necessary to manually select every retro-reflective target on-screen during processing.
- The software automatically selected the target centre which was then manually assigned a pre-determined label to identify that target during processing. This was a total of approximately five thousand manual selections. Subsequently, this process has been completely automated with the introduction of coded targets which allows automatic selection and unique identification of the targets.
- A minimum of six coded targets on a component allows the other standard targets on the component to be assigned a temporary label. These same targets can then be identified in the next photograph.
- For the survey to be undertaken at JET, use of coded targets reduced the processing time from about forty hours to eight hours.
- Analysis time is critical as survey results will be required before the installation of the new Gasbox tile carriers.
- The coded target technology also allows a first iteration at solving the survey calculations using about one tenth of the total number of targets i.e. the 'circle' is closed much sooner. This leads to a stronger solution with fewer iterations.

Targetless Analysis of Divertor Structure

- Preliminary trials with targetless analysis showed that accuracy of ±0.35mm is achievable. This compares to an accuracy for the targets on the frames of ±0.05mm to ±0.15mm.
- This needs to be qualified further in the context of the complete survey of the divertor structure, and in particular for the specific features to be analysed.
- An inspection schedule for the structure has been prepared, which defines the specific elements of the structure which must be analysed.
- This is extremely important in order to ensure that a satisfactory engineering appraisal of the structure is carried out. It also ensures that the analysis work will proceed quickly and efficiently, as personnel involved will be prepared and practised, and the maximum amount of information can be extracted from each picture in a single visit.

VIII. CONCLUSION

Special survey methods and data handling techniques have been developed over recent years to suit JET's particular geometry, difficult working conditions and unusual engineering requirements. The planned remote application of targetless digital photogrammetry during the first full remote handling intervention at JET will mark the achievement of the most challenging survey project to date. The problem of lack of access to carry out detailed engineering assessments in conjunction with maintenance and installation work will be a routine problem for ITER. Targetless surveying will need to be developed further in the future so that the process can be automated and ultimately lead to the production of models which can be interrogated as CAD models. This will, of course, be relevant throughout the broad spectrum of the nuclear and process industries.

ACKNOWLEDGEMENTS

The authors gratefully acknowledge the invaluable assistance of the JET's Data Management Group, the Remote Handling Group and the technical support received from ESIC, Geodetic Services Inc. and Leica.

REFERENCES

[1] Manufacturing and Installation of JET MKII Divertor Support Structure. G Celentano et al., 16th Symposium on Fusion Engineering, Champaign 1995.
[2] Alignment Systems for Pumped Divertor Installation at JET. B Macklin et al., 18th Symposium on Fusion Technology, Karlsruhe 1994.
[3] Application of 'Best-Fit' Survey Techniques Throughout Design, Manufacturing and Installation of the MKII Divertor at JET. B Macklin et al., 16th Symposium on Fusion Engineering, Champaign 1995
[4] Leica AG, Photogrammetry and Metrology, CH-5035, Unterendfelden, Switzerland.
[5] ESIC Reseau Eurisys, St. Quentin en Yvelines, France.
[6] Geodetic Services, Inc., Melbourne, Florida, USA 32901
[7] Preparations for Fully Remote Exchange of JET Divertor Modules. A C Rolfe et al., 17th Symposium on Fusion Engineering, San Diego 1997.

Closure of the Bypass Leakage around the JET Divertor with Polymer Seals

H Altmann, P Andrew

JET Joint Undertaking, Abingdon, Oxon, OX14 3EA, UK

ABSTRACT

An effort has been made to reduce the main chamber neutral pressure during plasma operation by reducing the conductance from the volume beneath the divertor target to the main chamber. A method of sealing gaps between metal structures using Aramid cloth was developed. These seals resulted in a nearly 2-fold reduction in the main chamber pressure relative to sub divertor pressure.

I. INTRODUCTION

During the design of the MKI JET divertor [1], closure of conductance paths around the outside of the divertor structure and coils was not a design requirement. The MKI divertor had a structure with many gas leakage paths between the radial beams supporting the plasma intercepting tiles. As a result, neutral particles could flow relatively freely between the main chamber and the volume beneath the tiles containing the divertor cryopump.

In the MKII divertor [2], the radial beams of the MKI have been replaced by three continuous rings of the support structure. Plasma facing tiles are supported on removable carriers attached to the rings, as shown in figure 1. Conductance to the cryo pump from the target plate region is through the water cooled louvres in the inner and outer corners of the support structure.

The MKII divertor is more "closed" than MKI, i.e., the divertor cross-section is designed to be a close fit around the divertor plasma. In this way neutrals recycled from the divertor target are more likely to be re-ionized and swept back to the divertor. The neutrals accummulated in the divertor are removed from the system by being pumped onto the divertor cryopump. However, if neutral particles are able to find another route to the main plasma without passing through the divertor plasma, the purpose of a closed divertor is defeated. Fig. 1 shows these paths between the walls and the divertor tiles which bypass the divertor plasma.

II. FIRST ATTEMPTS AT CLOSURE

Early attempts to close off the leakage paths involved the use of thin Inconel sheets (typically 0.8mm thickness) being spot welded to the walls either side of any gaps with a labyrinth clearance of about 3mm at the overlap between the sheets. Owing to the very irregular surfaces which formed the walls of the gaps, considerable difficulties were met in achieving any worthwhile closure of the gaps.

This state of leakage closure, referred to as MKIIa, existed for the first 6 months of MKII operation. Sections III - VI describe the efforts to bring the divertor to a state of reduced bypass leakage (plugged) referred to as MKIIap.

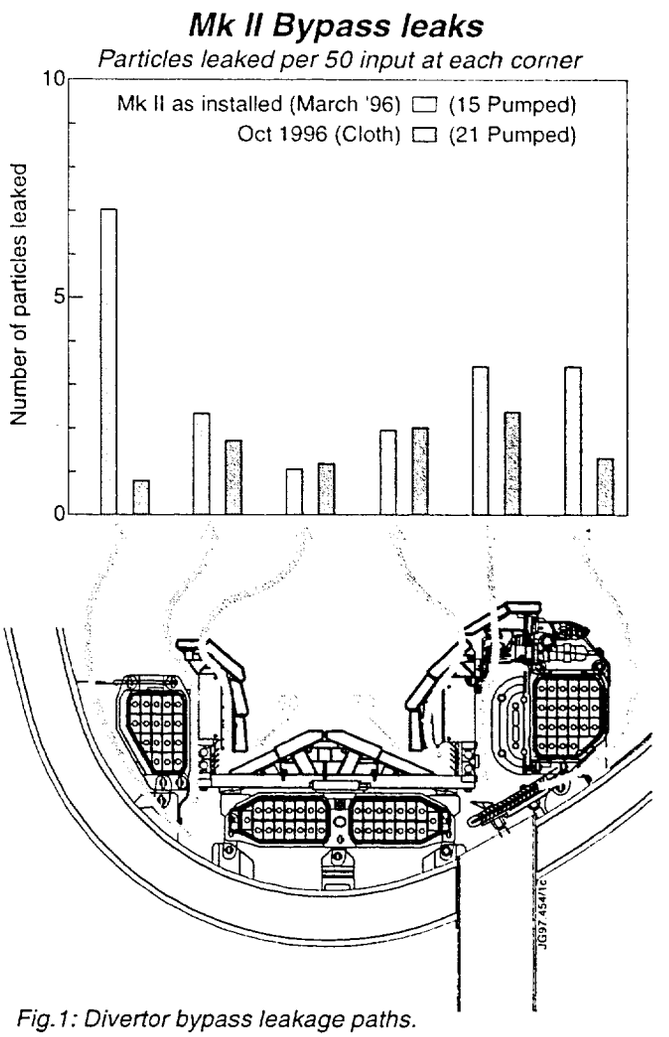

Fig.1: Divertor bypass leakage paths.

III. MATERIAL SELECTION

Any candidate material had to possess certain properties before it could be considered for long term use inside the JET vacuum vessel. These properties were:-

- non-shredding to avoid particles or fibres finding their way into vacuum valves to create leaks,
- non-electrical conductivity to avoid creating conducting paths and movement under magnetic fields inside the Torus,
- vacuum compatibility almost indefinitely up to 350°C without release of hydro-carbons or other contaminants,
- physical integrity in vacuum up to 350°C for repeated periods up to a year in length without deterioration,
- resistance to gamma radiation up to 10^8 rads,
- resistance to neutron radiation up to $5x10^{23}$ neutrons,
- non-retentivity of tritium compared to other material in the torus,
- suitability for installation by personnel dressed in restrictive protective clothing.

The following materials were considered:

A. *Metallic Woven Mesh, Wire Wool or Braid* - All the necessary properties were available except that of non-electrical conductivity.

B. *Glass Fibre Cloth* - Continual shedding of fibres made it unacceptable for use with the large number of metal-sealed valves on the Torus.

C. *Carbon Fibre Cloth* - This does not suffer from fibre shedding but its electrical conductivity, and the consequent magnetic forces acting on it, makes it impossible to guarantee that the material will not move around inside the Torus. Potential conducting paths would also have been a hazard.

D *Oxidized PAN Fibre* - The preliminary stages of carbon-fibre cloth manufacture involves the production of pre-carbon cloth. This has the advantage of being an electrical insulator at this stage.

A sample was subjected to a vacuum outgassing test but clearly showed an almost unlimited capacity for releasing water vapour.

E. *Ceramic Cloth* - A woven ceramic cloth designed for high temperature applications was subjected to an extended vacuum outgassing test at 350°C. The considerable outgassing rate showed almost no sign of decreasing.

F. *Polyimide* - At this stage it appeared as if none of the usual high temperature materials could meet all the requirements. Consequently the search was extended to include polymers such as polyimide. This is known to have good vacuum characteristics up to about 320°C. Unfortunately it appeared not to be available in woven cloth form.

G. *Polyaramid* - The next material to be tested was a polyaramid which sells under the trade name of Kevlar or Twaron. This material is usually chosen for its high strength and toughness at temperatures up to 250°C. At higher temperature in air it loses strength after a few hundred hours, apparently through oxidation of the fibres. A sample was subjected to a vacuum test at 350°C for several weeks and displayed very low outgassing rates after the initial loss of absorbed water vapour. It also appeared to lose none of its mechanical properties during this test, owing to the absence of an oxidizing environment. These results indicated that a polyaramid was the most promising candidate material so far and that further characterization was required.

IV. CHARACTERIZATION OF POLYARAMIDS

With reference to the previous section, the compliance of polyaramid with the required properties was as follows:-

- Shredding of broken fibres does not occur but individual fibres can unravel and this was to be avoided through the seal manufacturing process,
- Electrically fully insulating,
- Vacuum compatibility good with low hydrocarbon outgassing,
- Satisfactory physical integrity under vacuum and high temperatures,
- Irradiation by both neutrons and gamma radiation has been analysed on [3] with the conclusion that there should be no problem with any of the DT scenarios foreseen at JET, i.e. $5x10^{23}$ neutrons and 10^8 rads,
- Tritium absorption tests [4] carried out by AECL, Canada, indicated that this should not be a problem with $<5x10^{-5}$ ci/gm being taken up by the material,
- Installation feasibility would depend upon the design of the seals but the material itself would not present any special difficulty.

In view of these considerations, it was decided that the polyaramid would meet all the necessary requirements for sealing the bypass leaks.

V. SEAL DESIGN

With the choice of woven polyaramid the question of seal design had to be addressed. Thermal expansion leads to the gap sizes changing by a few centimetres and trials to fill the gaps with substantial rolls or bundles of folded cloth showed that the material itself does not have sufficient resilience or springiness to absorb this thermal expansion. The quantity of material required to implement such a solution would amount to many hundreds of square metres and the introduction of so much polymer into the JET vacuum was considered undesirable.

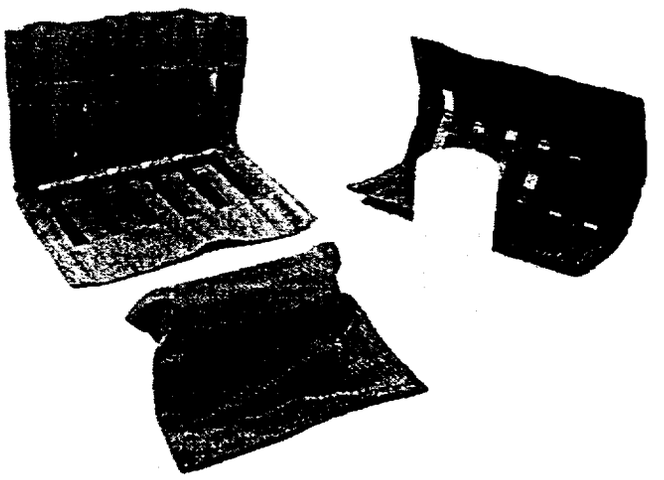

Fig.2: Seals prepared for installation.

The solution that was finally chosen is shown in figure 2. Woven cloth was folded to form rectangular sheets with all the cut edges tucked into seams to prevent the unravelling and shedding of fibres. Further folds and stitching were used to create multiple pockets about 15mm wide by 50mm long. Cold-rolled stainless steel 310 strip, 0.5mm thick and 10mm wide was used to form stiffening ribs that locate in the sewn pockets. Subsequent spot welding of cross strips created a flexible skeleton that could be bent to the required shape but still retain the springiness necessary to keep the seals located in the gaps. The individual steel strips allow the seal to follow the contour of an uneven wall fairly closely. The choice of SS310 was made because of its ability to retain its mechanical properties at the vessel temperature of 320°C.

VI. INSTALLATION

An important activity before installation was cleaning of the seals. Although the cloth is chemically scoured after manufacture to remove the surface coating needed during weaving, it still required a high temperature baking cycle to remove this coating. Both air and vacuum baking up to 350°C for a few hours were effective in cleaning the seals. The seals had to be located securely inside the vacuum vessel and not be displaced during operation. For this purpose, additional stainless steel locking strips were fitted into spare pockets on the seals and bent through 180° to form a tab suitable for spot welding on to the walls of leakage gaps. Four locking tabs were used on each seal with the many spare pockets giving flexibility for choosing suitable locations.

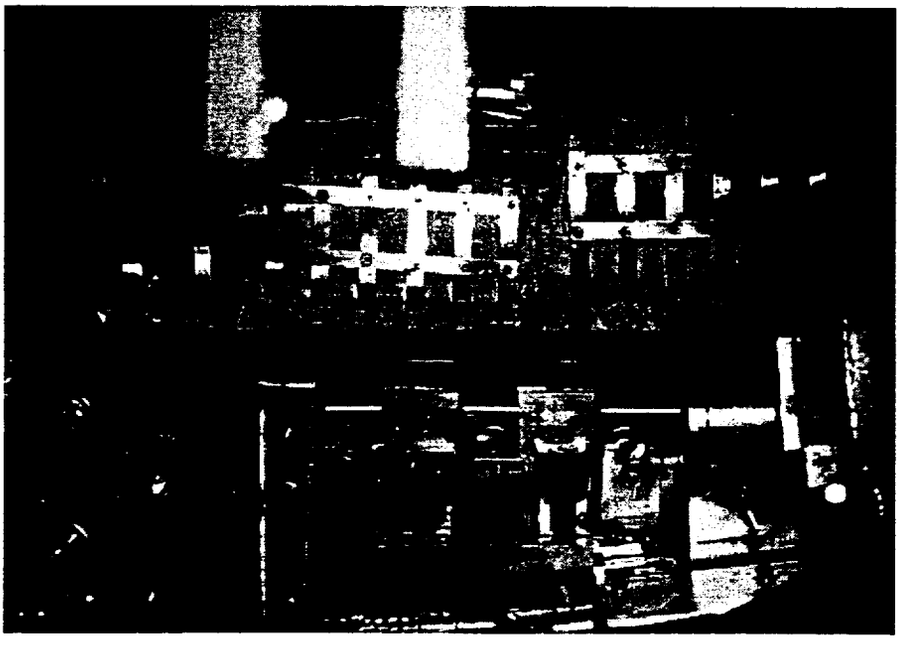

Fig.3: Seal installation between divertor and vessel wall

All seal installation had to be carried out by personnel in full protective clothing. This restricted the finger dexterity through three pairs of gloves and made it essential that the installation procedure was practised in advance in the In-Vessel Training Facility (IVTF). Figure 3 shows a photograph inside the IVTF of some seals fitted into the gap between the inner divertor coil and the vessel inner wall.

Access to carry out the spot welding of locking strips in the gap between the outer divertor coil and vessel wall was restricted by the hood of the protective suit to the extent that no locking strips could be attached to the divertor coil. Consequently the weight of a ø50mm alumina rod was used to assist in holding the seals in place. Polyaramid bags enclosed the rods and were sewn on to the seals. These components can be seen in figure 2.

Despite the reasonable flexibility of the seals, many gaps were very difficult, if not impossible, to close effectively. The space between the divertor support structure and inner divertor coil had so many brackets, diagnostics, clamps etc.,. around it that almost no serious closure could take place. The area above the cryopump also had limited access and many leakage openings were left unclosed. As a result of these difficult areas and the general contoured nature of all surfaces, an accurate assessment of the degree of closure could not be made.

VII. CONDUCTANCE CALCULATIONS

To quantify the bypass leak rates and the effectiveness of closure, the conductance of the various bypass leaks was estimated using simple analytical formulae for the conductances of apertures and narrow rectangular channels in molecular flow [5]. This is justified since the divertor pressure ranges from 10^{-4} to 10^{-3} mbar (i.e., mean free path is 0.1 to 1 m) while the leakage channels are typically ≤ 0.1m wide. The conductances were evaluated for a uniform deuterium gas temperature of 410K which represents an average for the various structures of 77K to 593K.

The cryopump pumping speed was assumed to be 500 m^3s^{-1} [6]. This figure refers to the naked cryo pump (LN_2 Chevrons + LHe surfaces) not baffled by any of the surrounding divertor structure.

Fig. 1 shows the particle flows based on theoretical estimates of the bypass leakage conductances. In the MKIIa, for 100 particles entering the divertor slots, 15 are pumped while a total of 19 are leaked to the main plasma. The remainder re-enter the divertor. In the MKIIap, the amounts pumped and leaked were estimated to be 22 and 8 respectively, i.e., a factor of 3 improvement in the ratio of leaked to pumped particles.

VIII. MEASURED CONDUCTANCES

It was not possible to measure the individual conductances evaluated above. Instead, it was possible to measure i) the overall pumping speed of the vacuum vessel by the cryo pump in series with the restrictions presented by the divertor and ii) the effective pumping speed of the cryo pump referenced to a point just below the cryo pump where a pressure measurement is available (see point P on fig. 1).

i) Pumping speed on the vacuum vessel, S_{torus}

The above model predicted an ~30% reduction in the value of S_{torus} from 265 m^3s^{-1} to 182 m^3s^{-1} at the vessel temperature of 320°C for the MKIIa and MKIIap respectively. This reduction is because the seals reduce the number of paths to the cryopump.

S_{torus} was deduced by measuring the fraction of gas pumped by turbo pumps (10m^3s^{-1} pumping the torus volume in parallel. Over a 10^{-5} to 10^{-3} mbar pressure range, this gave S_{torus} = 130 m^3s^{-1} for a vessel temperature of 320°C for the MKIIap. Other methods employed for both MKIIa and MKIIap, implied that S_{torus} was not significantly higher (i.e. <15%) during the MKIIa period, contrary to the theoretical expectations.

ii) Effective pumping speed near the pump, $S_{divertor}$

The model predicted that $S_{divertor}$ would increase slightly from 320 m^3s^{-1} to 335 m^3s^{-1} in going from MKIIa to MKIIap. These values are referenced to a point just below the divertor, assumed to be at 50°C, where a pressure gauge exists. The reason for the slight increase is that the reduction in the leak above the cryopump in MKIIap results in reduced leakage above the pump. The reason that both these pumping speeds are smaller than the nominal 500 m^3s^{-1} for the cryopump is the result of the conductance limiting surrounding structures.

$S_{divertor}$ was deduced experimentally from the time integrated pressure at the reference point compared to the cryopump gas inventory. This gave $S_{divertor}$ = 120 m^3s^{-1} which is much lower than the predicted value.

There are at least 2 possible causes for the poor agreement between measured and predicted pumping speeds:

1) the nominal speed of the cryopump is actually much lower than the assumed 500 m^3s^{-1},

2) the extent to which the existing divertor structure already baffle the cryo pump has been grossly underestimated.

Although it is not possible experimentally to distinguish between the above, the sensitivity to the assumed cryopump speed was checked by redoing all the calculations for a naked speed of 200 m^3s^{-1} instead of 500 m^3s^{-1}. This greatly improved the agreement with all 3 experimental observations: 1) the magnitude of S_{torus}, 2) the magnitude of $S_{divertor}$ and 3) the small change in S_{torus} from MKIIa to MKIIap.

Nevertheless, even with only 200 m^3s^{-1} according to the calculations, the effort of reducing the bypass leaks is still worthwhile. For the 500 m^3s^{-1}figure, the ratio of particles leaked to pumped decreased from 1.2 to 0.4 in going from MKIIa to MKIIap. If, however, 200 m^3s^{-1} is used the reduction is instead from 2.5 to 0.7.

IX. Effects on Plasma Performance

The aim of the bypass leakage reduction was to reduce main chamber neutral pressure and hopefully increase the plasma purity and confinement quality in the process.

i) Main chamber pressure

The clearest experimental result after the bypass leaks had been reduced was an ~30% reduction of H_α light at the inner main chamber plasma boundary, indicating a reduction in the flux of neutrals impinging on the plasma. It must be noted, however, that a change to the inner wall protection tiles which occurred during the change from MKIIa to MKIIap could conceivably be responsible for the reduced H_α light.

In addition, an ~50% reduction in the outer mid plane neutral pressure for a given divertor pressure was observed. The effect was especially clear for the case where the divertor cryopump was off (fig. 4).

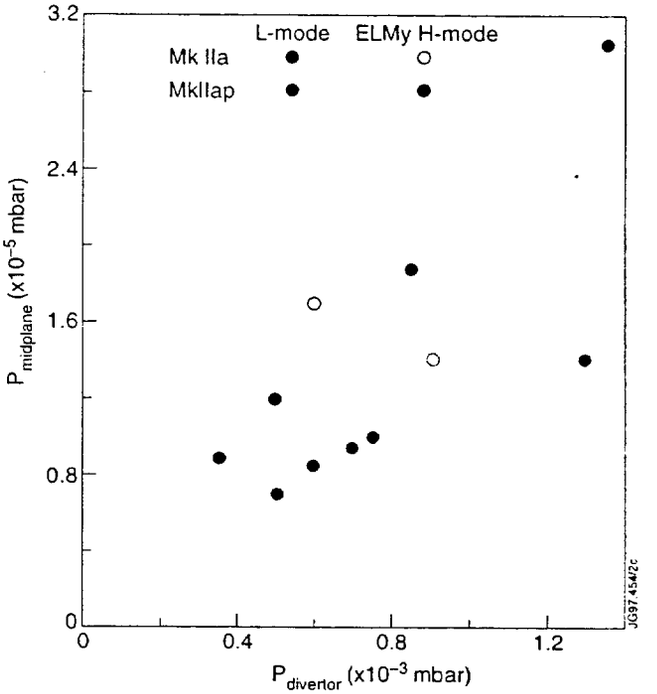

Fig.4: Midplane vs. divertor pressure (cryopump off cloth seals)

ii) Plasma performance

Unfortunately, no reduction in Z_{eff}or increase in confinement quality was observed as a result of the bypass leakage closure [7]. Indeed even the more dramatic reduction in closure in going from MKI to MKII divertors was not accompanied by a reduction in Z_{eff}. Unfortunately these results are not clear-cut because the degree of closure was not the only change to the machine. In going from MKI to MKIIa, the divertor target geometry and temperature changed and, in going to MKIIap, the inner wall material changed.

REFERENCES

[1] M A Pick et al. "The new first wall configuration of JET", *15th SOFE, Hyannis, USA*, Oct 11 - 15 1993.

[2] H Altmann et al. "Design of the MKII divertor with large carbon-fibre composite tiles", *18th SOFT, Karlsruhe, Germany*, 1994.

[3] Private communicaiton with J F Jaeger, *JET Joint Undertaking, Abingdon, UK.*

[4] Private communication with J Miller, *AECL, Chalk River Canada.*

[5] Methods of experimental physics: Vacuum Physics and Technology, Eds. G L Weissler and R W Carlson, Academic Press, 1979.

[6] W Obert et al. *16th SOFE*, 1995'.

[7] L D Horton et al. *24th European Physical Society Conference*, 1997

Plasma Vertical Stabilisation at JET using Adaptive Gain Adjustment

M Lennholm, D Campbell*, F Milani, S Puppin, F Sartori, B Tubbing

Jet Joint Undertaking, Abingdon OXON OX14 3EA, United Kingdom
***The NET Team, Max-Planck-Institut Für Plasmaphysik, Boltzmannstrasse 2, D8046 Garching bei München, Germany**

ABSTRACT

The plasma vertical position at JET is stabilised using the Fast Radial Field Amplifier (FRFA). This amplifier applies voltage to the radial field coils in steps of 2.5kV from -10kV to 10kV. It has a maximum current capability of 2.5kA. The amplifier is controlled in a closed loop by the Vertical Stabilisation controller. The best settings of the gains in this controller depend on the plasma growth rate which varies in an unpredictable manner during a JET pulse. An adaptive control algorithm, based on measurements of the switching activity of the FRFA amplifier, is used to adjust these settings in real time.

VERTICAL STABILISATION SYSTEM [1],[2],[3]

- 4 Radial Field Coils Outside Vacuum Vessel.
- Fast Radial Field Amplifier (FRFA).
- Magnetic Measurement for determination of Plasma Vertical Movement.
- Analogue Summing of Magnetic Measurements to reduce number of signals.
- Fast Digital Control system Calculates Control Signal for FRFA.
- FRFA Control signal (fig. 2):

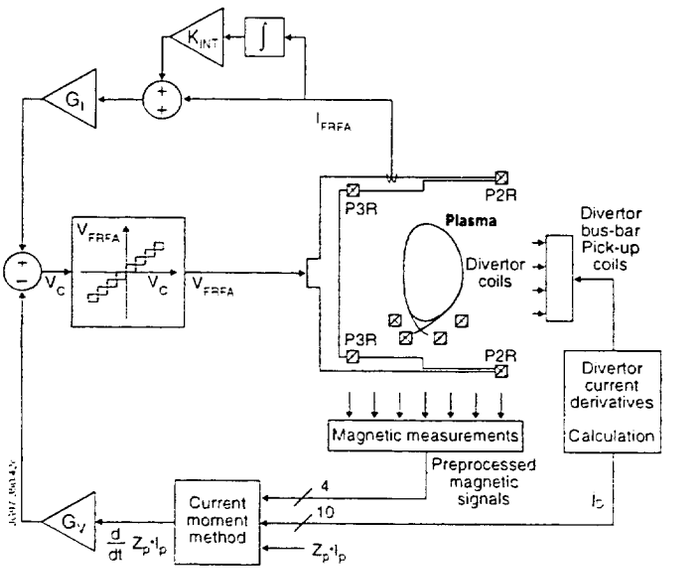

Fig. 1: The JET Vertical Stabilisation System

$$V_c = -G_v \cdot [I_P \cdot \frac{d}{dt} Z_P] + G_I \cdot [I_{FRFA} + k_{int} \int I_{FRFA}]$$

(I_P, Z_P = Plasma current and Vertical Position)

- Plasma + Coil system Transfer functions:

$$[I_P \cdot \frac{d}{dt} Z_P](s) = \frac{-(k_1 + k_3 \cdot \gamma) \cdot s}{(s+\tau)(s-\gamma)} \cdot V_{FRFA}(s)$$

$$I_{FRFA}(s) = \frac{k_2 \cdot (s-\alpha)}{(s+\tau)(s-\gamma)} \cdot V_{FRFA}(s)$$

- Typically: $\alpha \cong \gamma = 100 - 400 s^{-1}$, $\tau = 1.76 s^{-1}$

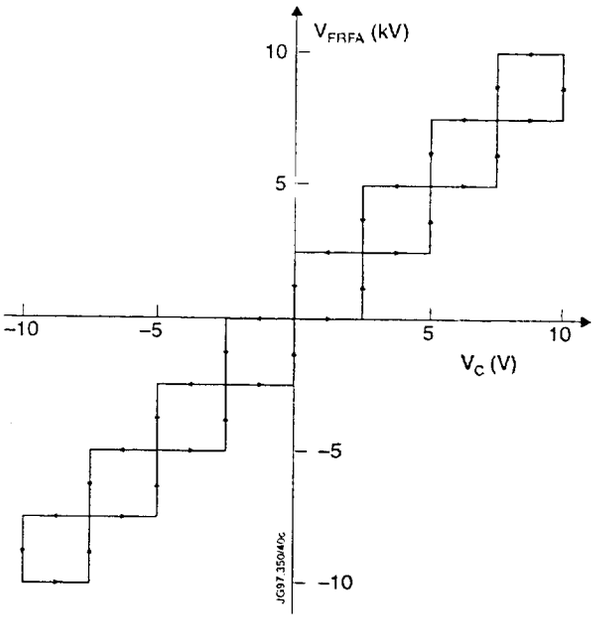

Fig. 2: FRFA characteristic

Fast Radial Field Amplifier (FRFA)[4]

- V_{FRFA}: -10kV → +10 kV in steps of 2.5kV
- I_{FRFA}: -2.5kA → +2.5kA
- Delay T_d: V_c → V_{FRFA} <300µs.
- Maximum switching frequencies:
  ±2.5kV: ~2.5 kHz
  ±10kV : ~1kHz
- Real Time simulation of thyristor junction temperature to prevent overheating.

Magnetic Measurements

- Magnetic measurements from 2 opposite toroidal locations are added to cancel any n=1 activity.

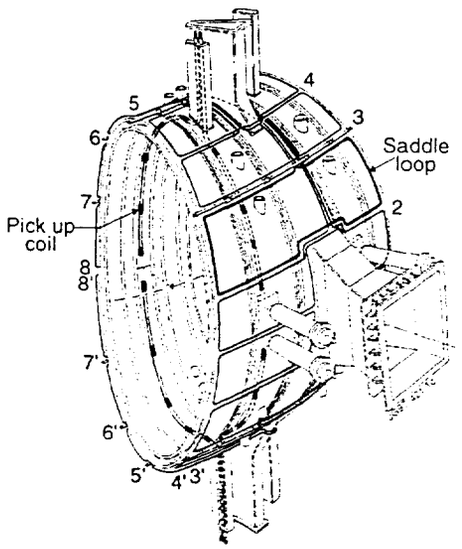

Fig. 3: Magnetic Sensors

- 18 Pick-Up coils situated inside the vacuum vessel at both toroidal locations, measuring the derivative of the poloidal field.
- 14 Saddle loops situated outside the vacuum vessel at both toroidal locations, measuring the derivative of the field perpendicular to the poloidal direction,.
- 4 pick-up coils measuring the derivative of the current in the 4 Divertor Coils.
- 8 Current shunts measuring the current in the toroidally conducting Divertor Support Structure.

The Full Current Moment Method [5],[6]

The value of $I_P \cdot \frac{d}{dt} Z_P$ can be determined by "Full Current Moment" method using the Zacharov-Shafranov integral. The method is described by the equations below, where I refers to the current passing through the poloidal crossection defined by the pickup coils and Z refers to the "centre of gravity" of this current. V_{pk} and V_{sad} are the voltages measured by the pickup coils and saddle loops and W_{pk} and W_{sad} are geometric weighting functions. $I_P \cdot \frac{d}{dt} Z_P$ is determined from $I \cdot \frac{d}{dt} Z$ by correcting for currents in the divertor coils and support structure.

$$\frac{d}{dt}(I \cdot Z) = \frac{1}{\mu} \oint \left[z \cdot \frac{dB_t}{dt} - 2\pi \cdot R \cdot \log\left(\frac{R}{R_0}\right) \cdot \frac{dB_n}{dt} \right] dl = \sum_n W_{pk} \cdot V_{pk} + \sum_m W_{sad} \cdot V_{sad}$$

$$I \cdot \frac{d}{dt} Z = \frac{d}{dt}(I \cdot Z) - Z \cdot \frac{d}{dt} I$$

The Flux Extrapolation Method

Due to Switching noise from the Amplifiers feeding the Divertor Coils signals from the lower part of the vacuum vessel could initially not be used. An alternative method, the "Flux Extrapolation" method, using only Pick-Up coil signals from the upper part of the vessel together with all the Saddle Loop signals was implemented. Filtering of the Divertor Coil Current and filtering of the affected signals has now made the use of the "Full Current Moment" method possible.

The VS Controller [7]

- VME based System
- 4 Digital Signal Processors (DSP's) 2 used for control, 1 for data acquisition, 1 for testing of new algorithms
- 24 low latency, "fast" ADC Channels, sampled at 20kHz for signals used for control.
- 32 high latency, "slow" ADC Channels sampled at 10kHz for diagnostic purposes.
- Optical link with FRFA.

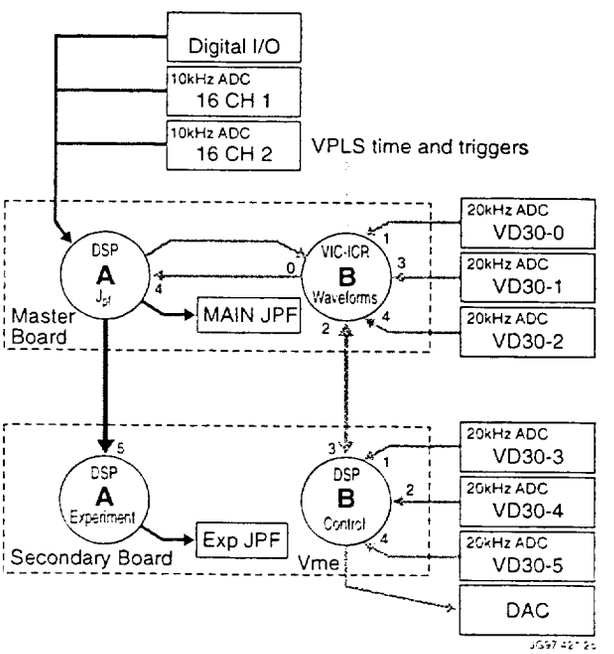

Fig.4 : VS controller- VME system.

THE STABILITY REGION IN G_I, G_v SPACE

Stability of the system depends on:

⇒ The Plasma Growth Rate: γ

⇒ The Velocity gain: G_v

⇒ The Current Gain: G_I

The boundaries of the stable region has the following characteristics:

- Small G_v, Large G_I ⇒ Slow, Large amplitude oscillation ⇒ FRFA current limit trip (Fig.5)
- Large G_v ⇒ Fast oscillations of smaller Amplitude ⇒ FRFA temperature limit trip (Fig.6)
- Small G_v, Small G_I ⇒ Very Slow, Large Scale Stable oscillation ⇒ Large movement of plasma vertical position (This is especially prominent when the "Flux Extrapolation" method is used).
- FRFA RMS voltage provides a good measure of system performance. The lower the RMS Voltage the better the performance.

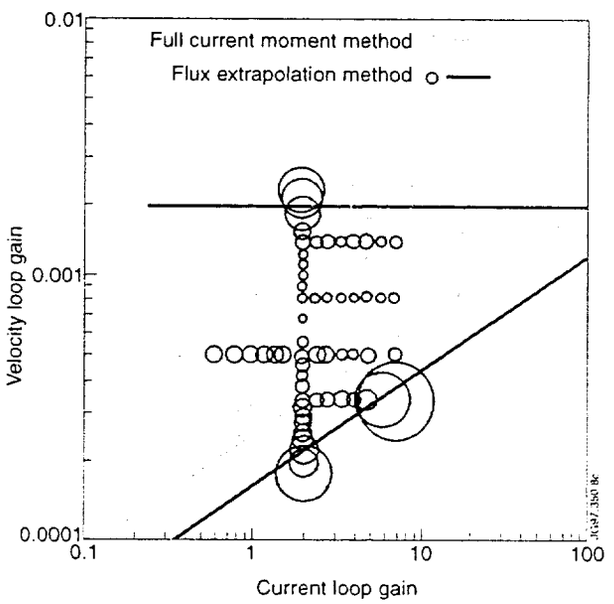

Fig.7 : Stability Region - Experimental. - The diameter of the circles is proportional to the FRFA RMS Voltage.

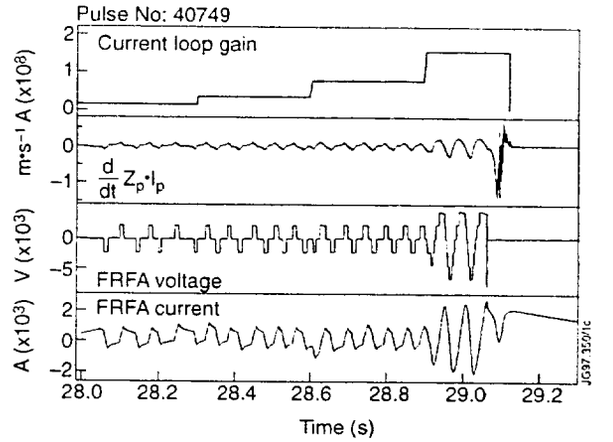

Fig.5 : Gain Scan G_v = 0.00025

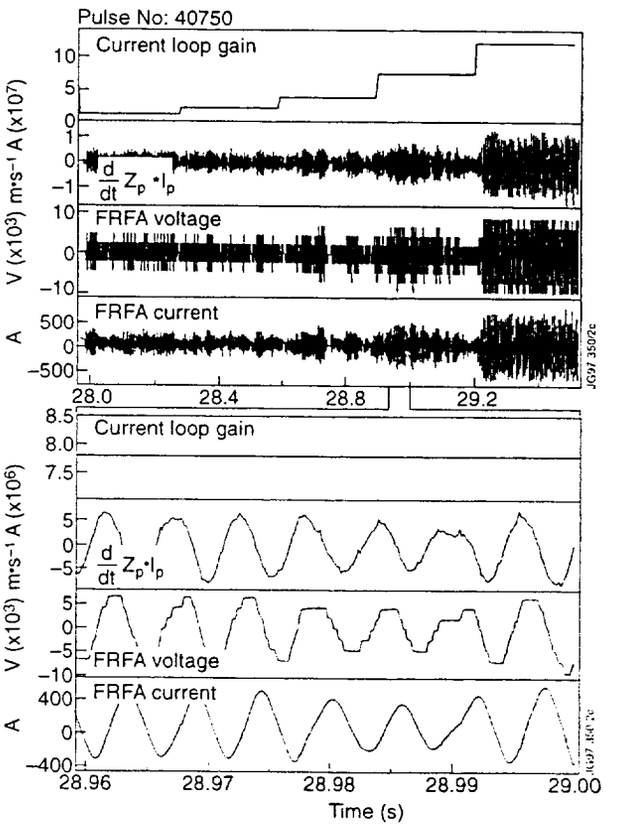

Fig 6 Gain Scan G_v=0.0013

- Simulation made with SIMULINK agrees well with measurements.
- Stable region moves towards smaller values of G_I and G_v for increasing plasma growth rate.

The best (most robust) behaviour of the system, is achieved with G_I *and* G_v centrally in the stable region.

Pre-programming G_I and G_v for optimal behaviour is very difficult – if not impossible.

Automatic adjustment of G_I and G_v as a function of plasma growth rate is desirable.

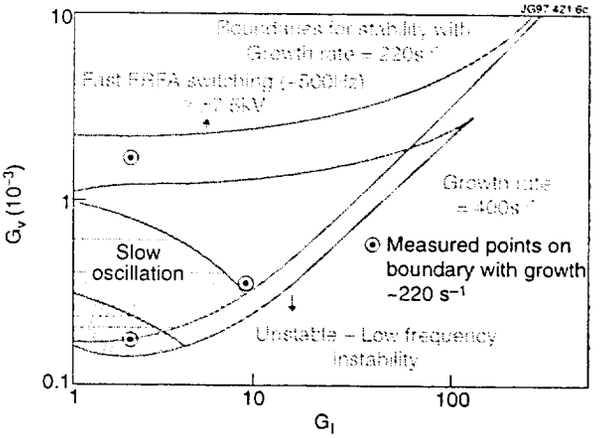

Fig. 8: Stability region from Simulations

ADAPTIVE GAIN ADJUSTMENT

- Real time determination of Plasma Growth rate is computationally demanding.
- The frequency with which V_{FRFA} changes sign, depends monotonically on G_I and γ for constant $\frac{G_I}{G_v}$: $f_{sw} \cong \frac{1}{\frac{1}{k \cdot G_v} + \frac{1}{\gamma} \cdot \ln\left(\frac{1}{k \cdot T_d \cdot G_v}\right)}$

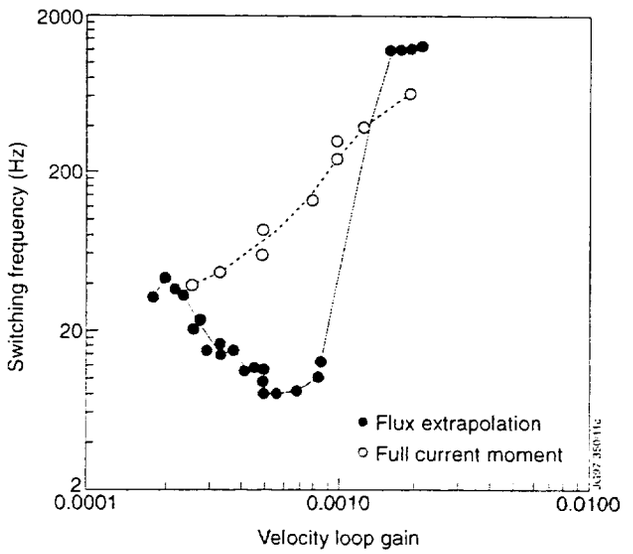

Fig.9 : Switching Frequency versus G_v

- When G_I and G_v are centrally in the stable region, f_{sw} is in a narrow interval for all γ.
- Algorithm for real time determination of f_{sw}:
  $f(n) = [k_a \cdot f(n-1) + k_b \delta[S_{FRFA}(n-1) + S_{FRFA}(n)]]$
  S_{FRFA}=Sign of V_{FRFA}.
- Adaptive controller adjusts G_v, keeping $\frac{G_I}{G_v}$ constant, to achieve the requested f_{sw}.
- Sawtooth like behaviour of Measured f_{sw} is smoothed by integrator.

EXPERIMENTAL RESULTS

Evolution through typical pulse (fig 11)

- Current ramp up - low growth rate: Adaptive controller adjusts G_v to large values.
- High performance phase - high elongation - large growth rate: Adaptive controller adjusts G_v to small values.

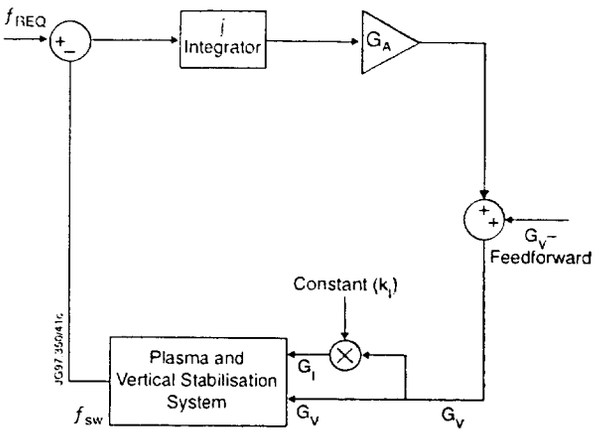

Fig. 10: Adaptive controller Block Diagram

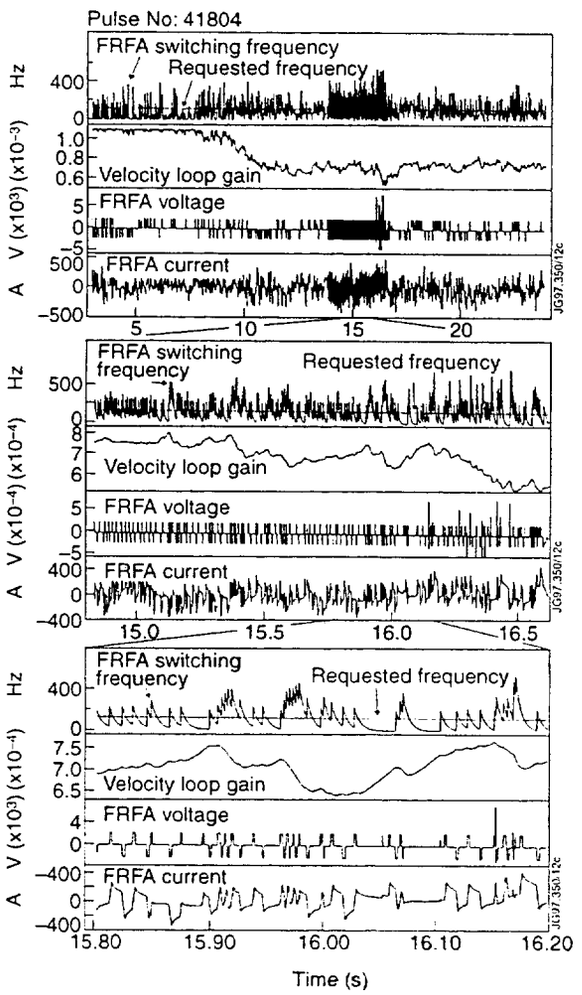

Fig.11: Adaptive Control - Typical pulse

Effect of fast pulse termination (fig 12)

- Fast Termination initiated at 10 seconds.
- Plasma current and elongation reduced rapidly.
- Fast reduction of Plasma growth rate.
- Adaptive controller increases G_v.

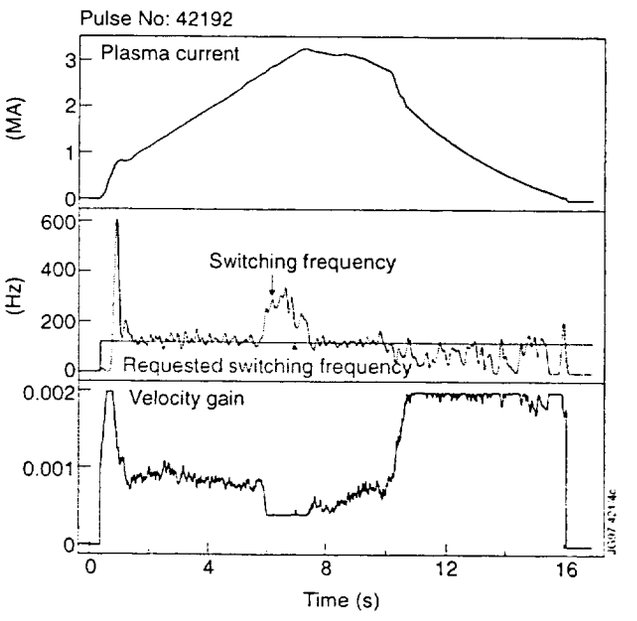

Fig.12:Adaptive Control - Fast Pulse Termination

Effect of ELM (fig 13)

- At the time of the ELM the Switching Frequency increases -
  - ⇒ G_v is decreased from 0.0008 to 0.0004 by the adaptive controller in ~100ms
  - ⇒ The frequency returns to the desired value.

Switching Frequency vs G_v - Non linearity

- The measured switching frequency can reach values of several kHz but can never be negative.
- Hence the Frequency error is asymmetric with respect to Zero (fig14).
- As a result G_v can be reduced much faster than it can be increased (fig. 15 - upper).
- To avoid this, the frequency error can be limited symmetrically about zero (fig. 14).
- Using this limitation the overall gain of the adaptive loop can be increased.
- The improvement achieved in this way is seen in fig. 15 - lower.

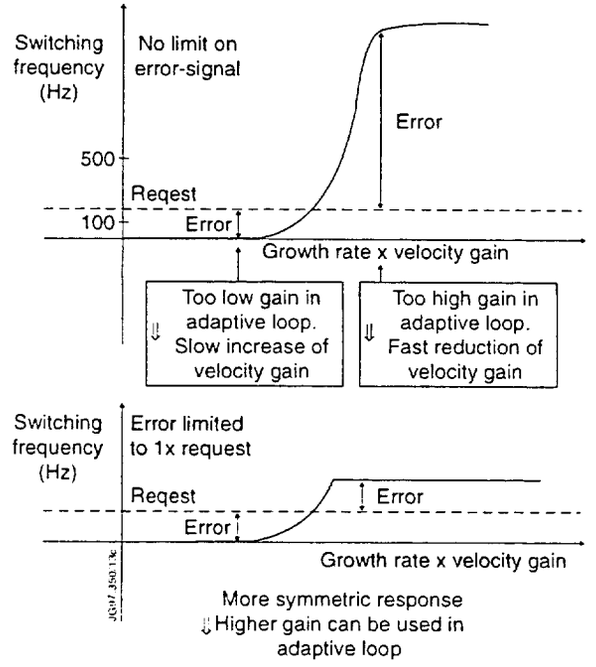

Fig. 14: Adaptive Control Non Linearity

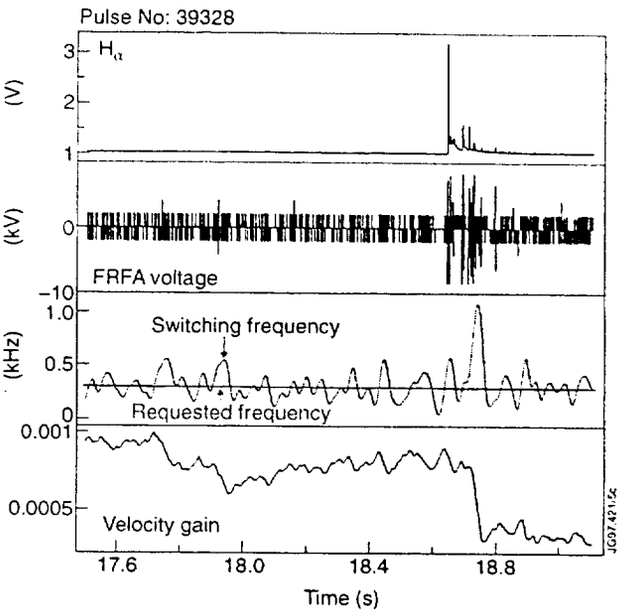

Fig 13: Adaptive Control at large ELM

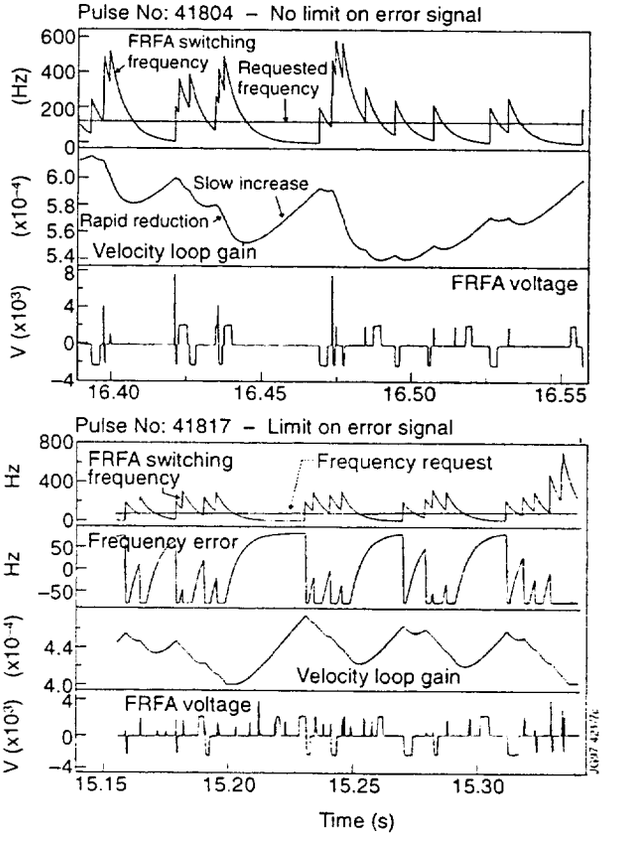

Fig. 15: Effect of Frequency Error Limit

Increased Switching Frequency can result from other phenomena than an increase of the plasma Growth Rate:

- **Frequent ELMs**:
  Each ELM results in a couple of fast switchings of FRFA.

- **N=2 Modes** (fig 16):
  Since no compensation for this mode is made in the determination of $I_P \cdot \frac{d}{dt} Z_P$ it appears as a real vertical oscillation resulting in very fast swithching of FRFA.

- **The lower Limit on** G_v must be set high enough to prevent slow oscillations and low enough to prevent overheating of FRFA.

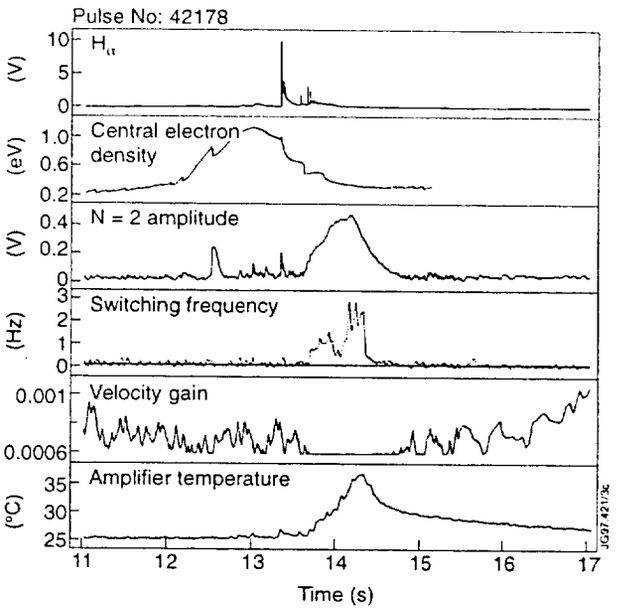

Fig.16 : N=2 Effect

CONCLUSIONS

The JET Vertical Stabilisation system uses magnetic measurements to determine the vertical velocity of the plasma multiplied by the Plasma Current. Using the result of this measurement the vertical position is kept stable by applying a Radial Field with the Fast Radial Field Amplifier.

Since October 1996 an adaptive gain adjustment algorithm has been used. This algorithm adjusts the gains in the Vertical Stabilisation controller in response to changes in plasma growth rate. The controller adjusts the gains in the loop to achieve a required switching frequency of the Fast Radial Field Amplifier.

After initial tuning of the Adaptive Controller, no loss of vertical control due to failure of the Vertical Stabilisation system has occurred, and pulse to pulse tuning of the settings of the Vertical Controller has virtually been eliminated.

ACKNOWLEDGEMENTS

The authors would like to thank the power supplies division for information about the FRFA amplifier and the personnel responsible for carrying out the experimental programmes from which the data in this poster has been taken.

REFERENCES

[1]: M.Garribba: Tesi di dottorato di ricerca, Universita di Padova 1994
[2]: M.Garribba et. al.: XV SOFE, Hyannis, 1993
[3]: M.Garribba et. al.: 18th SOFT, Karlsruhe, 1994
[4]: T.Bonnicelli et. al.: XV SOFE, Hyannis, 1993
[5]: L.E.Zakharov,V.D.Shafranov Sov.Phys.Tech.Phys., Vol.13.No.2, pg.151. 1973
[6]: F.Milani: Tesi di Laurea, Univesita di Padova, 1990-91
[7]: F.Sartori et.al.: RT95, 1995

The Development and Testing of a 66 kA By-Pass Switch with Arc Commutation Capability for the ITER Coil Power Supply System

T Bonicelli, D Hrabal[1], M Huart[2], J Neuser[2], E Sachs[1], B Bareyt[3].

JET Joint Undertaking, Abingdon, Oxon, OX14 3EA. UK.
[1]Siemens AG, Werner-von-Siemens-Strasse 50, D-91052 Erlangen, Germany
[2]Ritter Starkstromtechnik GmbH, Luisenglück 20, 44225 Dortmund (Barop), Germany
[3]ITER JCT, Naka, 801-1 Mukouyama, Naka-machi, Naka-gun, Ibaraki-ken, 311-01 Japan

I. INTRODUCTION

- The ITER discharging networks perform the discharge of the energy stored in the superconductive coils when a quench is detected.
- The current capability of the vacuum circuit breakers is far from been sufficient for the steady state operation.
- In normal conditions, the current flows therefore in by-pass switches rated for the full steady state current (60 kA).
- Upon the detection of a quench, the by-pass switch is opened and the current is commutated to the parallel path where the vacuum switch is installed.
- The by-pass switch must therefore be provided with some current breaking capability.
- The combination of high DC currents and high voltages is not normally encountered in industrial applications, the operating time is often also not of great concern.

II. RATINGS OF THE BY-PASS SWITCH

A commutating unit is essentially composed of a by-pass switch connected directly in parallel to a vacuum circuit breaker ⇒ the commutating loop inductance is minimized.

Table I

Ratings of the By-pass Switch for the ITER Discharging Networks

Rated voltage		17.5 kV
Rated DC current		60 kA DC
Rated peak withstand current		250 kA DC
Opening time (guaranteed)		<500 ms
Rated current breaking capability		66 kA DC
Resistance of main circuit		< 5 mW
Mechanical Life Expectancy		2000 cycles
Contact life time at the Rated DC current	- main contacts	1000 cycles
	- arc contacts	100 cycles

III. DEVELOPMENT OF THE BY-PASS SWITCH

- The protoype for the by-pass switch was based on an existing high current switch used in the electrochemistry industry.
- The standard voltage levels are up to about 2 kV and are therefore much lower than the ones required for ITER.
- The by-pass switch is pneumatically driven and it is of modular construction.

Areas of development work:

- **Contact distance**: the distance between the main contacts was increased from 20 mm to 45 mm (the arc contact distance was set to ca. 40 mm);
- **Clearances**: the clearance from the high voltage parts to the frame was increased from 30 mm to 135 mm;
- **Creepage**: the creepage distance was also increased from the standard 30 mm to 185 mm;
- **Bearings**: to achieve the specified mechanical life and to increase the switching speed, the original sliding bearings of the actuator and of the main shaft were replaced with needle (for the actuator) and cylinder (for the shaft) bearings;
- **Pneumatic drive**: a local 20 l reservoir was installed to reduce the pressure drops during operation;
- **Vacuum switch**: to define the actual characteristics of the commutating loop, a vacuum switch (two poles series connected) was connected in parallel as close as possible to the by-pass switch. A current shunt was installed between the two series connected poles. The inductance of the commutating loop was nevertheless 2 -2.5 times higher than for the original low voltage application.

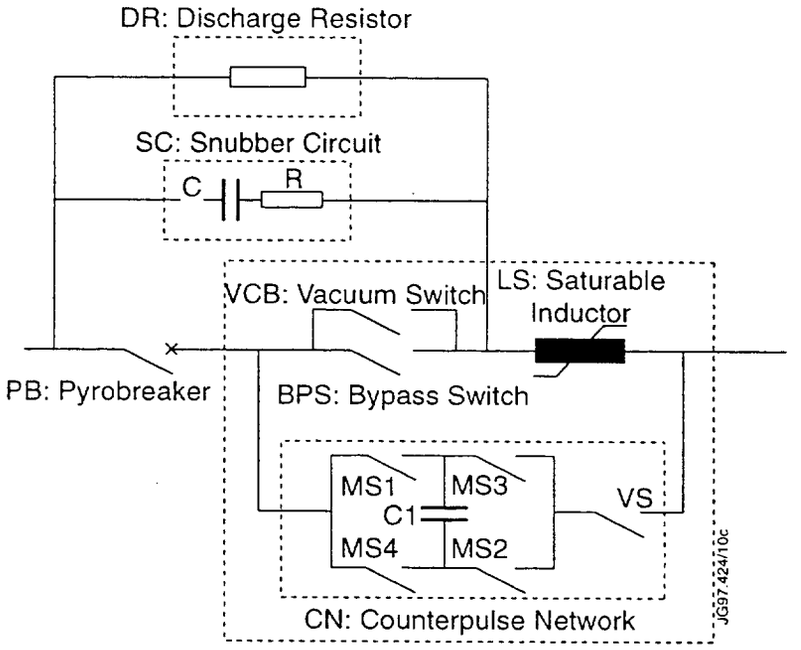

Fig. 1: Discharge Current Network

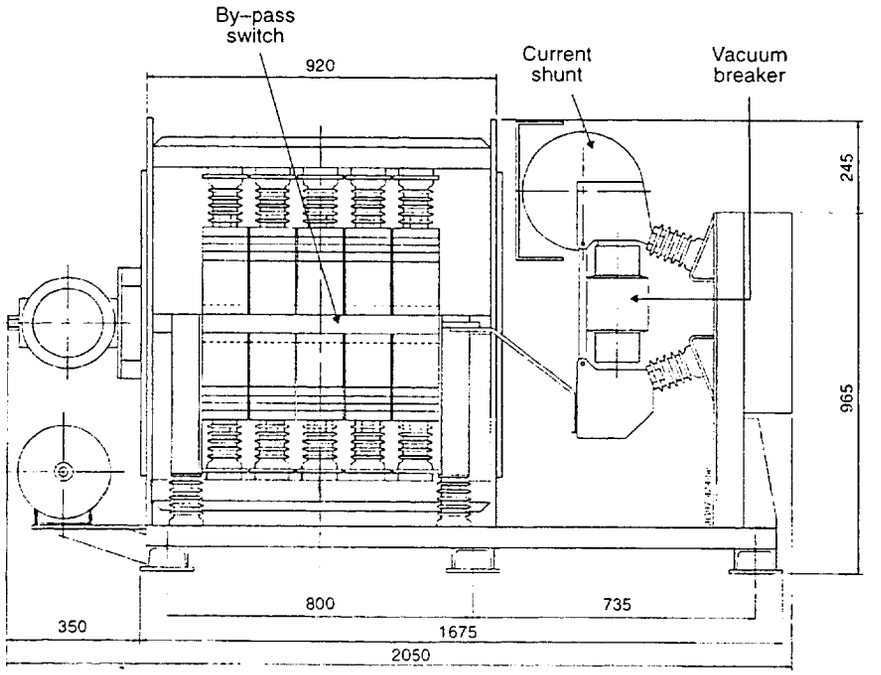

Fig. 2: General arrangement of the commutating unit

- Ten poles are connected in parallel, arranged in two rows of five poles each.
- Main contact size 120mm x 150mm (copper, silver plated).
- Each fixed contact is provided with four rows of special copper-silver-beryllium alloy multicontact strips.
- The movement of the contacts is linear.
- Two arc contacts were fitted, high tungsten graded-copper alloy (75% / 25%) soldered on a copper base. The size is 15mm x 50mm.
- The pneumatic driven rotating actuator operates at a nominal pressure of 6 bar.
- The switch is self-latching both in the open and in the closed position and its position is not affected by any loss of pressurised air.
- A force of ca 280 kg is applied on each contact in the closed position.

IV. TESTS

Power frequency withstand test at 38 kV

- **Measurement of the resistance of the main circuit**
- Contact resistance of each of the ten poles in the range from 5.1μΩ to 6.4μΩ.
  The average value was 5.95μΩ.
- The total resistance, including therefore the connections and the ten parallel poles, is 0.9μΩ.
- The resistance of the vacuum switch path was 62μΩ.

Temperature rise tests

- The ten poles were series connected for this test.
- The ITER water cooled busbars were simulated with water cooled cables.
- The test current of 6.8kA, simulating the effect of a total current of 60kA, taking into account the worst current mis-sharing.
- This approach produces an effective overload on the more resistive poles.

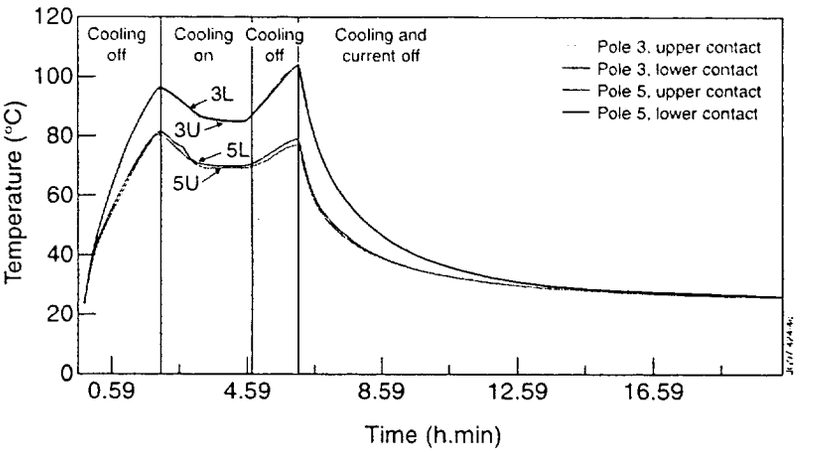

Fig.2: Temperature rise test

Peak withstand test

- The by-pass switch, with its ten poles parallel connected, was successfully subjected to a current with a peak value of 250kA, after a first failed attempt due to the spurious activation of an electrovalve (electromagnetic interference).
- **Commutating test in the range of 2 to 66kA**
- The current was increased in eight steps from 2kA to 67.6kA and five pulses were executed at each current level.
- The inspection at the end of the tests showed that all the arc and main contacts were in acceptable conditions, though some limited melting was noticed on one of the main contacts.

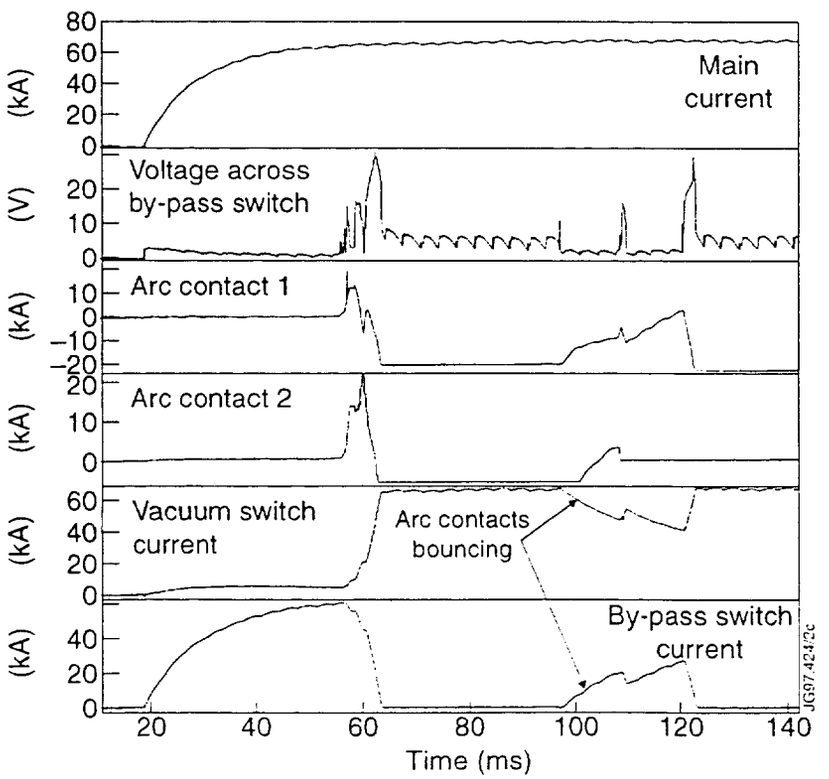

Fig.3: Commutating test at I = 67.6kA

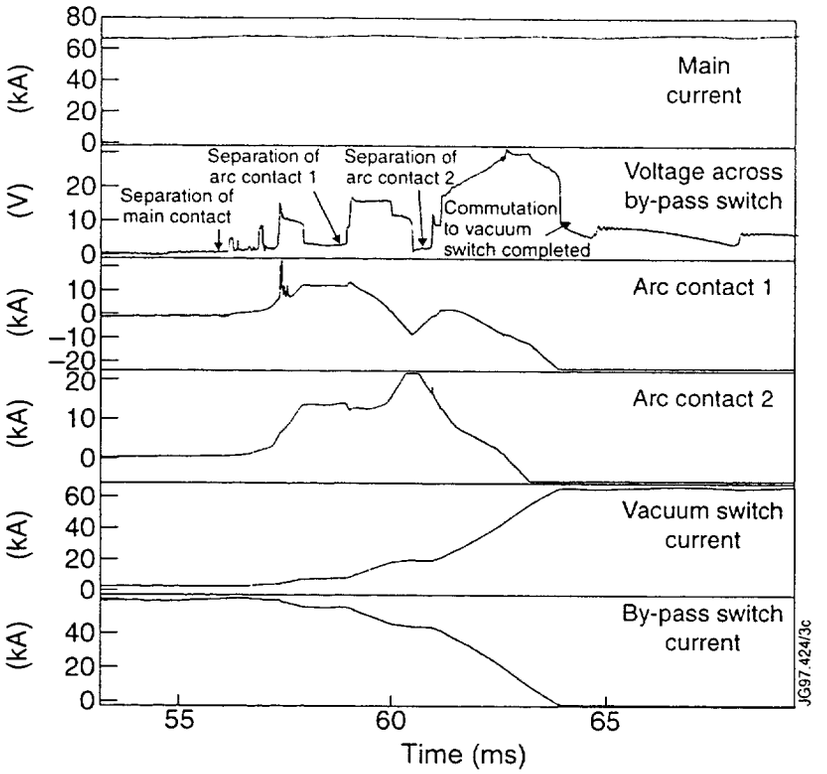

Fig.4: Commutating test at I = 67.6kA, expanded time base

Extended mechanical endurance test

- 2000 operating cycles without current.
- The opening and closing times were measured every 200 operations and the jitter over twenty successive operations was measured every 200 operations.
- The repetition rate was of 30 cycles per hour.
- A first test was stopped after 1408 cycles because of the failure of a weld on a pressure plate.
- The tests were therefore successfully repeated after improving the welding procedures and the quality control.
- Average opening time = 230ms (separation of contacts).
  (the limit switch indicates the "open" status only after ca. 400 ms).
- The jitter is within +/- 2ms of the mean opening time.
- Average closing time = 340ms.

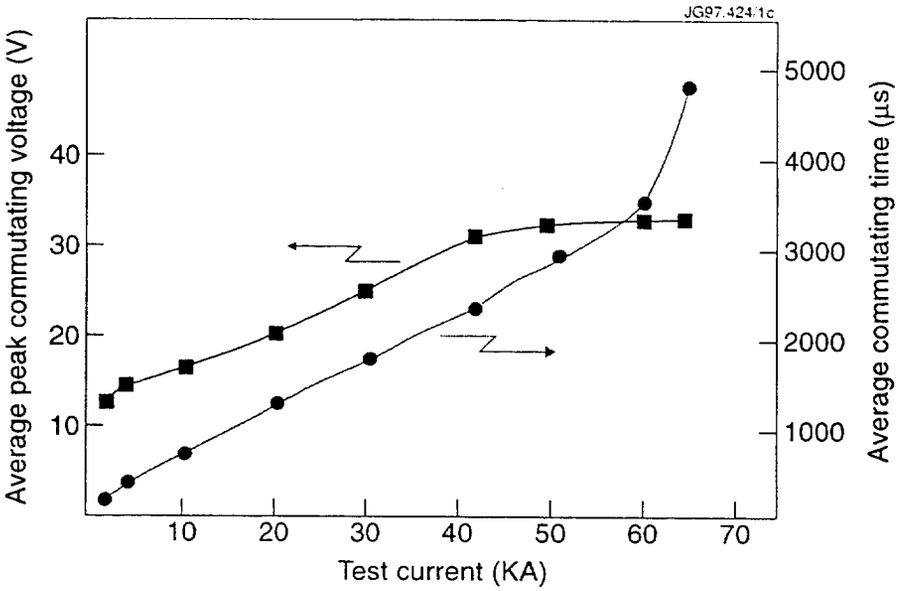

Fig.5: Main Resultsof the commutating tests

V. MODIFICATIONS TO THE SWITCH BEFORE THE CONTACT LIFE TEST

The results of the tests suggested some modifications.

- the weldings on the pressure plates were revised and the quality assurance procedures were improved;

- two more arc contacts were added to reduce the wearing on the main contacts by shortening the average commutating loop;

- the shielding between arc and main contacts was improved to reduce the deposition on the main contacts of vaporized material from the arc contacts;

- the adjustement range of the arc contact distance was increased to eliminate the contact bouncing;

- the electromagnetic valve was moved further away from the high current parts to avoid spurious operations due to elecrtomagnetic interference.

The contact life test essentially consists of 1000 operations of the by-pass switch at a current of 66 kA which is commutated to the parallel vacuum switch

Thr arc contacts may be replaced after every 100 operations.

The execution of the contact life test is planned to take place during the first months of 1998.

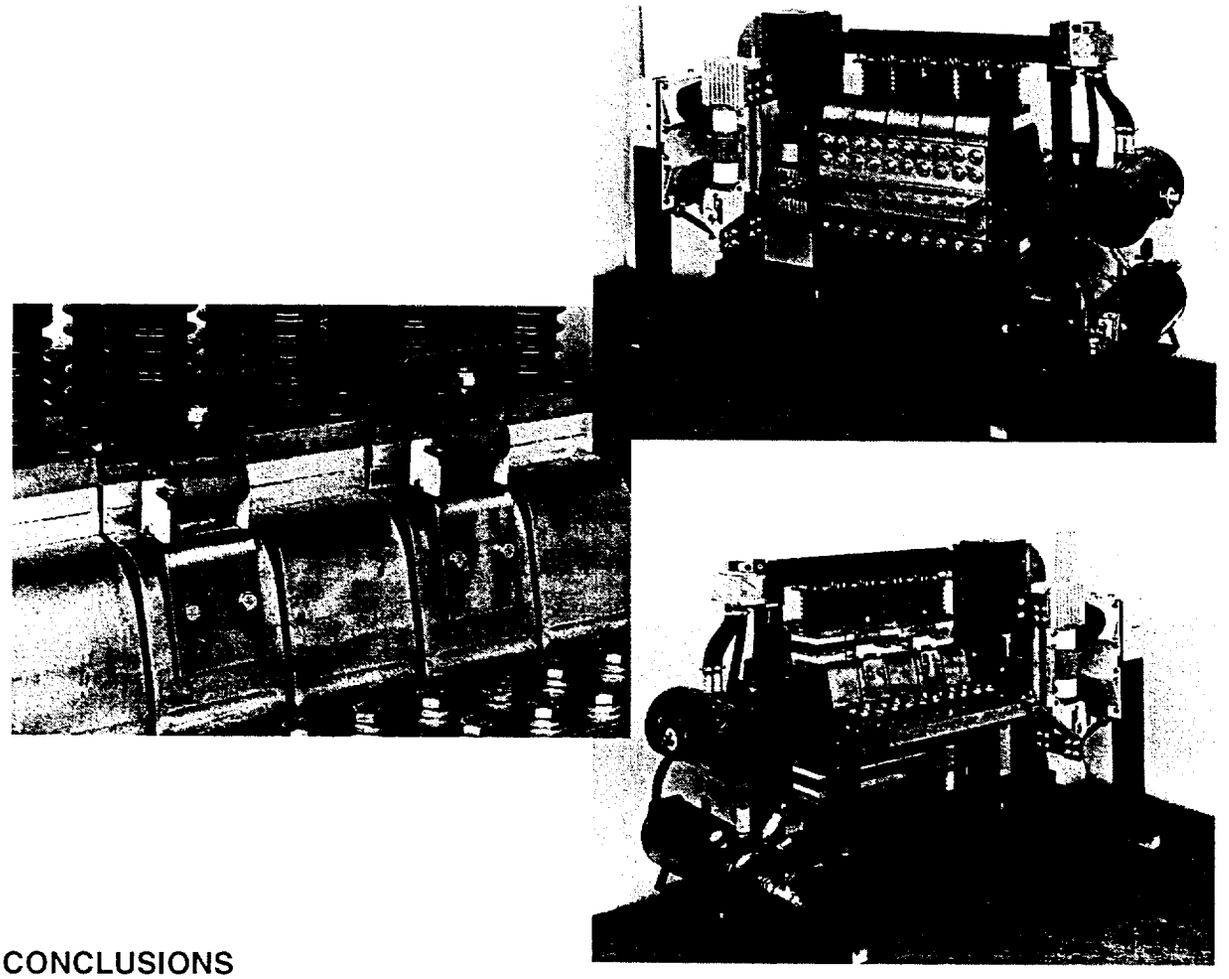

VI. CONCLUSIONS

- A fully sized and rated commutating unit has been developed and manufactured.
- A full set of type and characterisation test was performed and will be completed with the execution of the contact life test early next year.
- The by-pass switch satisfactorily passed all the tests, including the commutation to the parallel vacuum switch of a current 10% higher than the rated one. The operating time of the switch meets the requirements for the ITER application.
- Minor modifications were implemented mainly to improve the wearing and erosion of the main contacts.

Asymmetric Vertical Displacement Events at JET

V Riccardo, P Andrew, A Kaye, P Noll, T Raimondi

JET Joint Undertaking, Abingdon, Oxon, OX14 3EA, UK

1. INTRODUCTION

Asymmetric events have become an important issue for the integrity of the JET machine only after some mechanical components have been found damaged as a consequence of the vessel sideways displacements [1]. These are rare, but not new, phenomena. They are recorded only when the plasma kinks and the kink-locks long enough in the same toroidal position so that a net radial sideways impulse can build up [2].

2. SCALING OF SIDEWAYS DISPLACEMENTS

The radial sideways force is proportional to the product of the toroidal magnetic field with the difference of the vertical current moment in opposite cross sections.

Replacing the plasma with a current ring tilted about a radial axis and shifted about the same axis [2], the global force along the tilt axis is $F_x = \pi / 2\left(-\Delta M_{Iz} B_T + \Delta M_{IR} R \ \partial B_z / \partial R\right)$, where ΔM_{Iz} is the difference of vertical current moments in opposite cross sections and ΔM_{IR} of the radial current moments in the cross sections intercepted by the tilt axis. Considering uncertainties in the measurements the second term maybe neglected because the product of the plasma major radius with the gradient of the poloidal field (about 0.1 T/m times 3 m) is much smaller than the toroidal field (about 3T) and the difference of the radial current moment is generally found smaller than that of the vertical current moment.

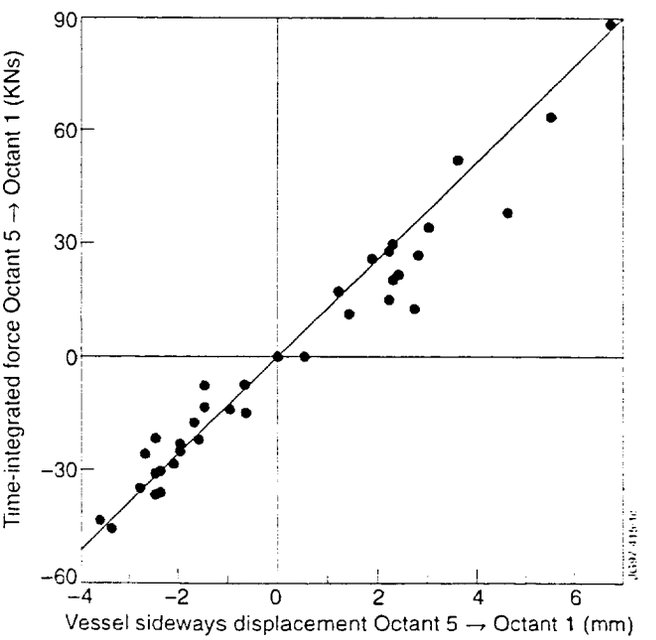

Fig. 1 *The vessel sideways displacement is proportional to the magnetic force impulse in the same direction (in this case the vessel movement has been projected on the direction normal to two magnetically instrumanted cross sections, octant 3 and octant 7).*

Experimental evidence (fig. 1) shows that the vessel sideways displacement is proportional to the impulse of the magnetic radial sideways force as evaluated using this simplified model. Besides, given the tilt axis, the direction of the vessel movement is determined, in fact the time integral of the magnetic force lays on the same direction of the vessel movement (fig. 2). Also the halo current toroidal distribution is determined by the plasma asymmetry (fig. 3).

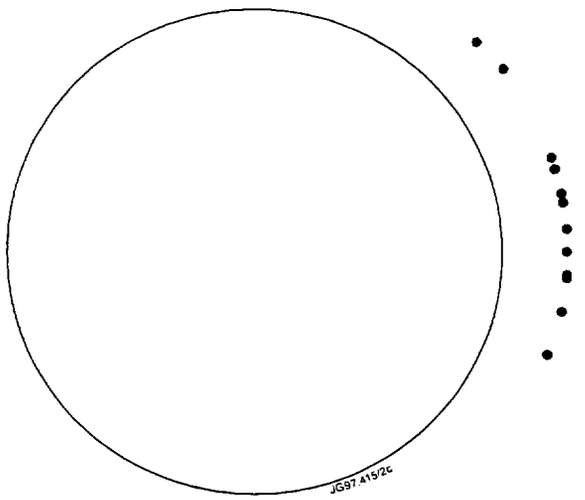

Fig. 2 *Aligning all large sideways displacements so that the vessel is moving from left to right of the figure, the time integral of the radial plasma force points almost in the same direction.*

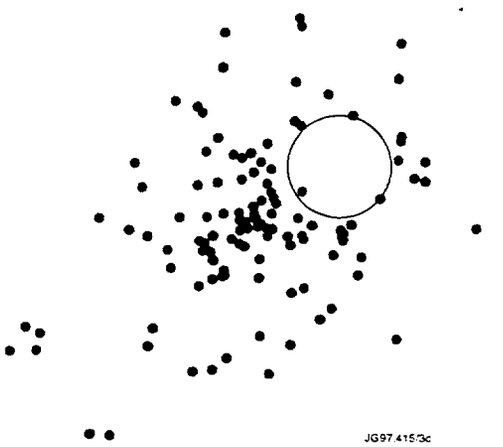

Fig. 3 *Placing on the right side the peak in the time integral of the halo current intercepted by shunts at the top of the vessel, the sideways displacements have a preferential toroidal direction (the distance of the points from the centre is proportional to the sideways displacement in that event, the reference circle is for a displacement of 1 mm).*

The upper envelope of the sideways displacements scales as the product of the plasma current with the toroidal magnetic field (fig. 4).

The maximum vessel displacement occurs only when the plasma kinks while it still has its full current, if the kink locks in a fixed toroidal location and stays there during the plasma current quench. If these conditions are only part satisfied, the sideways motion is smaller. Given the plasma current and the toroidal field, the largest possible vessel sideways displacement is limited by the degree of asymmetry of the plasma vertical displacement and by the duration of the plasma current.

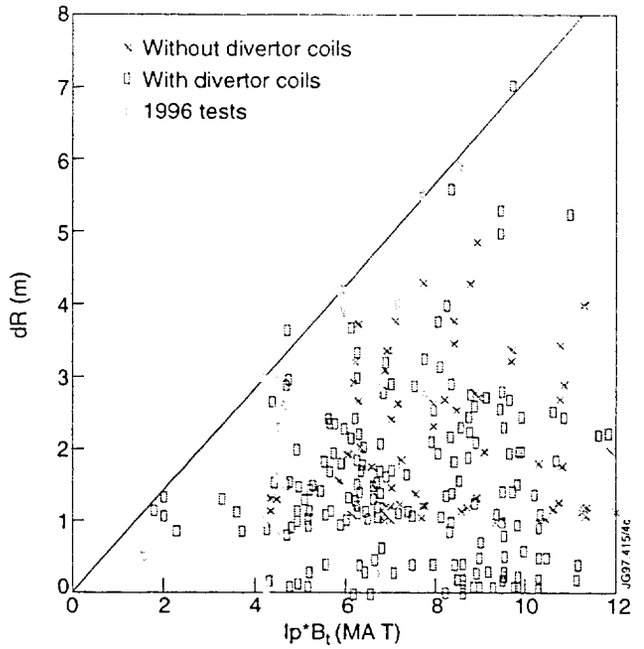

Fig.4: Collection of vessel sideways displacements plotted against the product of plasma current and toroidal magnetic field

Several attempts have been made to link the amplitude of the vessel sideways displacements to plasma parameters before the loss of confinement and test were carried for that purpose in November 1996. Only few variables seem to be relevant [2], however these are not free to be chosen or easy to control. More clear are the links with some disruption parameters, such as the disruption time. Fast disruptions would prevent asymmetric events (fig. 5). To this end killer pellets could be used, even if it would lead to other problems like high heat loads on localised areas of the first wall and increased eddy current loads on in-vessel components.

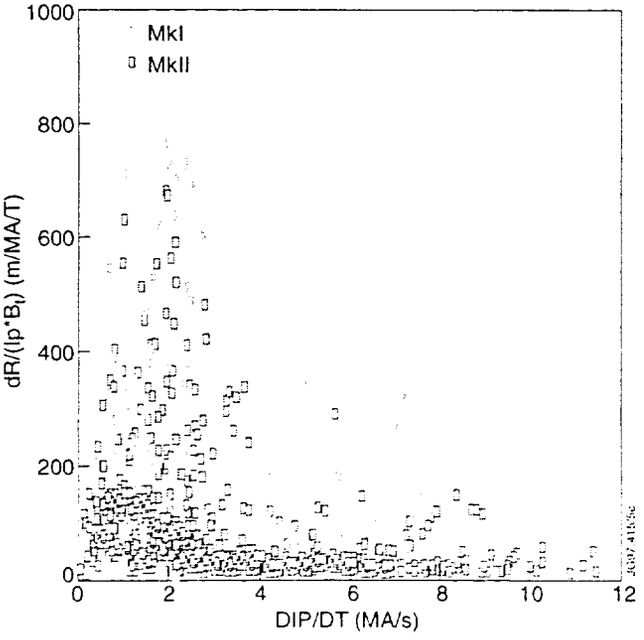

Fig. 5 *Normalised vessel sideways displacements plotted versus the plasma current quench rate.*

3. HIGHER POLOIDAL MODES

In the presence of a pure m=1/n=1 kink mode and assuming a simple plasma model with nested magnetic surfaces it is expected that the toroidal plasma current is smaller where the plasma is closer to the first wall, since there a larger fraction of the halo region is likely to be intercepted. Magnetic experimental data show the contrary in a number of cases: e.g. during pulse 38070, an upward VDE, the plasma current is larger and the vertical position is higher in octant 7 than in octant 3. This discrepancy between expected and measured plasma parameters may be explained taking into account the presence of the mode m=2/n=1. In this case the cross section of the plasma column is deformed along the toroidal angle [3] and the current centroid does not need to be at the highest position to have the smallest toroidal plasma current (fig. 7).

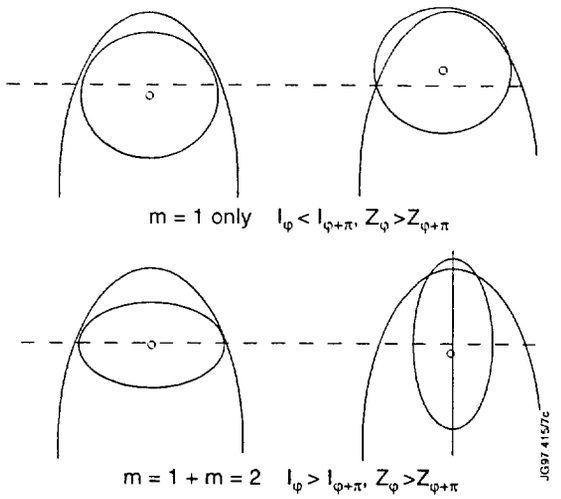

Fig. 6 Deformed/displaced plasma column in a vessel.

The effects of poloidal modes on the plasma position and current can be anticipated assuming a circular cross section for the undeformed plasma column. This simplification is acceptable since the plasma shrinks and its elongation decreases during VDEs. The cross section deformation can be modelled by a radial field perturbation

$$B_r = A_1 \sin(\alpha_1 + \varphi - \vartheta) + A_2 \sin(\alpha_2 + \varphi - 2\vartheta) + \ldots$$

Each poloidal mode can be obtained via scalar products

$$M_i(\varphi) = \oint B_r \cos(i\vartheta) d\vartheta = \pi A_i \sin(\alpha_i + \varphi)$$

and the amplitude and phase of the modes can be linked to magnetic measurements with appropriate toroidal and poloidal weights. In the cylindrical approximation, magnetic sensors located at a constant distance b from the centre of the original plasma measure the amplitude of the poloidal modes in terms of normal components of the field. Assuming a flat plasma current density $j_0 = I_p / \pi a^2$ over a circular cross section of radius a (which is indeed the case after the energy quench), the plasma deformations can be expressed as a function of the amplitude of the modes

at the magnetic sensors. The displacement due to m=1 is $\delta x = (2\pi b^2) / (\mu_0 I_p) \tilde{B}_1$ and the radial variation due to m=2 is $\delta a = (2\pi b^3) / (\mu_0 I_p a) \tilde{B}_2$; their ratio is $\delta a / \delta x = (b / a) \cdot (\tilde{B}_2 / \tilde{B}_1)$. The application of this simplified analysis to pulse 38070 shows that this ratio is as large as 1.5 when the vertical position asymmetry δx is about 9 cm. The result of a numerical evaluation of the effects of the superimposition of the two poloidal modes on the plasma column in the JET vessel is shown in fig. 7. The toroidal location of the current maximum comes rather close to that of the maximum vertical position, in qualitative agreement with observations.

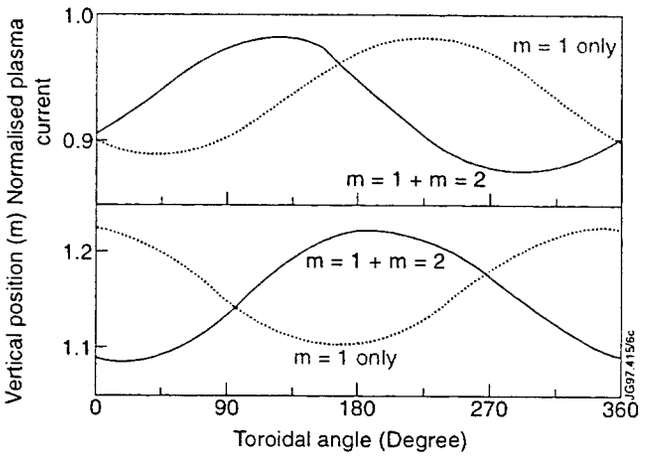

Fig. 7 *Plasma current and vertical position with m=1 only (broken line) and with m=1 and m=2 (solid line).*

4. FORCE BALANCE ON THE PLASMA

The force balance on the kinked plasma is due to the asymmetries of eddy and of halo currents.
Asymmetric eddy currents on the vessel have been computed with a finite element model. The torus surface has been replaced by quadrilateral plates. The vacuum vessel is such that the toroidal conductivity is much smaller than the poloidal one, and not uniform poloidally. The toroidal and poloidal resistivities are chosen to reproduce this anisotropy. The solution is carried out in terms of mesh currents. Branch currents are extracted from mesh currents to evaluate the force acting on the vessel. Two contributions are taken into account: poloidal currents interacting with the toroidal field and toroidal currents interacting with the plasma field. The driver is the change in the magnetic flux through the plates, provided by a shifting and tilting rigid current ring. The toroidal plasma current is assumed uniform. This is an approximation, since the distorted plasma intercepts the first wall differently in each cross. Furthermore, asymmetries in the plasma vertical position between opposite cross sections are usually smaller if taken from measured vertical positions $\Delta z_{pos} = M_{z,\varphi} / I_\varphi - M_{z,\varphi-\pi} / I_{\varphi-\pi}$, than if taken as moment-equivalent $\Delta z_{mom} = \left(M_{z,\varphi} - M_{z,\varphi-\pi}\right) / I_{ave}$:

because, in the presence of the second poloidal mode the vertical current moment may be larger where the plasma current is larger too. Since both the eddy current force on the vessel and the plasma force depend on the amplitude of the tilt, two limiting cases have to be taken into account: position-equivalent and moment-equivalent.

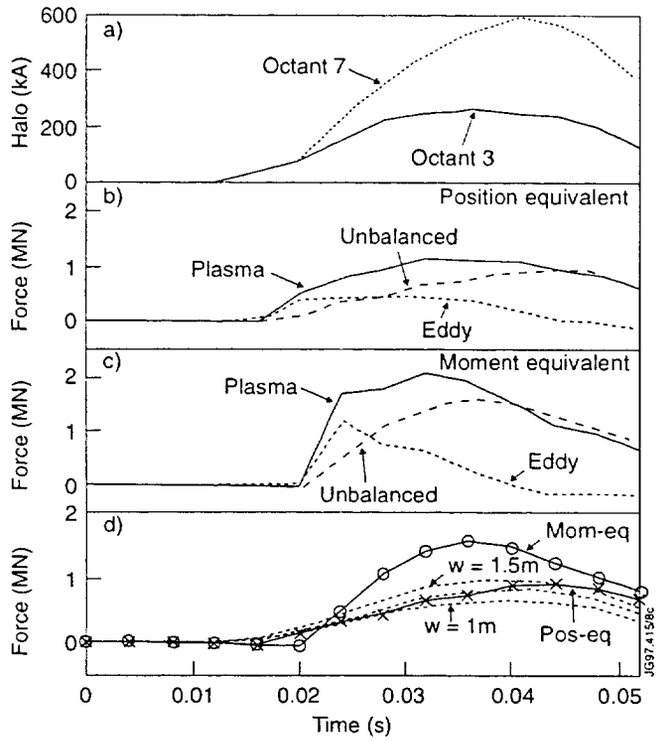

***Fig. 8** [a] Halo current in octant 3 and 7 during 38070 disruption; [b] position-equivalent and [c] moment-equivalent plasma net radial force (solid), eddy current force (dotted) and unbalanced force (dashed); [d] the unbalanced force from the position-equivalent (crosses) and the moment-equivalent (circles) cases compared with net radial halo current force evaluated for different reasonable values of the halo width (from 1m to 1.5 m). The initial time is 60.0 s.*

The net radial force due to the halo current can be estimated using a crude model. If a circular plasma kinks (m=1/n=1) in the centre of a circular vessel, at any toroidal position the halo linear force is $f_H = w I_H B_T / (2\pi R)$, normal to the vessel and pointing to its centre, the poloidal halo current (I_H) and the halo width of the halo region interception with the vessel (w) do not depend on the angle. The radial component is $f_{H,x} = f_H \cos\varphi \cos\vartheta$, and for m=1/n=1 it becomes $f_{H,x} = f_H \cos^2 \varphi$. Integration along the toroidal angle gives $F_{H,x} = 1/2\, w\, I_H B_T$.

Experimental data have been used for plasma current and position, halo current and toroidal field. The pulse chosen for the force balance test is 38070 (fig. 8): the vertical current moment and the plasma current are larger in octant 7 than in octant 3. Consequently the moment-equivalent case shows a plasma force almost double than the one of the position-equivalent case. The balance seems to be better satisfied for the position-equivalent case.

5. REACTION FORCES

The sideways force acting on the vessel in the worst asymmetric events is of the same order of magnitude as the vertical force (some mega newtons).

Even after the installation of a new lateral support system [4] large vessel displacements have been observed (up to 7 mm). The cause of the smallness of the improvement gained from the new supports can be in the previously neglected restraining action of toroidal field on the motion of the vessel. When the vessel is moving in the toroidal magnetic field, eddy currents are induced on its surface which tend to keep the flux constant inside the torus. Later they decay, because of the finite resistance of the vessel wall. The magnetic reaction force is proportional to the square of the toroidal field.

The restraining effect of the toroidal field can be approximately described by a magnetic damping coefficient and a stiffness constant. The numerical evaluation of the two parameters has been done using the same finite element model described before. In addition, a cross check was carried out against analytic calculations for a simplified geometry. The quasi-stationary solution (resistive only) gives the damping coefficient $\beta_M = b_M B^2$ with $b_M = 50\,\mathrm{MNm^{-1}T^{-2}}$ and the high frequency one (inductive only) gives the stiffness constant $\kappa_M = k_M B^2$ with $k_M = 0.41\,\mathrm{MNm^{-1}sT^{-2}}$.

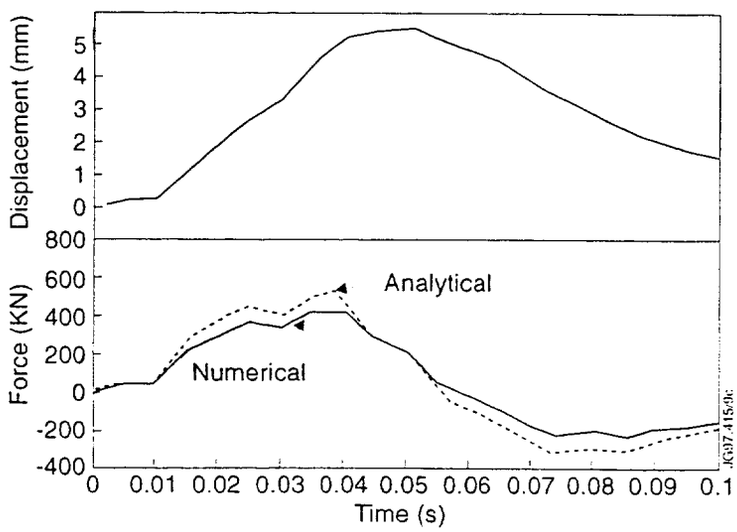

Fig. 9 *Analytical (dotted) and numerical (solid) solution for the magnetic reaction force at the vessel during pulse 38070.*

The magnetic damping coefficient and stiffness constant are used in lumped parameter mechanical models of the present vessel support system and of proposed designs. Because of the anisotropy of vessel resistance the eddy current pattern changes while the currents are decaying (different eigenmodes are present), whilst in the lumped parameter model only one time constant can be take into account. In order to understand if this simplification is acceptable the analytical solution of the force equation $\tau\dot{F} + F + \beta_M\dot{X} = 0$ where τ is β_M/κ_M, has been compared with the time dependent solution carried out on the finite element model (fig. 9): the two are reasonably similar.

According to the lumped parameter model of the present support system (fig. 10), during a 2.7 T disruption, the lateral supports reduce the sideways displacement by 12% and the magnetic damping by 20%.

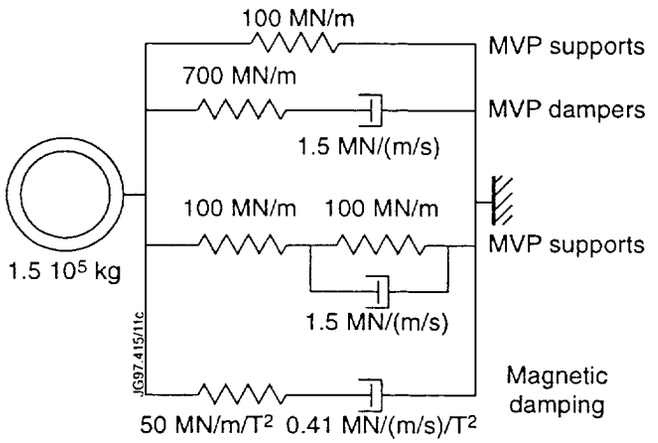

Fig. 10 Lumped parameter model of present vessel supports and restraints used for asymmetric load.

6. CONCLUSION

The sideways force scales as the product of the plasma current with the toroidal field and it implicitly depends on the amplitude of the asymmetry in the vertical position. The design of large machines has to account for this force or rely on prevention of asymmetric events by shortening the time between the loss of confinement and the plasma current quench.

REFERENCES

1. E. Bertolini et *al.*, Proc. of SOFE 1995, vol. 1, p.259.
2. P. Noll et *al.*, Proc. of SOFT 1996, p. 73.
3. N. Pomphrey, J. Bialek, W. Park, *Modelling the Toroidal Asymmetry of Poloidal Halo Currents in Conducting Structures*, submitted to Nuclear Fusion.
4. J. Hemmerich et *al.*, Proc. of SOFT 1996, p. 65.

An Active Phase Compatible Protection System to prevent Excessive Neutral Beam Shinethrough during JET Plasmas

S Cox, A Bickley, A Browne, T T C Jones, L Svensson, D Young

JET Joint Undertaking, Abingdon, Oxon, OX14 3EA, UK

ABSTRACT

The JET Fast Beam Interlock System (FBIS) removes the neutral beam power with a fast response (<20ms), under a diverse range of fault conditions. The configuration of FBIS for the tritium, or active phase of operation of JET is described, in particular its expansion to include inputs from a new interlock designed to prevent excessive neutral beam shinethrough.

This new system is based on visible bremsstrahlung emission from the plasma and is called the Bremsstrahlung Beam Interlock (BBI). Its main features are detailed here, including heated fibre-optics and a compensation fibre which make the interlock compatible with the active phase. In addition, the calibration of the BBI using JET's infra-red interferometer is described as well as operational experience with deuterium-tritium (DT) plasmas.

I. THE FAST BEAM INTERLOCK SYSTEM

The response requirements derive from the high power density (>200MW/m^2) of the beams [1] and the potential for damaging beamline and torus components, with the consequential risk of releasing large amounts of cooling water into a tritiated system or breaching the vacuum boundary itself. The FBIS [2] has been extended for the active phase of operation of JET with the inclusion of inputs from the tritium gas introduction system [3], and the BBI. FBIS features include:

- A fail-safe design based on the transmission and reception of 1kHz pulse-trains.
- A hierarchical structure (Fig.1) where certain fault conditions require a global beamline trip whereas others are specific to a bank or a pair of PINIs.

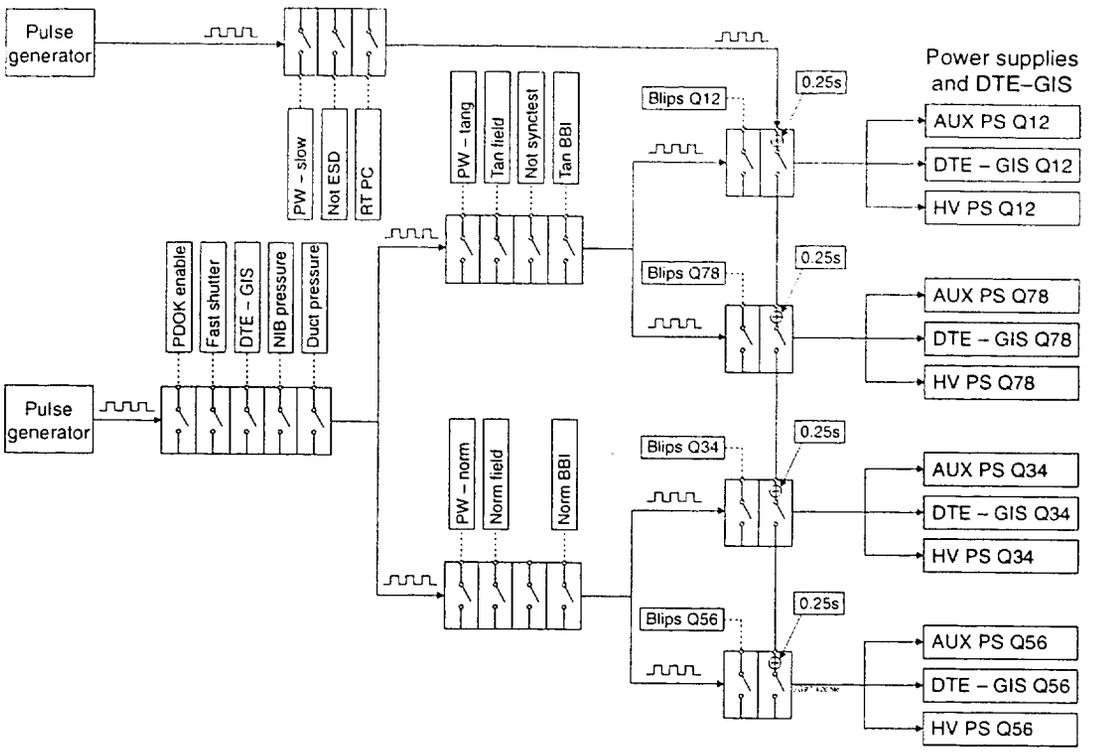

Fig.1. The structure of the Fast Beam Interlock System.

- A latched "first-fault" detector circuit which makes it easier to diagnose complex cause and effect scenarios (Fig.2).
- A stop-watch which records the time of a power supply trip with a resolution of 1ms (Fig.2).

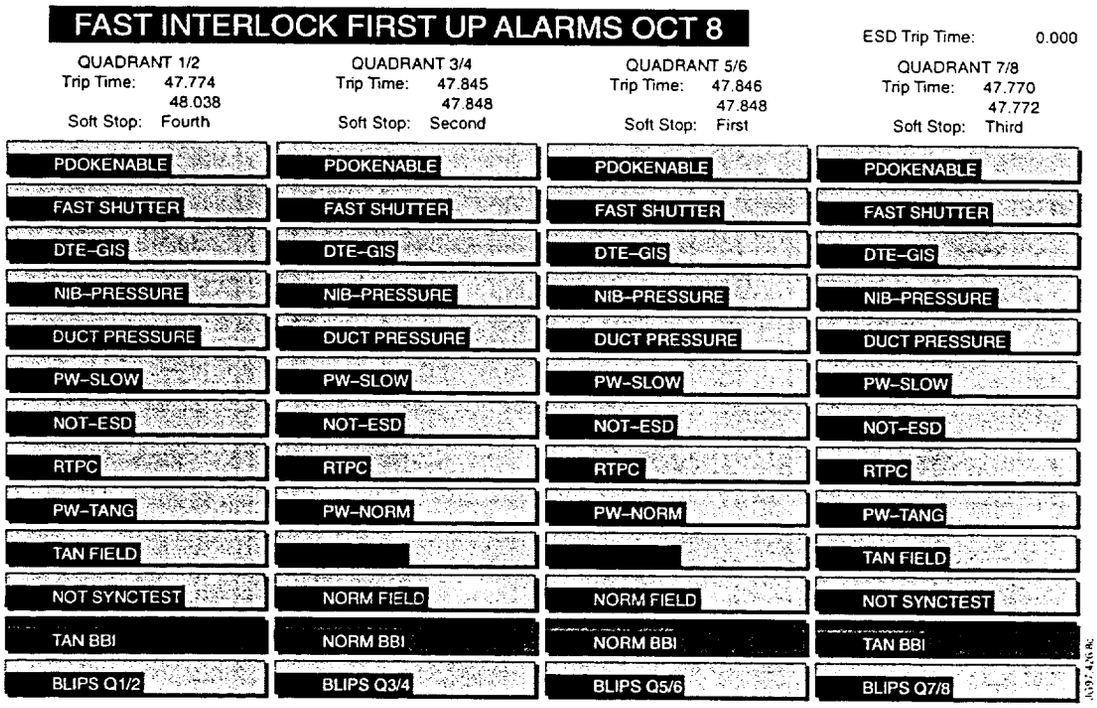

Fig.2. The "first-fault" alarm interface.

II. THE BREMSSTRAHLUNG BEAM INTERLOCK

Visible bremsstrahlung emission from a plasma at wavelength λ is given by,

$$\frac{dN}{d\lambda} = \frac{1.89\times10^{-35}}{4\pi}\,\bar{g}\,\frac{n_e^2 Z_{eff}}{\lambda^2\sqrt{T_e}} \qquad \frac{W}{m^3 nm\ sr} \qquad (1)$$

where $\bar{g}$ is the temperature averaged Gaunt factor, n_e and T_e are the electron density and temperature respectively and Z_{eff} is the effective ion charge. Thus it can be used as a measure of the electron density and hence the beam transmission through the plasma, i.e., shinethrough. In the event of a plasma of too low a density, the BBI (Fig.3) acts through the FBIS to remove rapidly the neutral beam power.

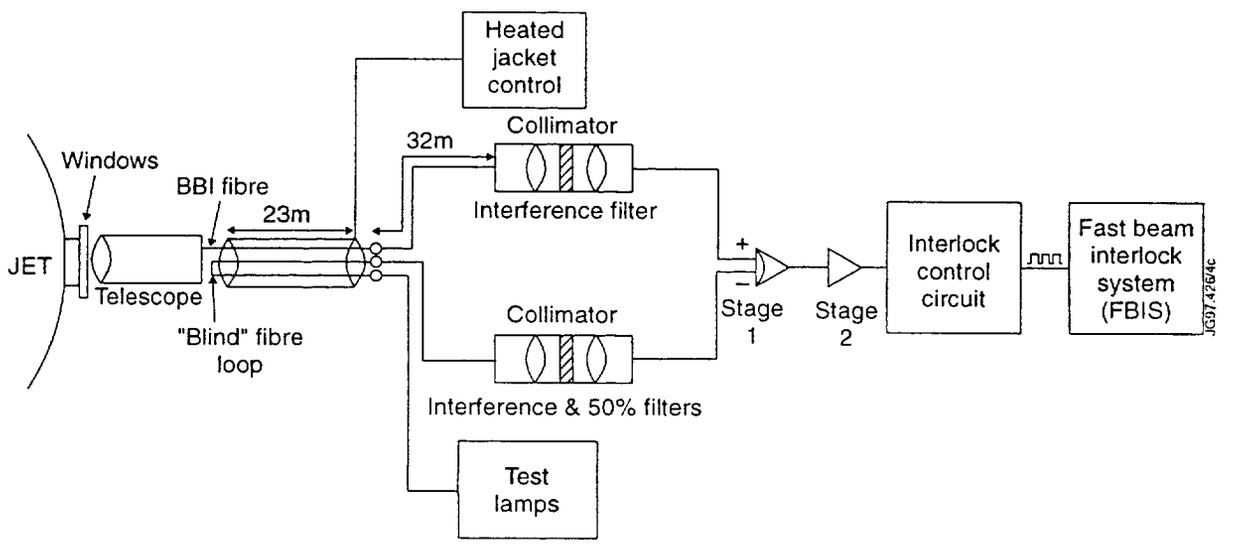

Fig.3. A schematic of the BBI.

A Optics

- 8m line of sight is through two fused silica windows (Fig.4).
- A large core diameter (1mm) fibre-optic has been selected in order to maximise power.
- The numerical aperture of the fibre is ~0.23 and this limits the optical étendue to ~$1.38\times10^{-7}m^2sr$.
- The interference filter transmits the bremsstrahlung radiation at 523.5nm with a bandwidth of 1nm which should be free from impurity line radiation.

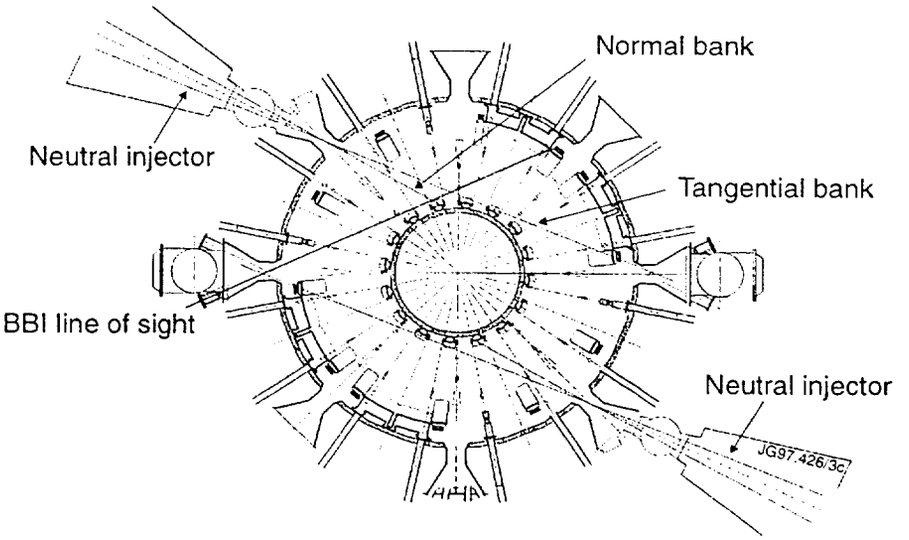

Fig.4. The line of sight of the BBI.

B Electronics

- A photodiode detector was chosen because of its simplicity and consequently higher reliability.
- A two stage, high gain (~10^{11}) transimpedance amplifier has been built with an ~50Hz bandwidth.
- To maximise the signal-to-noise ratio in the first stage (Fig.5):
  - Resistance R1 is as high as possible, consistent with the bandwidth requirements.
  - The photodiode's capacitance is minimised by making its active area as small as possible.
  - A low bias current op-amp is used to reduce shot noise and voltage offsets.
- The second stage comprises an instrumentation amplifier (gain~10^2) and a Butterworth filter.
- The signal-to-noise ratio is ~26dB for an output voltage of ~0.2V.

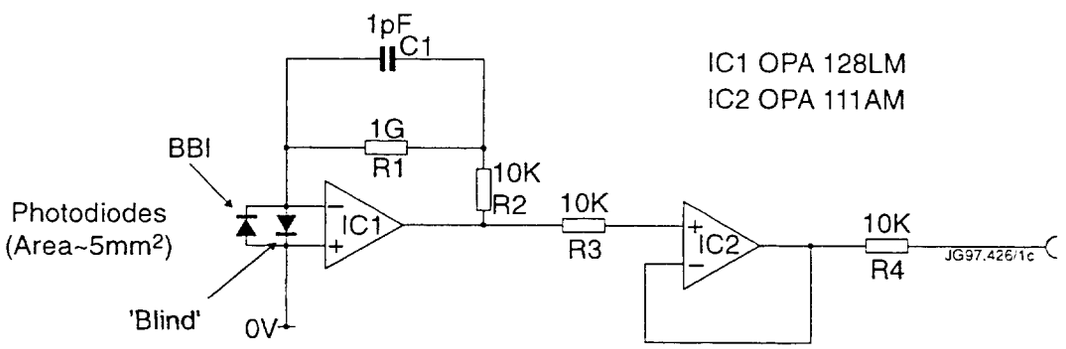

Fig.5. The first stage of the BBI amplifier.

C Active Phase Compatibility

Radiation effects on the BBI have been ameliorated by:

- Situating the electronics outside the biological shield.
- The use of large core diameter fibres which are more resistant to opacity effects [4].
- Heating the fibre-optics closest to the torus to ~300°C (Fig.3) which reduces the neutron induced transmission losses substantially [5].
- Using a second "blind" fibre to compensate for luminescence effects. This follows the same path as the BBI fibre (Fig.3), hence the bremsstrahlung emission can be obtained by subtracting the "blind" signal from the BBI signal (Fig.5).

These measures are effective as shown in Fig.6. The increased neutron and gamma radiation levels from the DT plasma had no significant effect on the BBI signal which confirms active phase compatibility at JET.

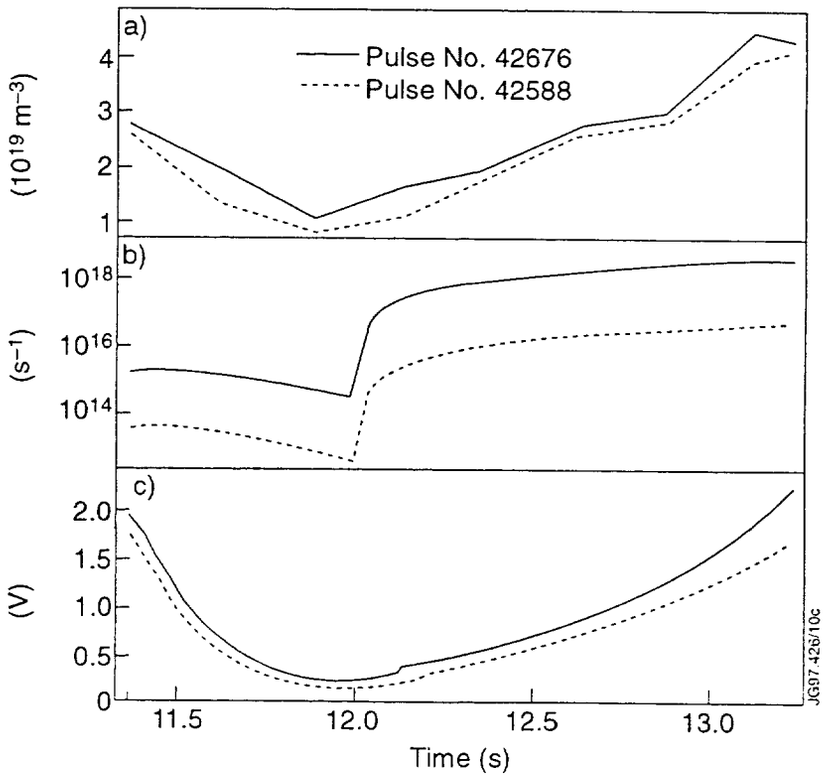

Fig.6. A comparison between JET pulses 42676 (DT) and 42588 (DD) showing: a) the electron density, b) the total neutron rate and c) the BBI voltage.

III. CALIBRATION

- A cross-calibration has been carried out using JET's infra-red interferometer.

A Calibration Constant

- The BBI and interferometer can be equated in the following manner:

  Assuming that the electron temperature and effective ion charge are constant, (1) can be re-written to give,

$$V_{BBI} = k \int_{BBI} n_e^2 \, dx \qquad (2)$$

  where k is the calibration constant and x is the distance along the line of sight. The electron density is a function of radial position, r, which in turn depends on x and can be written as,

$$n_e = n_0 f(r(x)) \qquad (3)$$

Fig. 2: General arrangement of the commutating unit

  where n_0 is a constant. Using the BBI and interferometer lines of sight gives,

$$V_{BBI} = k \left(\int_{inter} n_e \, dx \right)^2 \frac{\int_{BBI} f(r(x))^2 \, dx}{\left(\int_{inter} f(r(x)) \, dx \right)^2} \qquad (4)$$

- The form factor (third factor on the RHS) is computed from measured density profiles.

B Trip Levels

- For each PINI, the power density limit of the affected area of the vessel wall is used to calculate the limiting integral of electron density. Subsequently, an equation similar to (4) is used to derive the trip voltages for a number of ideal density profiles.

- The highest trip voltages from the tangential and normal PINIs determine the standard trip levels.

- The "notch" is a period (~0.5s) of higher than normal shinethrough at the start of beam injection allowing a lower density target plasma [6].

IV. OPERATION

- Data have been collected from over 500 JET plasmas.
- A typical BBI trip event is shown in Fig.7 for an optimised shear discharge in deuterium.

  The normal and tangential PINIs were timed to start at 5.0 and 5.4s respectively. The BBI voltage did not reach the normal standard trip level at the end of the "notch", and consequently the normal bank was tripped.

- The Plant Enable Windows System (PEWS), which uses the interferometer signal, was very close to tripping the beams on this pulse (Fig.8). This indicates that the cross-calibration method is accurate.
- The BBI is sensitive to reductions in the plasma purity, i.e., Z_{eff} . However, this is a fail-safe scenario as the density is interpreted as being lower than it really is.

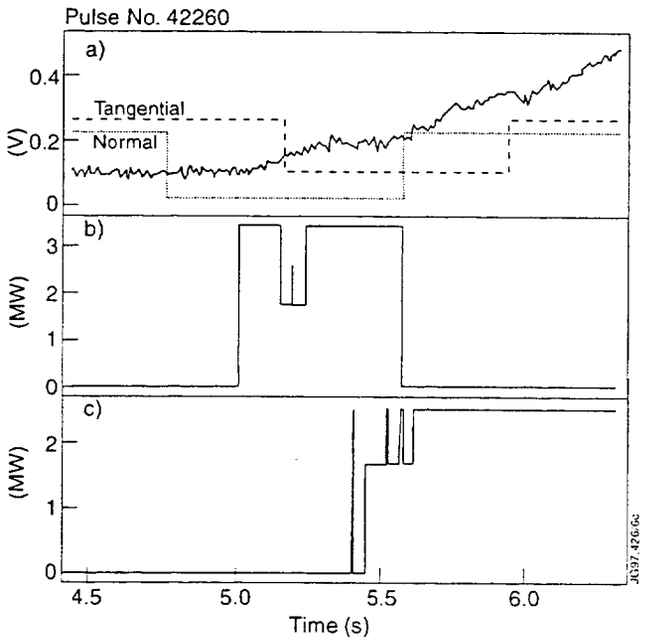

Fig.7. A typical BBI trip event showing:
a) the BBI voltage and the interlock trip levels,
b) the normal bank injected power and
c) the tangential bank injected power.

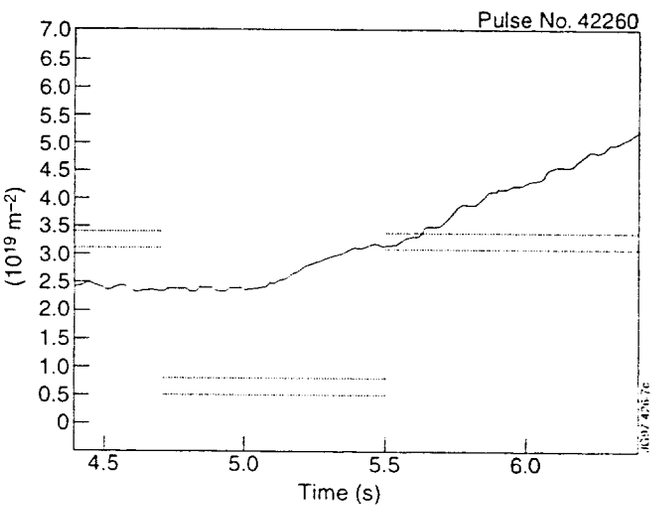

Fig.8. The PEWS data and trip levels for the normal bank.

V. CONCLUSIONS

The Bremsstrahlung Beam Interlock has worked reliably and with relatively few problems during its initial operational period, comprising over 500 JET pulses. The calibrated trip levels appear to be consistent with those in PEWS, which gives confidence in the interlock and in the cross-calibration using JET's infra-red interferometer. Being a hard-wired, fail-safe system, the BBI can be regarded as the primary protection against injection into a plasma of insufficient density. The interlock is compatible with the active phase of operation of JET ,i.e., neutron rates of ~4.3 $x10^{18}$ s^{-1}.

The success of the BBI shows that this is a relatively simple and therefore highly reliable method of protecting in-vessel components against excessive neutral beam shinethrough.

ACKNOWLEDGEMENTS

The authors would particularly like to thank P D Morgan who developed the heated fibre–optic system for active phase visible light diagnostics at JET and B Viaccoz for his technical assistance with the fibre terminations.

REFERENCES

[1] G. Duesing et al., "Neutral Beam Injection System," Fusion Technology **11**, January 1987, pp.163-202.

[2] D. Cooper, D. Stork, M. Mead, and D. Young, "The Fast Beam Interlock System for JET neutral injection," Proceedings of the 12th Symposium on Fusion Engineering, Monterey, 1987, pp.1096-1100.

[3] L. Svensson et al., "The JET active phase gas introduction systems for neutral beam injection and commissioning and operation with tritium," these proceedings, in press.

[4] H. Adler, K. Hill, A. Ramsey, and W. Tighe, "Luminescence and transmission measurements on fibers exposed to high neutron fluxes," Rev. Sci. Instrum. **66**, January 1995, pp.904-906.

[5] A. Ramsey, "D-T radiation effects on TFTR diagnostics," Rev. Sci. Instrum. **66**, January 1995, pp.871-876.

[6] The JET Team, "The route to high performance on JET," Plasma Phys. Control. Fusion **37**, (1995), pp.A359-A370.

Operator Interfaces for JET Remote Handling Equipment

P Carter, B Haist, A Rolfe.

JET Joint Undertaking, Abingdon, Oxon, OX14 3EA. UK.

INTRODUCTION

Operator interfaces play an important role in remote handling operations at JET. A new approach to design, has greatly increased flexibility. Interfaces are now more intuitive and readily adaptable to new scenarios.

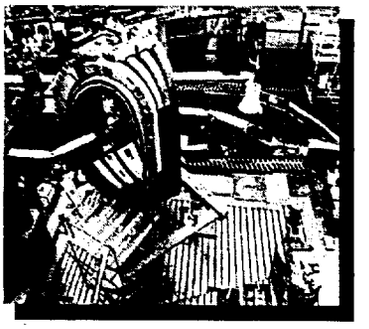

Articulated Boom

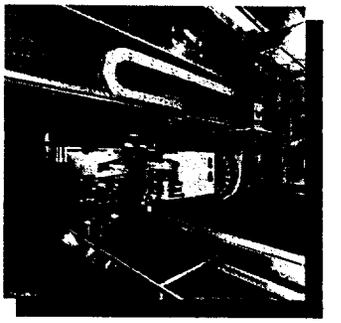

TCTF (Tile Carrier Transfer Facility)

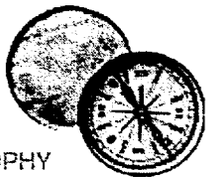

PHILOSOPHY

DESIGN

PROTOTYPE

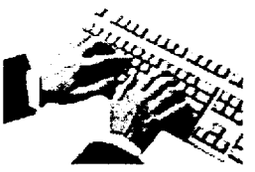

CODE

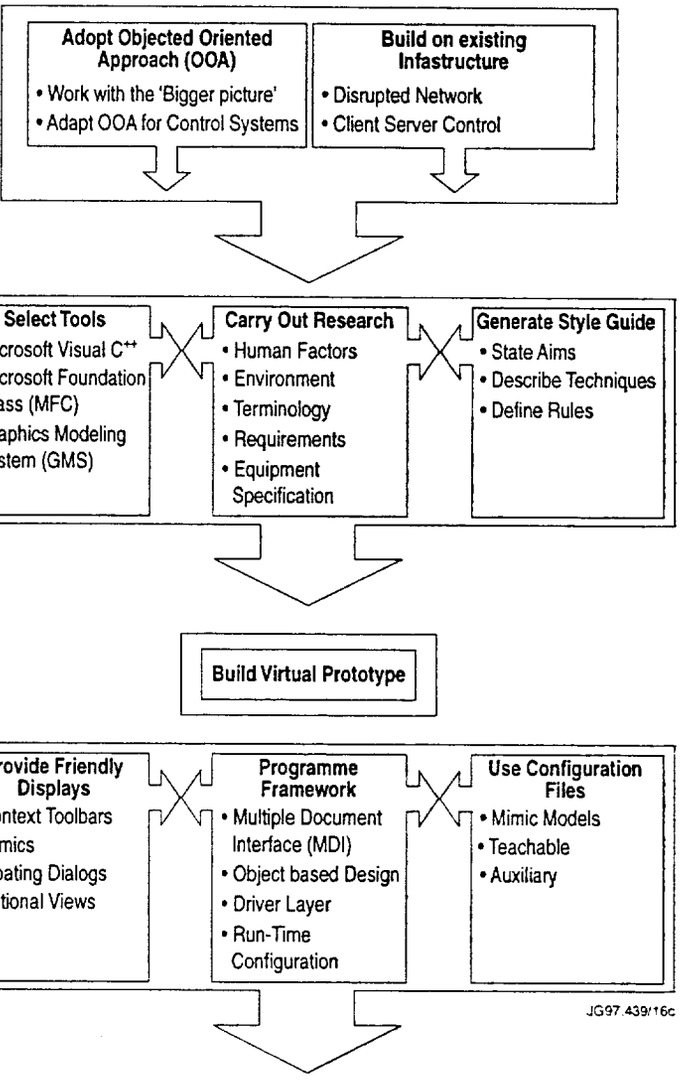

The Articulated Boom Mill

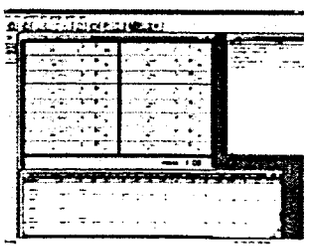

The TCTF MMI

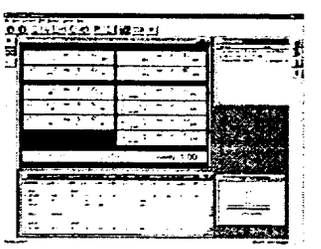

ABSTRACTION

Abstraction is not a new concept. Everybody is affected by it to some degree. For example, car owners work at a high level of abstraction. Somebody else defines and implements a 'car', and all that is visible to the owner is the behaviour of the car. Details of how that abstract behaviour is implemented are hidden so that they can be changed as necessary without impact to the end user.

The new Remote Handling interface is structured using abstract layers. The lower layers provide services to higher ones. Irrelevant internal details of the lower services are hidden from the higher layers. The layers are aligned with classes of users. A high degree of flexibility is achieved by giving tools to the classes of users. The tools correspond to a layer of the operator interface.

The software life-cycle in remote handling thus includes extra feedback paths. This contrasts with the typical software life cycle where only the software developer can make the changes

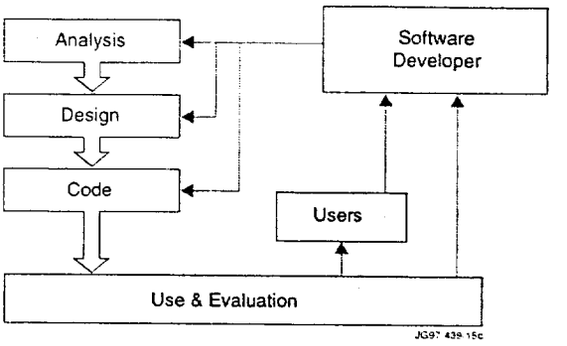

A Typical Software Life Cycle

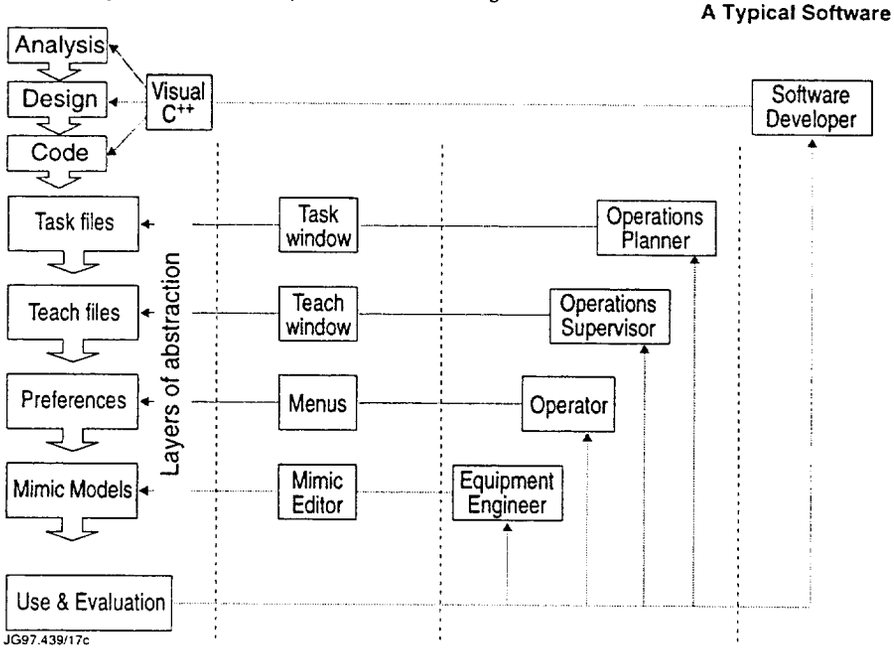

Remote Handling Software Life Cycle

Current and Future Development

The focus of the operator interface has now moved on to tasks and associated procedures. As a result the design framework has extended to include:

- Task descriptions
- System wide mimics
- Inter-MMI communications
- Client Server objects within the framework

Additionally we are curently investigating the followinf possible additions:

- Web integration
- ActiveX controls
- Audio prompt for operators